**Finite Element-based Parametric and Probabilistic Analysis of Structural
Deterioration in Corroded Pre-stressed Concrete Girders**

by

Liying Huang

A thesis submitted in partial fulfillment of the requirements for the degree of

Master of Science

in

STRUCTURAL ENGINEERING

Department of Civil and Environmental Engineering
University of Alberta

ABSTRACT

Deterioration of concrete structures caused by corrosion have caused worldwide concerns especially for pre-stressed concrete (PC) structures because of their extensive use in important infrastructure, such as highway bridges. PC girders that have been in service for a long time in natural environment are highly susceptible to various corrosion-induced deteriorations, which can in turn affect the structural behaviour of PC girders. Therefore, it is important to understand and quantify the corrosion effects on the flexural and shear behaviours of PC bridge girders.

In parallel with the experimental testing of the PC girders salvaged from a decommissioned 28-year old bridge, this thesis aims to take an analytical approach to investigate the residual performance of PC girders with various deteriorations. In this thesis, two-dimensional (2D) non-linear finite element (FE) method was used to model the flexural and shear behaviour of concrete beams/girders, and relevant modeling strategies were first validated using experimental tests of reinforced concrete beams with artificial corrosion defects. After that, 2D FE models for PC girders were developed to study the flexural and shear behaviours of corroded PC bridge girders. A 2D FE model was developed for the PC girder #1, which was in a visually intact condition, and it was firstly used to back-calculate the possible pre-stress loss (30% - 40%) in this PC girder as a preliminary forensic analysis. This was verified by the 2D FE models for the flexural and shear girder tests, as well as the one-dimensional beam model using fibre-based beam elements for the flexure test. The 2D FE models were validated against the tests to be capable of predicting both the flexural and shear behaviour of PC girders.

The validated 2D FE models were then used to conduct comprehensive parametric studies for both flexural and shear critical girders, respectively, focusing on the corrosion effects on the structural behaviour (e.g., stiffness, residual strength). The deterioration features considered in the parametric studies include pre-stress loss, the steel cross-sectional area loss, material degradation, concrete spalling, and complete or intermediate loss of bond between steel and concrete, which were all related to corrosion degrees. It was found that the pre-stress loss, the steel cross-sectional area loss, and bond loss played significant roles on the residual capacities of corroded PC girders. In contrast, the material degradation and concrete spalling on the tension side played less role on the residual load bearing capacities. Based on the parametric analysis results and the FE modeling of girder #1, the 2D models were used to understand the possible deteriorations inside other corroded girders (i.e., girder #2) with severe corrosion or to predict the behaviour of other girders (i.e., girder #3). The models provided fairly good results for both flexural and shear behaviour of girders under different deterioration levels.

Eventually, to further understand the effect of corrosion on the capacity of PC girders, the FE models for corroded girders were integrated with probabilistic analysis algorithms (e.g., subset simulation) to study the residual capacity of PC girders. The probabilistic capacities for specific corrosion scenarios with three different corrosion degrees (0%, 10%, and 30%) were compared. It is found corrosion affects both the mean and variance of the residual capacities of PC girders, especially for high corrosion degrees (e.g., 30%).

ACKNOWLDEGEMENTS

TABLE OF CONTENTS

LIST OF TABLES

LIST OF FIGURES

CHAPTER 1: INTRODUCTION

1.1   Background

Reinforced concrete (RC) and Pre-stressed concrete (PC) highway bridges are widely used as integral parts of the transportation network, as their functionality and safety has been playing an important role towards the socio-economic development globally. However, both RC and PC bridge structures are prone to various deteriorations caused by chloride intrusion, carbonation, alkali-aggregate reactivity, freeze-thaw as well as other aging effects.

The structural deficiency due to deterioration of bridge structures is revealed by the following statistics. According to the Canadian infrastructure report card (2016), 26% of bridges were in fair/poor/very poor physical conditions compared with 74% in good/very good conditions in Canada. The Bureau of Transportation Statistics (2008) reported that about 25% of the bridges in the United States of America were structurally deficient or functionally obsolete. Over 30% of the existing bridges were estimated by the Federal Highway Administration (2011) to exceed their 50-year service life, which necessitated costly maintenance in the near future. BRIME (2001) suggested that a significant portion of the concrete highway bridges were affected by deterioration and thus considered to be substandard in Europe (e.g., 39% in France, 37% in Germany, 26% in Norway and 30% in the United Kingdom).

Furthermore, the importance of deterioration effects due to corrosion or other aging effect on bridges can be highlighted by catastrophic failure of bridges as reported in the literature. For example, Figure 1-1 shows four failure events of bridge girders due to deterioration: the collapse of the Lake View Drive Bridge in the US in 2005 (Harries 2009), the collapse of the Saint Stefano Bridge in Italy in 1999 (Darmawan 2009), the collapse of the Ynys-y-Gwas Bridge in the UK in 1985 (Woodward and Williams 1988), and the collapse of the Melle Bridge in Belgium in 1992 (Mathy et al. 1996). As such, structural deficiency due to deterioration is highly concerned by the government and engineers as a universal phenomenon all around the world.
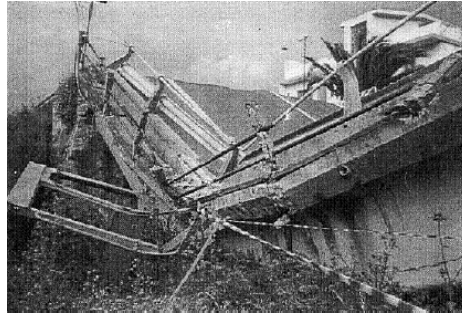
Figure 1-1 Photos for the collapsed bridges: (a) the Lake View Drive Bridge in the US, (b) the Saint Stefano Bridge in Italy, (c) the Ynys-y-Gwas Bridge in the UK, and (d) the Melle Bridge in Belgium

Among various causes of deteriorations aforementioned, chloride corrosion has been identified as one of the main factors. Through decades, considerable research has been devoted to study the effects of deterioration due to corrosion on structural behaviours of RC beams by experimental testing and numerical modelling. The experimental tests provided significant and detailed knowledge on corroded RC beams, and these experimental studies include, but is not limited to, Rodrguez et al. (1997), Mangat and Elgarf (1999), Castel et al. (2000a and 2000b), Xu and Niu (2004), EI Maaddawy et al. (2005), Malumbela et al. (2010), Xia et al. (2011), Dang and François (2013), Zhao and François (2014), Zhu and Francois (2014), Kotsovos et al. (2015). Complementary to the experimental approach, numerical analysis was also used by many researchers (e.g., Coronelli and Gambarova 2004, El Maaddawy et al. 2005, François et al. 2006, Azad et al. 2007, Wang 2008, Kallias and Rafig 2010, Jnaid and Aboutaha 2016). Similar studies (i.e., experimental test and numerical analysis) were conducted on PC beams or girders (e.g., Darmawan and Stewart 2007, Coronelli et al. 2009a and 2009b, Li and Yuan 2010, Guo et al. 2010, Rinaldi et al. 2010, Castel et al. 2010, Cavell and Waldron 2001, Wang et al. 2017,

2

Zhang et al. 2017a and 2017b). Those work available in the literature for PC beams or girders is relatively less compared with RC beams, and many of them had specific research focuses or limitations. For example, most of them focused on experimental studies with a special focus (e.g., corrosion on strands only), or considered limited deterioration levels or types based on real-world bridge girders (e.g., Halsey and Miller 1996, Labia et al. 1997, Czaderski and Motavalli 2006, Pape and Melchers 2013, Pettigrew et al. 2016, Murray et al. 2017). However, inspections of aged pre-stressed bridges indicate that PC girders, after long-time service in natural environment, are highly susceptible to different corrosion-induced deteriorations, which affect the structural behaviour of PC girders. As such, further research is needed for a comprehensive study of corroded PC girders.

1.2 Problem Statement and Motivation

The central problem to address in this thesis is understanding and quantification of the corrosion effects on the flexural and shear behaviours of PC bridge girders. In the current practice, a typical load evaluation procedure, e.g., as specified in the Alberta Transportation Bridge Load Evaluation Manual v.1.1 (2016) and/or the Section 14 of Canadian Highway Bridge Design Code (CSA S6-14), is used to rate bridge condition based on visual inspections and experience of bridge evaluators. This procedure does not involve quantification of the residual capacity of deteriorated structure members, but highly relies on the knowledge of deterioration effects on bridge girders. This calls for a comprehensive study using a wide range of corrosion degree and deterioration types in PC girders, and possibly consider pertinent uncertainties.

Specifically, a PC bridge constructed in 1990 near Barrhead in central Alberta was recently rated as unsafe and removed in 2017. Thus, the nine girders salvaged from this abandoned bridge offered a great opportunity to investigate the behaviour of aged PC girders experimentally and analytically. In parallel with the experimental study conducted in this project by the research team in the Department of Civil and Environmental Engineering, at the University of Alberta, computer modeling can be complementary to the experimental work by providing further insight into salvaged girders tested. Because the girders are under different deterioration states that are unknown, it is challenging to develop models

to predict all tested girders. However, reliable models can be used to infer the possible deterioration states for preliminary forensic analysis. It is also worth mentioning that it is unlikely to have an intact girder to be used for comparison as a control sample (i.e., a un-corroded PC girder); a virtual control specimen through numerical modeling is needed.

For PC girders with similar deteriorations, the residual structural performance is uncertain due to inherent uncertainties associated with the concrete and steel material properties. For reliable assessment of the residual performance of PC girders, the effect of corrosion on probabilistic capacity of PC girders needs to be explored.

1.3   Objectives and Methodology

The overall goal of this work is to study the flexural and shear behaviours of corroded PC bridge girders comprehensively and to provide insights into the corrosion effects on the PC girders. Since it is impractical to test a large number of aged full-scale bridge girders with a wide range of corrosion degree and deterioration types, a numerical analysis approach is taken in this study. To the end, this study will develop numerical models that can consider deteriorations in PC girders, and use models developed to investigate the effect of corrosion on structural behaviour of PC girders through (1) parametric studies considering different deteriorations and (2) probabilistic structural analyses for PC girders under given corrosion scenarios. Various corrosion-induced deterioration features in concrete structures will be considered, including changes in geometry (e.g., concrete spalling, steel area deduction), material properties (e.g., yield strength of steels, compressive stress of cover concrete), and composite actions between steel and concrete (e.g., de-bonding and intermediate bonding). All these in turn affect the structural behaviour of PC girders. The corrosion-induced deteriorations are incorporated into non-linear finite element (FE) models for PC girders developed in 2D software VecTor2 (Wong et al. 2013). The FE models for corroded girders are then combined with probabilistic analysis algorithms (e.g., subset simulation) to study the corrosion effect on the probabilistic capacity of PC girders.

To achieve the goal of this research with the aforementioned methodology, the research tasks are presented as follows:

1. Literature review on the relevant studies for corroded concrete beams/girders.

2. Investigation and validation of modeling strategies for corroded concrete beams/girders using test data available from the literature.

3. Development and validation of FE models for flexural and shear critical PC girders with least corrosion damage through visual inspection.

4. Parametric studies using FE models developed for both flexural and shear critical girders to investigate the effect of different deteriorations on corroded PC girders, and inference on the deterioration states of other girders salvaged from the same bridge abandoned.

5. Probabilistic analysis of the residual capacity of PC girders under specific corrosion scenarios using the FE models developed for corroded PC girders.

1.4 Organization of Thesis

This thesis consists of seven chapters as follows:

- Chapter 1 of this thesis is a brief introduction to the background, problem statement, motivation, objectives, methodology, and specific tasks of this research.
- Chapter 2 presents a literature review regarding the investigation on corroded RC and PC beams.
- Chapter 3 provides the investigation and validation of numerical modeling strategies for corrosion-damaged RC beams using test data from the literature.
- Chapter 4 presents the simulation results of flexural-critical PC bridge girders with comparison to the test results, as well as a parametric study for flexure-critical PC girders with different corrosion-induced deteriorations.
- Chapter 5 presents the simulation results of shear-critical PC bridge girders with comparison to the test results, as well as a parametric study for shear-critical PC girders with different corrosion-induced deteriorations.
- Chapter 6 presents the probabilistic analysis of the residual capacity of PC girders under specific corrosion scenarios.

- Chapter 7 summarizes conclusions of this research, with recommendation for future works.

CHAPTER 2: LITERATURE REVIEW

2.1 Deteriorations in Concrete Structures

Deterioration of concrete structures can be caused by physical (e.g., thermal changes such as natural freeze-thaw cycles, mechanical actions such as impact), chemical (e.g., chloride intrusion, carbonation, acids/sulfates attack), and biological processes (e.g., fouling, biogenic attack). Among them, deterioration due to chemical processes (e.g., corrosion) is most common for concrete structures under aggressive environments. As commonly observed for concrete bridge girders, corrosion can influence both concrete and steel bars and thus it is considered as a primary cause of capacity degradation of RC and PC structures (Broomfield 1997, Harries 2009). Ideally, the reinforcement is protected from corrosion in alkaline environment of concrete, with a pH value between 12 and 14 (Minkarah and Ringo 1982, Coggins and French 1990). This is because a passive oxide film forms around the reinforcement and it can prevent the penetration of moisture and oxygen (Minkarah and Ringo 1982). However, concrete bridge girders are generally exposed to various environmental conditions and susceptible to chemical attacks (Enright and Frangopol 1998). Concrete carbonation and the intrusion of chloride ions (e.g., from the use of de-icing salt) can reduce the pH value of concrete and damage the passive film around the reinforcement. This will result in the depassivation of reinforcing steels (Bohni 2000), and in turn initiate reinforcement corrosion. The breakdown of the oxide film due to chloride intrusion is usually local and random, and thus chloride attack typically leads to pitting corrosion (Bertolini et al. 2004). By contrast, carbonation typically induces general or uniform corrosion along steel reinforcements, see Figure 2-1. The corrosion of steel reinforcements together with other accompanying effects (e.g., bond deterioration, concrete spalling and cracking) will in turn impair the bridge condition and degrade its structural performance.
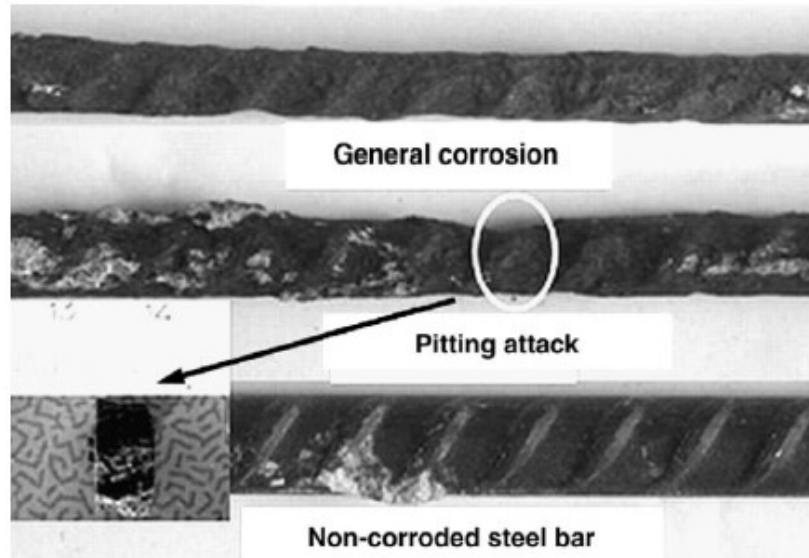
Figure 2-1: Corrosion of reinforcement steel in concrete (Zhang et al. 2010)

2.2 Bridge Condition Assessment

The American Society of Civil Engineers reported in 2017 that the average age of more than 600,000 bridges in the U.S. was 43 years old. It was also estimated that almost 40% of the existing bridges in the U.S. were in service more than 50 years (i.e., the expected design life), and thus needed rehabilitation or replacement in the near future (ASCE 2017). As such, billions of dollars are spent each year in repairing and replacing aged bridges to keep the infrastructure structurally sound and functional. In order to assess the safety and condition of existing bridges and to prioritize the rehabilitation and maintenance of deficient ones, inspection is usually the first step to proceed.

2.2.1 Bridge Inspection

In the current practice, bridge condition is typically inspected visually first by bridge evaluators. Visual inspection, as a non-destructive method without the aid of tools or devices, is easy and straightforward to get apparent damage features such as cracks, spalling, and potholes (Bertolini et al. 2004). Whereas this method can only indicate superficial damages, reliable assessment of bridge condition requires advanced bridge inspection methods, such as non-destructive testing (NDT). NDT consists of a variety of analysis techniques to evaluate material properties or structural components without

causing damage to inspected structures (Cartz 1995). Those techniques can be used to detect, characterize, and measure damage such as corrosion and cracks inside reinforced concrete structures. There are different types of NDT technologies commonly used, penetrating radiation (e.g., electromagnetic radiation for ground penetrating radars), sound waves (e.g., acoustic emission, ultrasonic testing, laser ultrasonic testing), and other signal conversions (e.g., electrical method, infrared thermography, magnetic method). For example, acoustic emission testing can detect the presence of cracks, delamination in concrete (Chotickai 2001); ultrasonic testing can accurately determine the thickness and depth of a crack or void in concrete (Mohamed and Rens 2001, Toutanji 2000); ground penetrating radars can assess delamination and the thickness of concrete, as well as the depth of reinforcement embedment (Huston et al. 2000). Their applications to bridge structures can be found in the Bridge Inspector's Reference Manual published by FHWA in 2006 (Ryan et al., 2006). NDT has been used extensively for bridges as it can be performed without disrupting the use of bridges and it is economical, safe and effective on structure assessment.

Nevertheless, NDT is limited to detection and quantification of local damages with certain restrictions, but unable to provide full information of bridge condition (e.g., the remaining strength of corroded reinforcement), or the safety-related aspects in particular. As a result, destructive testing (DT) needs to be conducted by testing material or structural specimens (e.g., load carrying capacity testing) to failure in order to understand their mechanical behaviour better for safety evaluation and condition assessment.

2.2.2 Testing of Aged PC Girders from Real-world Bridges

In order to investigate the residual performance of bridge girders after years of service under natural environment, inspection and destructive testing can be conducted on aged or deteriorated bridges. Limited PC girders removed from real-world bridges have been used for such an investigation with a specific focus, such as flexural and shear capacities, chloride contents in concrete, pre-stress loss of strands, remaining strength of materials. Selected experimental works on PC bridge girders affected by corrosion or other aging effects are summarized in Table 2-1. They are also reviewed in detail in the following

subsections categorized by the research focuses: flexure behaviour, shear behaviour, and others in general.

2.2.2.1 *Flexural Behaviours*

Shenoy and Frantz (1991) studied two PC box beams (914 mm × 686 mm) removed from a 27-year-old bridge in East Hartford, Connecticut. Visual inspection of the bridge showed that severe deterioration of some beams was observed and was attributed to the use of de-icing salt. The deteriorations included large holes on the top of two most deteriorated beams, concrete cracking and spalling on the sides and bottoms of some beams, exposed prestressing strands, and strand rupture. Two beams with different deterioration features were removed from the bridge to study the remaining strength and prestress loss. Each of the two girders was tested under two-point loading monotonically until the ultimate flexural capacity was reached. It was found that both beams were ductile and had similarly good performance; their flexural behaviour was accurately predicted by ACI Code methods (ACI 1989) based on the material properties measured from coupon tests. However, the service load estimated according to AASHTO (1989) was only half of the applied load corresponding to the start of flexural cracking. Regarding the prestress loss, the general method in PCI (1975) was used and it over-predicted the prestress loss in the strands.

Table 2-1 Brief summary of the experimental work reviewed on aged bridge girders

Reference	Location (Year)	Bridge	Age (years)	Girders	Inspection and testing
Tassios and Aligizaki, 1990	Arta, Greece (1959)	PC (46 m × 3)	30	5 I-shaped	inspection, truck loading test, measurement of corrosion content, material test
Cullington and Raggett, 1991	Manchester, Britain (1961)	PC (16.1 and 8.5 m)	30	10 I-shaped	shear test, inspection
Shenoy and Frantz, 1991	Hartford, Connecticut, US (1960)	PC (15.6 m)	27	2 box beams	visual inspection, flexural test, prestress loss measurement, material test
Rao and Frantz, 1996	Connecticut, US (1960)	PC (17.1 m × 13)	27	2 box beams	fatigue test, static test
Labia et al, 1997	Reno, US (1968)	PC (21.34 m × 2)	20	2 box beams	flexural test, remaining prestress test
Bruce and McCarten, 2006	Gisborne, New Zealand (1966)	PC (19.9 m)	35-48	3 I-shaped	visual Inspection, concrete compressive test, chloride ion contamination and carbonation depth
Lau et al., 2010	Canada (1965)	PC (19.87 m)	40	6 channel girders	flexural tests, shear test, load ratings, chloride ion contents test, material test
Osborn et al., 2012	Utah, US (1968)	PC (7.1, 14.5, 20.4 m)	42	7 I-shaped	cracking moment test, shear test
Setty, 2012	Ohio, US (1967)	PC (14.36 m × 3)	43	1 box beam	visual inspection, truck load test, chloride testing, load rating test
Pape and Melchers, 2013	Tasmania, Australia (1957)	PC (13 m × 34)	45	3 T-shaped	destructive load test, visual inspection, material test
Dasar et al., 2016	North-west of Japan (1975)	PC (24 m)	35 and 40	6 rectangular beams	visual inspection, bending test，prestressing force measurement
Floyd et al., 2016	Tulsa, US (1968)	PC (9.14 and 14 m)	47	2 I-shaped	shear test, non-destructive testing
Pettigrew et al., 2016	Utah, US (1965)	PC (16.3 m × 1)	48	3 double-Tee	inspection, cracking test, flexural test
Murray et al, 2017	Oklahoma, US (late 1960's)	PC (9.75 and 14 m)	45	2 I-shaped	non-destructive flexural tests, destructive shear tests
Kramer et al., 2018	Western Cape, South Africa (1963)	PC (18.5 m × 4)	54	1 I-shaped	visual inspection, material test, carbonation and durability tests

Labia et al. (1997) tested 2 full-scale pretensioned box girders removed from a bridge in Reno, in the U.S., to investigate their behaviours after 20 years of service. The girders were tested under simply supported condition with two-point loading applied in the middle, creating a 1.828 m long constant moment region. Both cracking tests and ultimate load tests were conducted for both girders. During the tests, strain profiles, deflection, crack opening, and strand strain were recorded. The residual prestress of the girders was also tested. It was found that prestress losses were significantly underestimated by using different methods (i.e., from ACI. 1989, AASHTO 1992, and PCI 1975). The authors inferred that the high prestress losses were attributed to severe creep and shrinkage due to a large range of daily temperature and humidity from the environment. For the ultimate load tests, the measured ultimate loads agreed well with those calculated by ACI code (1989) for both girders, as indicated in Figure 2-2. However, tested girders failed suddenly, which might be due to low concrete ultimate strain and high level of prestress loss, which delayed the yielding of strands.
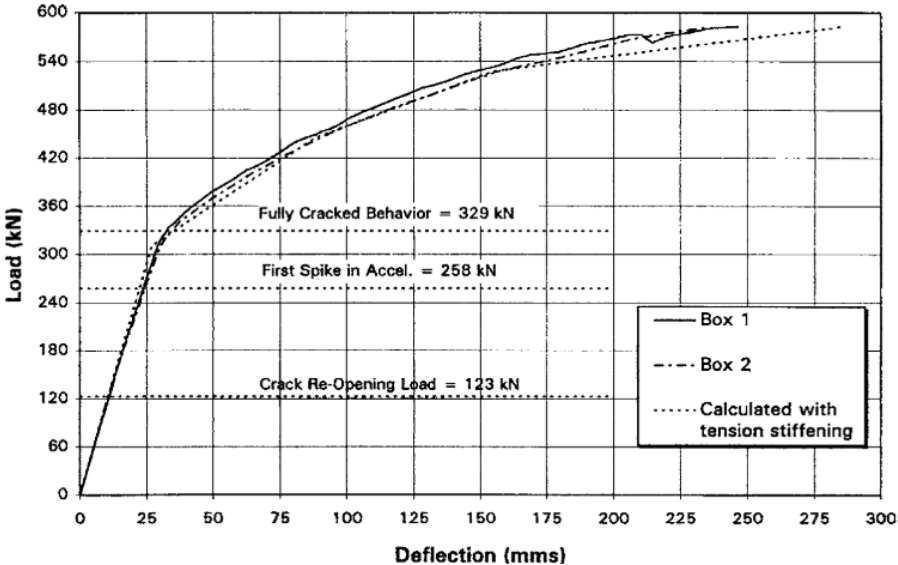
Figure 2-2: Load versus deflection: calculated and measured (Labia et al. 1997)

Pape and Melchers (2013) reported the destructive test results of three PC girders removed from a bridge exposed to an aggressive marine environment for 45 years. The bridge was the first prestressed, precast bridge in Australia constructed in 1957 (Coombs, 1957).

Among the three girders selected, two had severe deteriorations with tendon corrosion and cracking (i.e., severe for one and moderate for the other one), and the third girder was in good condition with little deterioration based on visual inspection. All these three girders were tested under a simply supported condition with two-point loading through displacement control. All tested girders failed before reaching the expected design capacity and the prestressed wires were observed to have progressive and premature failure even for the girder with least visual damage. Note that the measured capacity was lower than the ultimate capacity estimated on the basis of design specifications using actual material properties yet ignoring cracking and corrosion damage. It was claimed that significant loss of load capacity, as well as the deformation capacity, might be caused by corrosion damage (e.g., tendon loss) in PC girders in marine environments for a long time. It was also observed that as the loss of tendons due to corrosion degree increased, both ultimate load-carrying capacity and corresponding deformation capacity reduced.

Dasar et al. (2016) tested six PC beams (i.e., four post-tension and two pre-tension), to study the influence of cracks on prestress loss and load bearing capacity after 20 years' exposure in marine environment. Visual inspection of the cracking traces showed that cracking occurred due to internal pressure resulted from corrosion of tendon, in spite of the fact that the tendon was covered by grouted mortar and sheet. The prestress loss was evaluated using the crack re-opening method during the bending test and determined by comparing the initial prestressing force with the effective prestress back calculated from the test. It was found that the prestress loss increased due to pre-cracked for post-tension beams and pre-tension beams about 26% and 30%, respectively. In addition, the reduction of flexural moment capacity due to pre-cracking was about 5.58% and 4.44% for post-tension beams and pre-tension beams, respectively.

Pettigrew et al. (2016) conducted cracking tests and flexural tests on three 48-year old pre-stressed bridge girders made with lightweight concrete to determine the effective pre-stress loss and the flexural capacity. The in-site inspection of the girders showed that a few rebars were exposed at some locations on bridge deck surface but no deterioration was observed for the webs. In the cracking tests, all the girders were simply supported with a 14.94 m

long span under two-point loading applied in the middle (see Figure 2-3). The applied loads increased monotonically until visible cracks formed on the bottom of the girder in the constant moment region; then the cracks were recorded under some reloading and unloading without making any permanent damage to the girders to determine effective pre-stress loss. After the cracking test, using the same test setup, the load was reapplied and monotonically increased until the girder failed in flexure. Additionally, material tests were conducted, including 5 concrete samples, 15 pre-stressing strands and a mild steel bar. The effective pre-stressing force for girders was determined using decompression loads recorded from cracking tests, and the average loss was 32.1% for the bridge girders after 48 years' service. This prestress loss was found to be (17.6%) higher than the one estimated based on the refined method from AASHTO LRFD Bridge Design Specifications (AASHTO 2012). Similarly, it was found that the methods in AASHTO LRFD specifications (AASHTO 2012) overestimated the flexural capacities of the girders by an average of 34% compared with the test results.
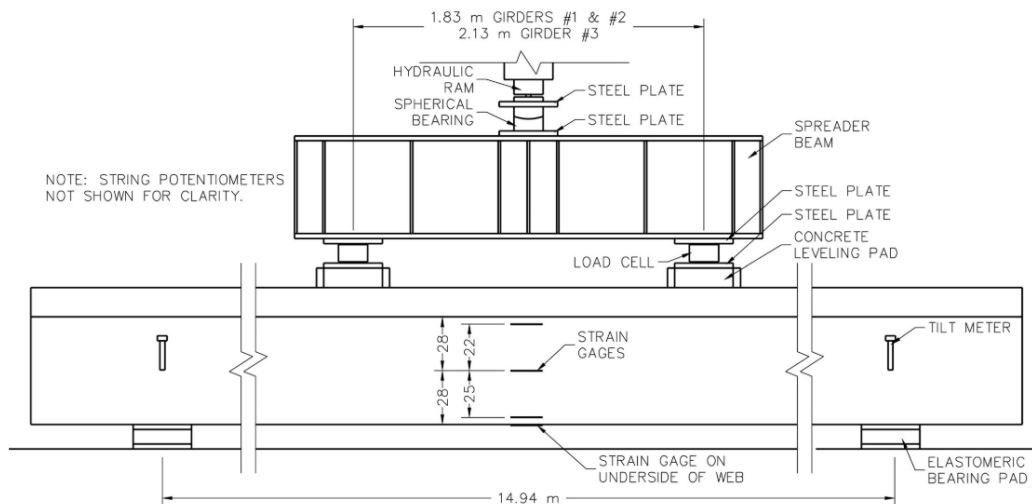
Figure 2-3 Cracking and flexural tests setup (Pettigrew et al. 2016)

As revealed from these inspections and tests of aged PC girders from real-world bridges, some girders could still perform very well after long time service even though with some deteriorations (Shenoy and Frantz 1991). However, most of tested PC girders had a loss of load-carrying capacity and corresponding deformation capacity due to corrosion (Pape and

Melchers 2013, Dasar et al. 2016, Pettigrew et al. 2016). It was also found that corrosion can reduce the concrete ultimate strain and prestressing force, leading to a sudden failure of a flexural girder (Labia et al. 1997). In addition, a number of researchers compared the tested girder capacities and prestress loss, as two of the most concerned factors, with those estimated using different codes and calculation methods. It can be observed that flexural behaviour of some lightly deteriorated PC girders was predicted relatively well by ACI code (1989) (Shenoy and Frantz 1991, Labia et al. 1997), compared with other codes. But the code provisions failed to incorporate detailed deteriorations and thus was not capable of predicting the general behaviour under various deterioration levels. In contrast, prestress loss was usually underestimated by different methods in different codes (Labia et al. 1997, Pettigrew et al. 2016).

2.2.2.2   *Shear Behaviours*

Cullington and Raggett (1991) conducted shear tests on a number of pre-tensioned I-beams without links removed from a 30-year-old bridge during demolition to identify the load at cracking, failure mode, and the strength of the girders without shear links. Through the inspection, the bridge was generally in good condition with no obvious sign of deterioration, and chloride penetration and carbonation were both determined to have little effect on the bridge deck. In the test, each girder was simply supported with a single point displacement-controlled load applied. The test results were compared with the calculation results in BS5400 standards (1990) and it was shown that strengths and behaviours calculated in BS5400 standards were relatively conservative. For regions cracked in flexure, instead of failure with flexural-shear cracking that was assumed to govern in the calculation, I-beams without shear reinforcement were found to likely fail by web cracking. As a result, the authors stated that it should be cautious when evaluating I-beams without shear reinforcement but having cracks in the webs.

Osborn et al. (2012) tested seven 42-year-old PC bridge girders to determine the remaining effective prestress force and ultimate shear capacity. Girders #1 to #6 were all 7.1 m long and had an I-shaped cross section, salvaged from a bridge in Utah, US, and Girder #7 was 10.5 m long from another bridge which had similar conditions with the other girders.

Cracking moment test was performed on Girders #1 to #5, which were simply supported with a span of 6.8 m and a single point loading applied at midspan. The load applied was increased monotonically and held constant when the cracks were visually observed, then the cracks were traced; once the load was removed, the cracks were closed by prestress force. This allowed to determine the prestress losses experimentally, which were compared with estimated values based on the procedures (i.e., approximate method and refined method) recommended in the AASHTO LRFD specifications (2009). Although both methods overestimated the residual prestress loss, refined method provided better prediction than approximate ones, which were 10% and 15% larger than measured values, respectively.

Ultimate shear tests were conducted on Girders #6 and #7 to quantify their shear capacity, which were then compared with the calculated values on the basis of simplified and nominal shear design procedures in the AASHTO LRFD specifications (2009) and strut-and-tie methods, respectively. The girders were simply supported with a single point load applied near the D-region (shear span over depth ratio = 1:5), and the load was increased until girder failure. The test results showed that the simplified and nominal shear design procedures in the AASHTO LRFD specifications (2009) provided very conservative predictions, i.e., the calculated shear capacities were between 28% and 55% of the measured values. In contrast, strut-and-tie models predicted the shear capacities within an error of 2% and 22% compared with the tested values. This could be because of better applicability of strut-and-tie methodology for D-region shear calculations compared to the AASHTO procedures.

Floyd et al. (2016) inspected and tested two 47-year-old PC girders taken from a bridge in Oklahoma. In addition to a series of non-destructive tests to evaluate the applicability of different NDT methods for detecting damage in PC bridges and assessing material properties, shear tests were conducted. The tested girders were representative ones from the bridge with cross sections shown in Figure 2-4: Girder A, 9.8 m (32 ft) long with six straight prestressed strands and four harped strands, and Girder C, 14 m (46 ft) long with

ten straight strands and six harped strands. During the tests, both ends of each of the two girders were simply supported and loaded at a single point under a load-controlled protocol.
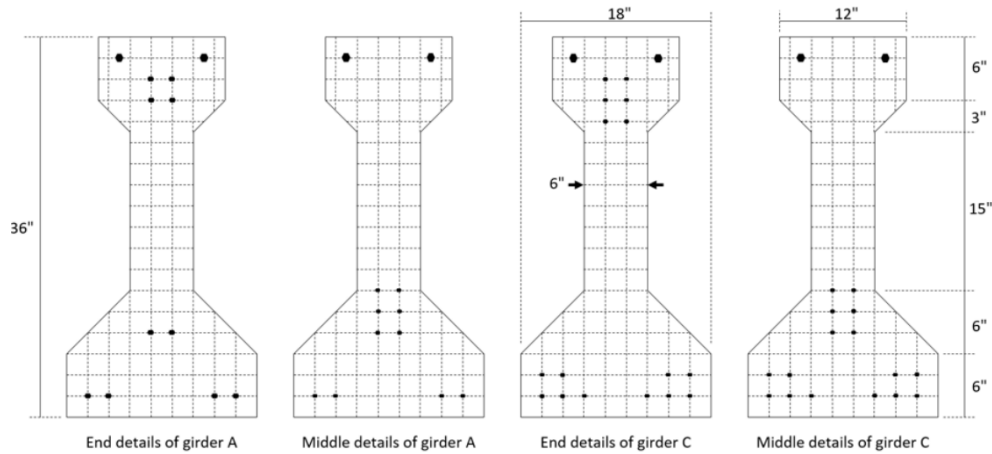
Figure 2-4: Cross-sections of two types of girders (Floyd et al. 2016)

The comparison between tests and predictions showed that the AASHTO simplified method over predicted the shear capacity of tested girders, and the Modified Compression Field Theory (MCFT) methods in AASHTO LRFD (2004) was more accurate. This research also pointed out that due to the difficulty in accounting for the creep effects, camber measurement was not an effective method to identify effective prestress; in contrast, cracking moment test was found to be a better method if the cracks occurred mainly due to flexure. For the tests focused on the effects of deteriorations caused by corrosion, it was claimed that corrosion at the ends of a girder could caused issues in structural behaviour, especially at high load levels. For example, spalling was usually initiated by the cracking due to corrosion at the ends, resulting in bond loss that can affect structural behaviour of the girder, which was common deterioration of simply supported precast concrete girder bridges.

More recently, Murray et al. (2017) conducted non-destructive and destructive shear tests on two 45-year-old AASHTO Type II bridge girders to assess their shear strength and failure mode. The two girders selected, which had mild to moderate corrosion damage at the ends, were taken from separate spans, having different representative configurations of reinforcement used for the AASHTO Type II girders. The first girder (girder I244A) was

9.1 m (30 ft) long was prestressed with 10 strands and the second one (girder I244C) was 14 m (46 ft) with sixteen prestressed strands, as shown in Figure 2-5. Before destructive tests, non-destructive tests were performed on I244A to evaluate the residual stiffness by recording the deflection and tensile strain due to bending under varying location of point loads.

After that, destructive shear test was conducted once on each end of both girders respectively with different shear to depth ratios. All the tests were performed under a single point load and the girders were tested to failure in a load-controlled manner. It was found that the two girders performed well in general after 45 years' service and they failed after significant deflection with both shear and flexural cracking. Different levels of corrosion at the ends of girders did not affect the shear strength much; however, corrosion at the ends was believed to cause strand slip, which was observed in two of the tests, resulting in flexure-shear failures yet did not lead to sudden failures. The measured capacities of the girders were compared with the shear capacities calculated using the equations in various design specifications. It was claimed that the shear capacities were higher than the predicted values using MCFT shear method from AASHTO LRFD specifications (2015). More accurate predictions were provided by ACI 318 (2014) shear method and the simplified method in AASHTO LRFD specifications (2015), although their calculated values were slightly greater than the measured capacities, which were 97% and 80% of calculated values, respectively.
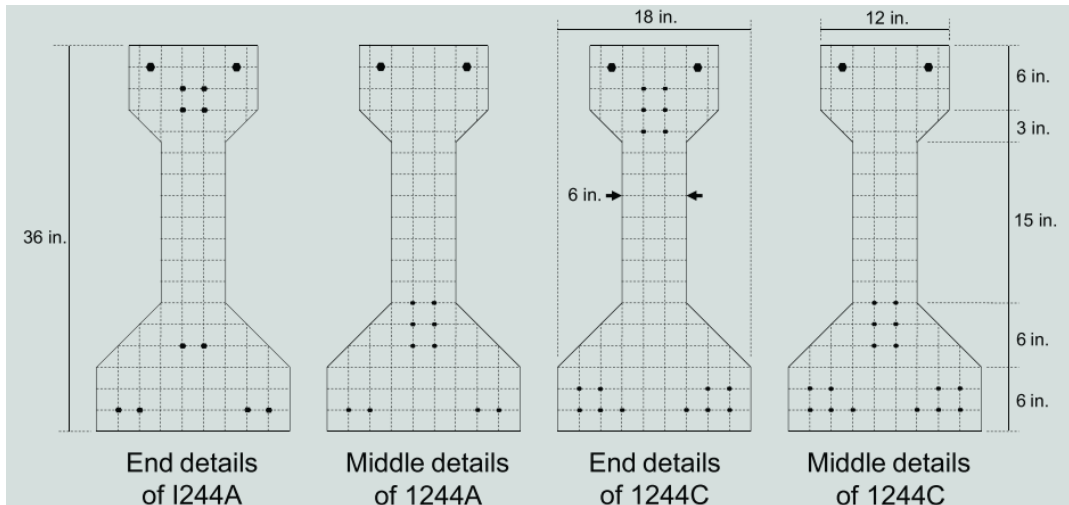
Figure 2-5: Section details of I244A and I244C (Murray et al. 2017)

There are limited studies focusing on shear behaviour of PC girders compared to flexural behaviour. Shear capacities of deteriorated PC girders were overestimated by most of methods in different codes according to some tests (Cullington and Raggett 1991, Osborn et al. 2012, Floyd et al. 2016, Murray et al. 2017). Among all the methods studied, ACI shear method and MCFT methods in AASHTO LRFD (2004) were mentioned to be able to calculate the shear capacity relatively accurate (Floyd et al. 2016, Murray et al. 2017). It was believed that corrosion at the ends can cause bond loss that may affect structural behaviour of the girder (Floyd et al. 2016); however, Murray et al. (2017) reported that different levels of corrosion at the ends of girders did not affect the shear strength much from the test results. The contradictory observations regarding the effect of corrosion at the ends on the shear strengths needs further investigation.

2.2.2.3   General Tests on Aged PC Girders or Girder Components

Instead of focusing on the flexure and shear behaviour of aged PC bridge girders, a number of researchers performed inspections, experimental studies in-site such as truck test to study their general condition, material properties, and residual performance.

Tassios and Aligizaki (1990) inspected and tested a girder from a 30-year-old bridge to determine the depth of corrosion content (e.g., carbonation and chloride) and its global structural behaviour. The inspection showed the concrete was generally in good condition

19

with only slight honeycombs and poor finishing near water stains and the soffit of side beams. This was confirmed by a rebound hammer test and the concrete cores taken from the slab. In-site and laboratory tests were also carried out to measure the carbonation depth and chloride content of concrete by spraying phenolphthalein solution on concrete surface and analyzing wet chemical in concrete respectively. It was found that both carbonation depth and chloride content in concrete were far below the maximum acceptable value. However, more defects were detected in the steels. Severe corrosion was observed on some tendons in side beams with inadequate cover and located near the drainage pipes that discharged water containing de-icing salts (as shown in Figure 2-6). Nevertheless, static load tests carried out by placing heavy vehicles in the middle of the two of the spans of the bridge confirmed structural safety, and led to the conclusion that the good overall behaviour of the bridge was attributed to the good quality and condition of the concrete.
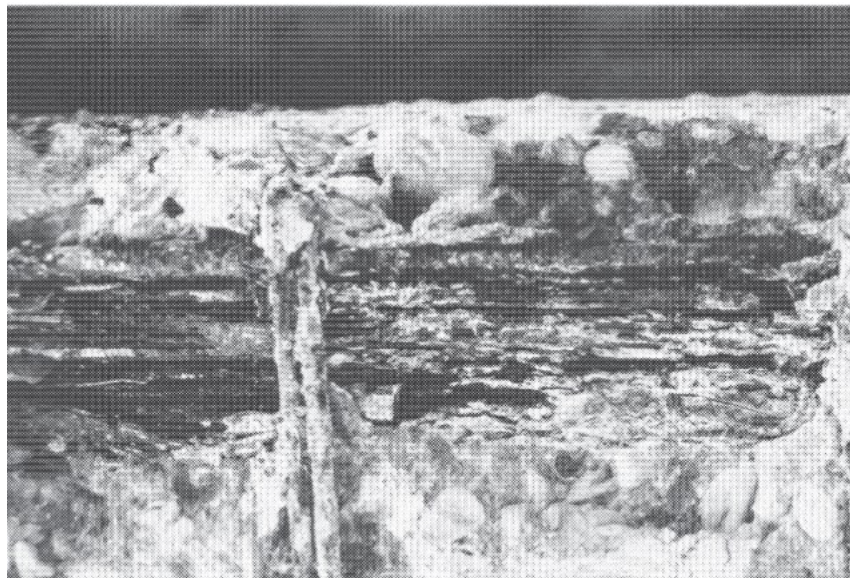
Figure 2-6: Total corrosion of tendons in the inner face of some side-beams near drain areas (Tassios and Aligizaki, 2010)

Rao and Frantz (1996) tested two 27-year-old precast PC box beams with fatigue loading after being removed from a deteriorated bridge. The beams were generally in good condition visually but had two large vertical cracks, which indicated the corrosion of the strands. The tested beams were simply supported with a span of 16.5 m (54 ft) and

subjected to periodic overloads after the pre-cracking load. One beam with precracks due to initial tests still retained excellent performance after 1,500,000 load cycles of loading, while the other beam failed due to the rupture of strand wires and the strength was reduced significantly after 145,000 cycles.

Bruce and McCarten (2006) inspected and investigated some deteriorated I-beams from bridges in New Zealand to identify the cause of deteriorations and assess the risk of prestressing steel corrosion in other similar bridges. The bridge had three spans with PC I-beams, in which some prestressing strands were corroded, causing concrete spalling along the bottom flange of the beams. In order to identify the effect of such deteriorations on similar bridges, twenty-nine prestressed I-beam bridges, constructed from the late 1950's through to the early 1970's, were assessed by a series of tests. The tested samples, whose age ranged from 35 to 48 years, consisted of 16 bridges in inland environment, 5 bridges in the coastal perimeter, and 8 bridges in the coastal frontage. It was found that the concrete had good durability performance and its compressive strength met the requirements of the specifications. The tested beams were generally constructed well; specifically, most of bridges in coastal perimeter and inland environment were generally in good condition with no obvious effect caused by reinforcement corrosion. Only one bridge in coastal perimeter spalled because of corrosion in prestressing steel and three other bridges got affected by corrosion of stirrups due to insufficient concrete cover, which in turn could affect the durability of the adjacent prestressing steels.

Lau et al. (2010) evaluated the flexural and shear behaviours of six channel PC bridge girders to study the load carrying capacities of the deteriorated girders after 40 years in service. The six girders were representatively removed from a part of Trans-Canada Highway constructed in 1965. Flexural tests were performed on three girders and shear tests were performed on the other three girders. Besides, compressive strengths and chloride ion contents were tested on concrete sample cored from the girders before the tests. All the girders were subjected to load ratings in accordance with the methods in Load Factor Rating (LFR), AASHTO Allowable Stress Rating (ASR), and the Load Resistance Factor Rating (LRFR).

Two of the test girders (G1 and G4) were in good condition which had no obvious cracks at the prestressed region, another two (G2 and G6) were in fair conditions which had some horizontal cracks in prestressed region but no concrete cover loss, and the last two (G3 and G5) were in poor condition, which had concrete sectional loss as well as strand deteriorations. In the test, girders were supported at the ends with a static monotonically increased single load applied in the middle of the girders in the flexural tests and at quarter point in shear tests. During all the tests, to record and inspect the cracks, the load was held at each increment. Theoretical predictions were also performed for all six beams using the equations in AASHTO-LRFD code (2009) and Moment-Curvature method.

The tests showed that all measured load-carrying capacities of the girders were greater than the calculated values using sectional analyses. The higher load-carrying capacities was considered as the attribution of the plastic deformation prior to the collapse of the girders created by adjacent sections of the loaded section, which is not uncommon to monotonic single point loading. Regarding the load rating, when ratings under the standard AASHTO vehicles, all the girders failed both ASR and the LRFR service limit. LRFR method was recommended to girder load ratings according to the analysis of different methods and the comparison with the test results.

Setty (2012) tested a 43-year-old prestressed concrete box girder bridge in Ohio after failing a visual inspection. Truck load testing was also conducted, after which, the spans were tested to failure with various degrees of controlled damage to investigate the capacities and the corresponding experimental load rating of the spans. The measured response in truck test indicates that truck moving at a slow speed will generate more variation in dynamic deflection. However, the maximum dynamic deflection remained the same. Load rating using the experimentally determined ultimate capacity proved that rating factors calculated using span rating are still conservative. Due to the differences in Load Resistance Factor Rating (LRFR) and Load Factor Rating (LFR) methodology, LRFR resulted in rating factors were less than those calculated using LFR.

Kramer et al. (2018) studied the condition of a PC bridge that suffered from many damages after 54 years of service, to provide a reference for other similar bridges in terms of general condition, structural behaviour, and material quality. The bridge was in South Africa with four simply-supported spans, and was demolished due to repetitive vehicular impacts as a result of insufficient vertical and horizontal clearances. After visual inspection, durability tests and carbonation infiltration tests showed that the bridge was still in fairly good condition, and no corrosion in steel reinforcement was detected. The prestressed wires, ducts and blocks were also in fairy good condition and showed no deterioration and distress. Carbonation infiltration tests on different concrete fragments showed that intrusion of CO_2 did not reach the reinforcement steels in general, except that at the expansion joints, where CO_2 ingression depths reached about 60 mm deep. The compressive testing of concrete samples cored from the bridge showed that the strengths, from both the superstructure and substructure, were above the designed compressive strengths of concrete cubes: 50% to 80% higher for the superstructure concrete, and 104% to 200% higher for the substructure concrete. In general, the assessment indicated that the workmanship and material quality of tested bridge had a fairly good durability.

The majority of existing studies focusing on general behaviours of bridges found that they performed well in a series of tests of girders in good conditions. Such good performance was attributed to the good quality condition of the concrete and good construction (Tassios and Aligizaki 1990, Rao and Frantz 1996, Bruce and McCarten 2006, Kramer et al. 2018). However, from the inspection of aged PC girders, cracking, concrete spalling, corrosion in prestressing steels and stirrups were very common deterioration features that could affect the structural behaviour of PC girders under aggressive environmental conditions. Their effects on PC girders with various levels of deterioration need to be examined comprehensively.

2.3 Experimental Studies of Naturally Corroded RC/PC Beams

Due to practical limitations of using real-world PC bridge girders, considerable research has studied experimentally the effect of corrosion on structural behaviours of RC and PC beams in the laboratory condition. There are very limited PC girders that were corroded

naturally in the lab; as a result, more studies on corroded RC beams are reviewed here due to the similarity to corroded PC beams. In order to study the naturally corroded RC/PC beams, a few researchers placed RC and PC beam specimens in corrosive environment for certain time and conducted experimental tests and relevant work were reviewed here.

2.3.1   Reinforced Concrete Beams

Castel et al. (2000a) tested four 14-year-old RC beams (i.e., two for control beams and two for corroded beams) in order to investigate the effects of corrosion-induced deterioration on the structural behaviour of RC beams at both service and ultimate limit states. The four beams were all 3,000 mm long with a 150 mm × 280 mm cross-section, two of which were placed in a confined room that sprayed salt fog from the top corner of the room for 14 years as corroded beams, denoted as B1CL and B2CL. The first corroded beam (B1CL) revealed a secondary cracking more developed in the tensile zone than in the compressive zone, while the second corroded beam (B2CL) suffered significant damage in the compressive zone and the damage in the tensile area was light. It was observed in the test that the concrete cracks due to the corrosion of compressive reinforcements had insignificantly influence on the global behaviour in service. In the service limit-state stage of beam B1CL, a 35% loss of stiffness was found, which was claimed to be caused by both steel cross-section deduction and the deterioration of bond strength in the tensile zone. For the ultimate stage of corroded beams, it was reported that only the reduction of cross-section of tensile steel affected the load-carrying capacity, since the effect of bond loss was negligible on the residual capacity.

To further understand the behaviour of corroded RC beams and the necessity of repairing, Castel et al. (2000b) studied the individual and coupled effects of the losses in bond strength and steel cross-section area behaviour. The loss of bond of steel and surrounding concrete was achieved by removing the concrete cover of the tensile reinforcements on variable lengths. The reduction in the steel cross-section due to pitting corrosion was simulated by creating local notches. It showed that a local steel cross-section reduction located between flexural transversal cracks had negligible influence on the global behaviour of the beam when the bond strength was not weakened. The global behaviour of

24

the beams was greatly affected when both loss of steel cross-section area and bond strength existed.

Dang and François (2013) investigated the structural performance of a 27-year-old corroded concrete beam through a bending test and compared that with a control beam. The corroded beam was stored in a chloride environment under sustained loading and the control beam was stored in a non-aggressive environment for 27 years to achieve natural processes without any impressed current. Each of the beam was 3,000 mm long with a 150 mm × 280 mm cross-section, tested in three-point bending. It was observed that the long-term corrosion was independent of the initial flexural cracking pattern according to the corrosion distribution in the steel re-bars. The corrosion was different from one reinforcing bar to another even though all conditions were identical and was not uniform in terms of distribution along the perimeter or the length of re-bars. The loss of steel cross-section for tensile steels of the corroded beam locally reached 50% of the initial cross-section area. It was concluded from the test that the decrease in both yielding moment and ultimate moment in the corroded beam was closely related to the reduction of steel cross-section at the failure location, and the corrosion led to a failure mode change compared to the un-corroded beam (i.e., from concrete crushing to tensile steel failure). The ultimate deflection of the corroded beam was reduced considerably (50%) in comparison with the control beam, which was because of the corrosion-induced reduction of ultimate deflection of the steel bar in tension. Similar observations were made in Zhao and François (2014). Despite the high corrosion level of the corroded beam with 26% drop in the yielding load, the ultimate capacity was still largely above the ultimate limit-state design load and the deflection at the service load was still way below the permissible value specified in the design standards.

Zhu and François (2014) tested a highly corroded beam (150 mm × 280 mm × 3000 mm) after being exposed for 26 years to a chloride environment, which was formed by the salt fog generated by four sprays located in top corner of a confined room. This study confirmed that the main influences of corrosion on mechanical characteristics included the load-bearing capacity, the stiffness, and the ductility. To be specific, the corrosion of reinforcement changed the failure mode of the beam: the control beam failed from steel

yielding followed by concrete crushing, while the corroded beam failed with less ductility as a result of the reduced ductility of corroded tension bars. The ultimate deflection capacity of the corroded beam (denoted as B2T2) decreased greatly compared to the control beam (denoted as B2CL2) (see Figure 2-7). The reduction of ultimate elongation of the steel bars in tension due to corrosion was confirmed by the tensile test performed on corroded bars extracted from the beam. Additionally, corrosion led to large corrosion cracks and spalling in concrete, which in turn reduced the bond between steel re-bars and the surrounding concrete. The bending stiffness of the beams was also reduced, but not as obvious as the loss of deformation and strength capacity. It was interesting to note that, according to the tension test on the steel re-bars, the ultimate tensile strength of the bars was found to be about 30% higher than that of the un-corroded bars. This surprising result could be due to the natural variation uncertainty of the material strength.
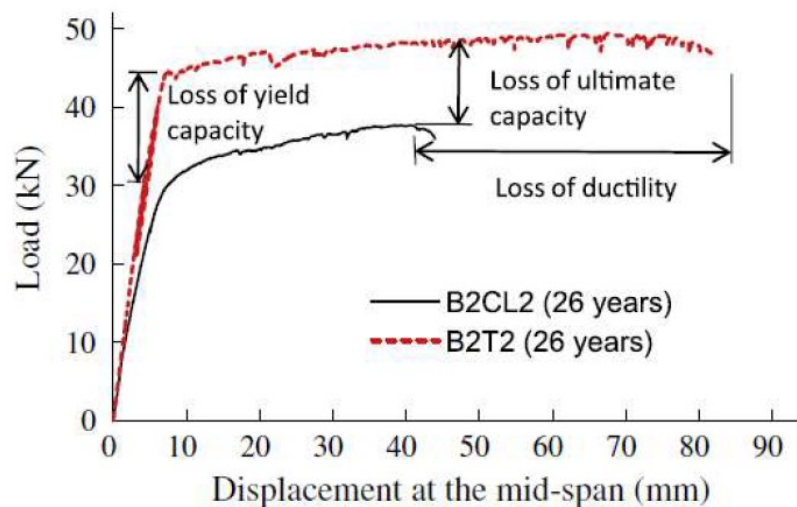
Figure 2-7: Comparison of load-displacement behaviour of corroded beam and control beam (Zhu and François 2014)

2.3.2   Pre-stressed Concrete Beams

Li and Yuan (2010) studied the deterioration of flexural property of pre-stressed concrete beams with steel strands corroded. Five pre-tensioned pre-stressed beams (250 mm × 200 mm × 2600 mm) and five post-tensioned pre-stressed beams (250 mm × 200 mm × 2000 mm) were tested in four-point bending. For each group, 4 beams were mixed with salt to be corroded for 13 months and the corrosion degree, which was defined as strands mass

loss, was range from 0.94% to 2.87%. The tests results showed that under the condition of low corrosion degree (less than 2.87%), the effects of corrosion were not remarkable on the cracking moment, the initial hardening moment, and the ultimate moment; but corrosion effects were significant on the ultimate deflection of the beam with strands rupture. The tests also showed that after the ultimate load, the beams could still sustain a relatively high level of load and develop moderate residual deformation.

As concluded from the tests of naturally corroded beams in the lab, tion, eels or even rupture on strands, which can affect the ultimate deflection of the corroded beams (Li and Yuan 2010, Dang and François 2013, Zhu and François 2014).

2.4   Experimental Investigations for Artificially Corroded RC/PC Beams

Compared to investigations on naturally corroded RC/PC beams in the lab, more studies are based on accelerated corrosion on beams to avoid the long process of natural corrosion. This also allows to focus on the interested structure behaviour since the artificial corrosion is more under control on tested specimens, such as limiting the failure mode of the beam to flexural or shear. As such, the literature is surveyed with a special attention to the flexure and shear behaviours of corroded RC/PC beams as follows.

2.4.1   Flexural Behaviour

2.4.1.1   Reinforced Concrete (RC) Beams

Mangat and Elgarf (1999) tested 111 under-reinforced concrete beams with different degrees of artificially accelerated reinforcement corrosion to study their residual capacities. The beams were 910 mm long with a 100 mm × 150 mm cross-section and reinforced with two deformed reinforcement steels with diameters of 10 mm and 8 mm. The accelerated galvanic corrosion was applied on tensile longitudinal re-bars only and tubular steel collars were used on shear zones as external reinforcement to prevent shear failure. The corrosion degree was defined by a percentage reduction to reinforcing bar's diameter, which was related to the rate of corrosion, the original reinforcing bar diameter, and the time elapsed in years after corrosion initiation. According to the test results, it was reported that the reinforcement corrosion in concrete beam had a significant effect on both flexural capacity

and deflection of beams. However, the corrosion-caused reduction in reinforcing bar area had moderate effect on the residual flexural strength of beams. The resulted reduction in residual strength was primarily due to the loss or degradation of the steel/concrete interfacial bond. In addition, failure mechanism could change to failure with horizontal splitting of concrete along the tensile steel interface and vertical tensile cracks for the corroded beam compared to the classical flexural failure for the control beam.

Malumbela et al. (2010) conducted experimental tests on corroded nine RC beams with different mass loss of deformed longitudinal tensile steel reinforcement to study its effect on the flexural capacity. The beams were 3,000 mm long with a cross-section of 153 mm × 254 mm, tested under a sustained load. The three steel bars on the tension side were artificially corroded locally in the mid-span of the within a length of 700 mm (see Figure 2-8). There was no corrosion at shear spans; as a result, flexural failure could be expected. It was observed that attributing to the location of the cracks due to corrosion, the bar in the center usually had the severest corrosion damage. In other words, the steel cross-section had a maximum loss in the center of the corrosion region and little loss at the ends of the corrosion region. The reduction of ultimate moment capacity was linear to the corrosion level and correlated best with the maximum mass loss of the steel compared to the average mass loss. In more details, there was a 0.7% reduction in the ultimate capacity of beams for every 1% maximum mass loss of steel.

Side view of beams (inverted)
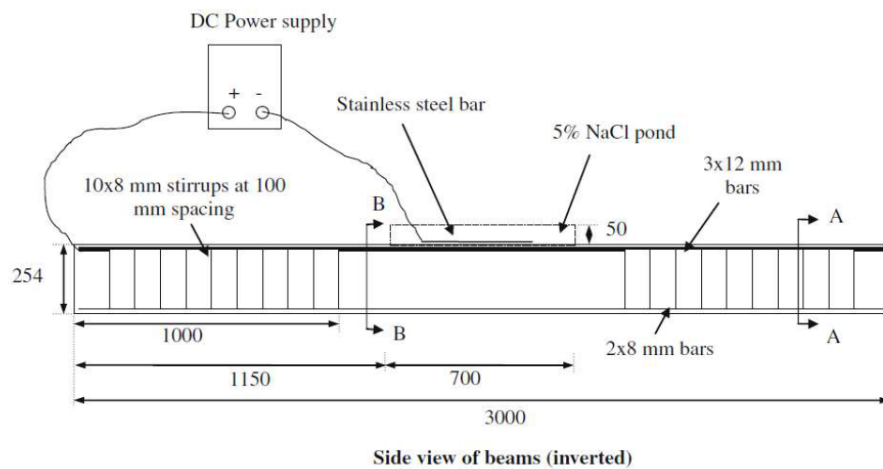
Figure 2-8: Accelerated corrosion set-up for test beams (Malumbela et al. 2010)

2.4.1.2 Pre-stressed Concrete Beams

Minh et al. (2007) carried out accelerated corrosion tests on two series of PC beams to study the chloride-induced corrosion of a sheath and a pre-stressing tendon in post-tensioned beams with different grouting conditions. Two series PC beams were tested under flexural loading: series A was to investigate the effects of grout ratios in straight sheath, and series H was to study the effect of length of grout filling in curved sheath. It was shown that corrosion-induced cracking tended to occur earlier in fully-grouted beams than in insufficiently-grouted beams. As the grout ratio inside the sheath increased, width of cracks increased and the corrosion cracks propagated earlier during the corrosion. It was also shown that the bonding between steel and concrete could be deteriorated due to corrosion of the sheath, leading to a significantly reduction on load-carrying capacity of the PC beams.

Rinaldi et al. (2010) carried out an experimental program to evaluate the effects of the corrosion on PC beams. Nine PC beams were tested under four-point bending, before which the beams were corroded artificially with different damage levels. Three beams (200 mm × 300 mm × 3000 mm) were kept in ordinary environmental conditions as control specimens, while the strands of the other six beams were artificially corroded, up to a mass loss of about 7%, 14% and 20% for each strand. The corrosion was only applied to the central zone at the bottom of the beams, to avoid corrosion-induced bond loss at the extremities of the strands because such loss might trigger a shear-type failure, which was not of interest for this research. It was shown that corrosion in pre-stressed strands strongly affected the global behaviour of simply supported PC beams subjected to bending, in term of both load-carrying capacity and failure mode. The ultimate bearing capacities of corroded beams were significantly decreased compared with un-corroded beams. In addition, the failure of corroded PC beams with mild and severe corrosion levels (14% and 20%) occurred because of the local rupture of pre-stressed strands, while the failure of un-corroded reference was governed by concrete crushing.

Zhang et al. (2017a) performed an experimental program to investigate the residual flexural behaviour of bonded post-tensioned beams with different corrosion levels (i.e., maximum

strand area loss from 0 to 84.7%). Eight post-tensioned concrete beams with the same dimension of 150 mm × 220 mm × 2000 mm were manufactured and tested in four-point bending, in which one control beam was in normal environment and seven PC beams were subjected to accelerated corrosion in lab condition to different corrosion levels. A special corrosion tank was designed and installed along the beam to prevent the submergence of strand ends in the saline solution. The tests showed that the degradation of cracking load and the loss of pre-stressing force had almost a linear relationship with increasing strand corrosion levels. As shown in Figure 2-9, the ultimate bearing capacity and post-cracking stiffness of beams were decreased significantly with the increase of strand corrosion levels. In addition, the failure modes of PC beams changed from concrete crushing to strand rupture with the increase of corrosion loss and the rupture of the strands degraded the ductility significantly.
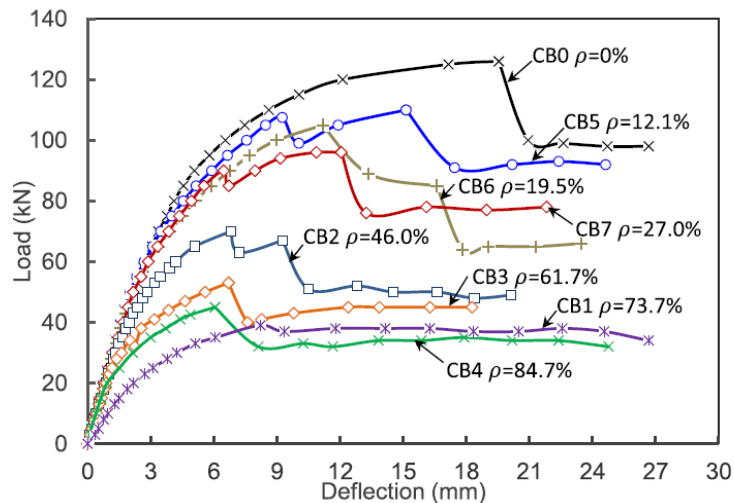
Figure 2-9 Load-displacement curves (Zhang et al. 2017a)

Zhang et al. (2017b) conducted tests on corroded strands for constitutive law development and flexural tests on locally ungrouted post-tensioned beams after strand corrosion behaviour. In the test, the specimens were exposed in an artificial salt fog to accelerate corrosion and the corrosion level was represented by the maximum area loss of the strand. The results showed that strand corrosion loss had small effects on the yield strength and elastic modulus, but decreased significantly the ductility. Especially when the specimens were severely corroded, the strand failed immediately after the elastic stage and the

ultimate strain was almost equal to the yield strain of un-corroded specimen. The eight PC beams in the flexural test were all of size 150 mm × 220 mm × 2000 mm under four-point bending. One beam was set as the control beam with no corrosion and seven beams were corroded by soaking the ungrouted region in a saline solution tank. It was shown that when the corrosion level was low, the beam failed with a lot of cracks; in contrast, when the corrosion was severe, the beam failure with fewer but wider cracks. In addition, severe corrosion degraded significantly the flexural capacity and the local post-cracking stiffness of beams as shown in Figure 2-10. It was also shown that the corrosion of the strands changed the failure modes of the beam from concrete crushing to wire rupture with the increase of corrosion level.

(a) (b)
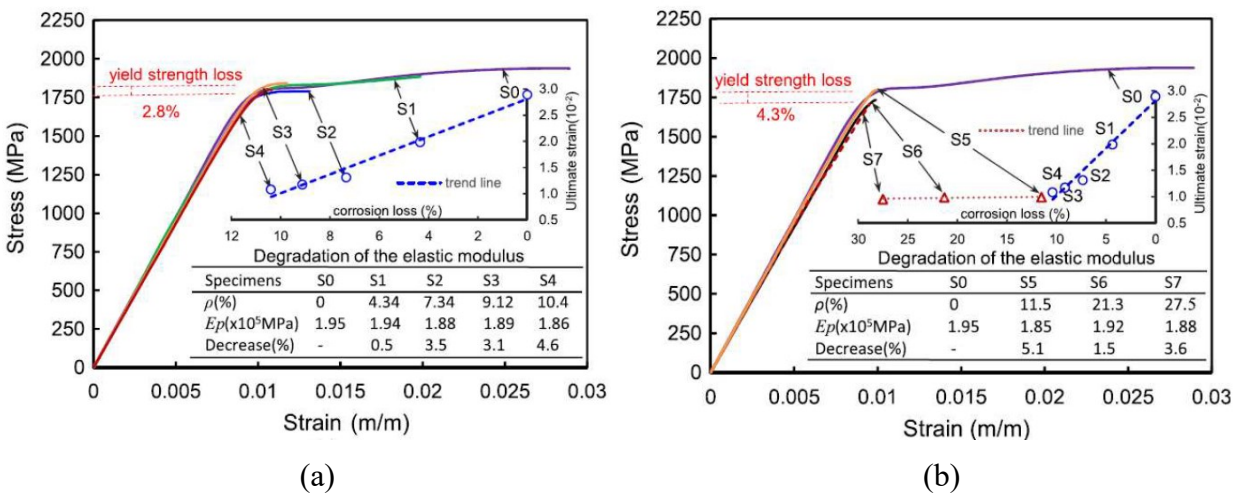
Figure 2-10: Stress-strain curves of the specimens: (a) slightly corroded strands, and (b) severely corroded strands (Zhang et al. 2017b)

2.4.2 Shear Behaviour

Xia et al. (2011) carried out an experimental program to investigate the shear capacity of RC beams with different levels of corrosion in both longitudinal reinforcement and stirrups. In this program, a total of 18 RC beams (120 mm × 230 mm × 1200 mm) were tested in three different groups, each group including 5 corroded beams and 1 un-corroded beam. The corrosion was introduced by attaching sponges soaked up in NaCl solution on the two shear zones near the beam ends, as shown in Figure 2-11. The experimental test results showed that both the average and maximum corrosion-induced cracks in concrete cover

became wider as the corrosion level of the steel reinforcement increased and the maximum crack width increased more quickly with the average crack width. According to this correlation, the crack width could be used as an indicator of the corrosion level. Both the stiffness and shear capacity of the beam decreased as the corrosion level increased. It was also found that shear failure mode of the beams may be characterized by stirrup failure instead of concrete crushing when corrosion level became severe.
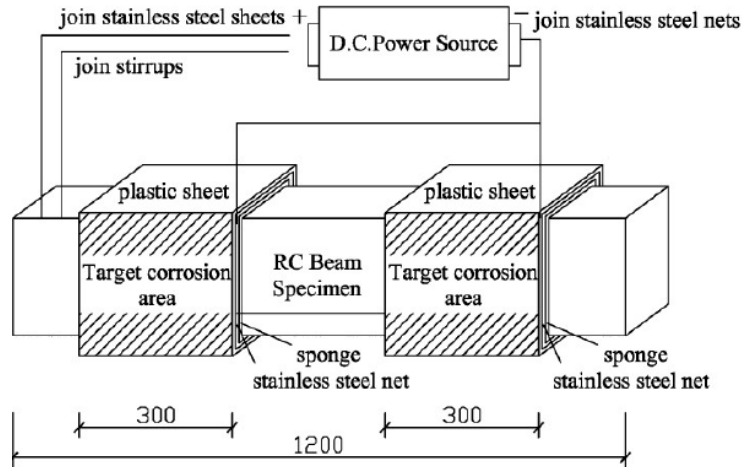
Figure 2-11: Schematic representation of accelerated corrosion test setup (Xia et al. 2011)

Kotsovos et al. (2015) studied the effect of bond loss between concrete and longitudinal reinforcement on the behaviour of RC beams. No stirrups were provided for all beams so shear failure was expected for the majority of the tested beams. Two groups of beams with different de-bonding lengths and locations were tested (6 beams with dimension of 150 mm × 270 mm × 1950 mm and 6 beams with dimension of 170 mm × 200 mm × 1950 mm), subjected to transverse loading and an axial force. The de-bonded areas were mainly located in the shear spans. It was shown that loss of bond between concrete and longitudinal reinforcement within the shear span resulted in an increase in shear capacity, which became larger as the non-bonded length increased from the point load towards the support. It was also shown that the failure mode changed from shear to flexural when the bond between concrete and steel was eliminated throughout the whole span.

Wang et al. (2020) investigated the shear behaviour of corroded post-tensioned PC beams. Two groups of beams were tested: four beams with fully grouting and four beams with insufficient grouting. For each group, three of the beams were corroded artificially. The beams were all with dimension of 160 mm × 450 mm× 3000 mm. In the test, all the beams were simply supported with a span of 2,600 mm and under two-point loading applied monotonically. The shear span to effective depth ratio was 2.1. It was found that corrosion of strands could degrade the post-cracking stiffness and the shear capacity of the fully grouted girders. The degradation of the post-cracking stiffness will become more severe if the beam was insufficiently grouted. In addition, it was observed that the failure mode did not change for fully grouted beams with corrosion loss in strands less than 31.7%, but changed from shear compression failure to rupture of strand wires for insufficiently grouted beams.

2.4.3 General Behaviour

Rodrguez et al. (1997) tested 31 beams (i.e., one specimen with dimension of 200 mm × 150 mm × 2050 mm, and 30 specimens with dimension of 200 mm × 150 mm × 2300 mm) to study the effects of steel corrosion (i.e., longitudinal bars and transverse stirrups) on the structural performance by considering different influencing variables. These variables included the corrosion level, tensile reinforcement ratios, compression reinforcement ratios, shear reinforcements, and curtailment of bars, and interaction between corrosion and loads. The corrosion was introduced by adding calcium chloride and applying a constant density up to 100 ~ 200 days. It showed that the corrosion increased the deflection and crack width at the service load, reduced the load capacity, and changed failure modes (i.e., from flexure for sound beams to shear failure for corroded beams) at the ultimate limit state.

Coronelli et al. (2009a) investigated the structural behaviour of post-tensioned beams with bonded wires and the effect of brittle failure of the wire due to stress corrosion induced cracking. Four beams of size 150 mm × 200 mm × 3000 mm were tested in the study, one of which was the control beam and the other three corroded beams were designed to simulate having the wire failure near the support, wire failure happened at higher bending moment area and have no pre-stressing wire but have same ordinary reinforcement,

respectively. Results showed that the effect of wire failure depended on the position of the break with respect to the shear and flexural load effects. When the break happened closed to the supports, the remaining wires and strands can still provide some pre-stressing force and resistance on load effects but when the wire broke at midspan, the pre-stressing force in the wire is almost lost. The consequence in terms of strength, stiffness and local damage may be rather low if the wire breaks where bending effects are limited. By contrast, if wire failure occurred in the area subjected to large bending, very significant consequences should be expected, with a sizeable reduction of both flexural stiffness and capacity. In beams with low amounts of transverse reinforcement, the breaking of the wires in the shear-span could trigger brittle shear failure.

To sum up, from almost all the experimental tests for corroded flexural and shear RC/PC girders, a reduction on load-carrying capacity and the post-cracking stiffness were observed. Specifically, it was found from the flexural tests of corroded RC and PC beams that reinforcement corrosion in PC an RC beams had a significant effect on both flexural capacity and deflection of beams (Mangat and Elgarf 1999, Zhang et al. 2017a). Malumbela et al. (2010) claimed that the reduction of flexural capacity was almost linear to the maximum mass loss of the steel. In addition, the behaviour of bond between concrete and steel was also of great importance since the loss or degradation of the bond can cause a significant reduction of the load carrying capacity (Mangat and Elgarf 1999, Minh et al. 2007). However, for shear beams, loss of bond may result in an increase of the shear capacity (Kotsovos et al. 2015). It was also commonly found that the failure mode of the corroded PC and RC beams could change from classical flexural failure to failure with splitting of concrete, or due to pre-stressed strands rupture for flexural beams (Rodrguez et al. 1997, Mangat and Elgarf 1999, Rinaldi et al. 2010, Zhang et al. 2017a, Zhang et al. 2017b). Similarly, failure mode change was also observed in shear-critical beams due to corrosion of stirrups or bond loss (Xia et al. 2011, Kotsovos et al. 2015, Wang et al. 2020).

2.5 Numerical Studies of Corroded RC/PC Beams

Compared with experiment tests, analytical approach is more economic and efficient to study the residual performance of corroded RC and PC structures. Different types of

analytical/numerical models can be used, behaviour including approximate analytical models (Jnaid and Aboutaha 2016) and various finite element (FE) models. FE method is one of the most powerful and efficient structural analysis methods that can assist the understanding of the structural behaviour and failure mechanism. FE model includes 3D continuum-based FE models combined with tri-axial material constitutive models, 2D continuum-based FE models with quadrilateral elements, and 1D models with frame elements. This section will mainly focus on the relevant research related to FE analysis of corroded RC/PC beams, with particular attention to the modelling techniques of corrosion effects.

2.5.1   3D FE Models

Jnaid and Aboutaha (2016) developed an FE model, which can consider material degradation and geometry change due to corrosion, to evaluate the residual strength of corroded RC beams. The developed FEA model was a 3D model in a commercial FE software (i.e., ANSYS 13.0) as shown in Figure 2-12. In the FE model, 3D *SOLID 65* elements behaviour were used to model concrete with tri-axial constitutive material laws; 3D *LINK 180* elements, which were uniaxial tension–compression, were used to model steel reinforcements; *COMBIN 14* spring elements, which were uniaxial elements with three degrees of freedom at each node, were used to model the de-bonding between steel and the surrounding concrete for corroded regions. Note that the reinforcing bars were assumed to be completely de-bonded in corroded regions but perfectly bonded to the surrounding concrete in the un-corroded regions. The residual cross-sectional area and yield strength of corroded reinforcing bars were defined following the method proposed by Du et al. (2005). The FE model was verified against 29 experimental results of corroded beams obtained by other researchers (Cairns and Zhao 1993, Sharaf and Soudki 2002, EI Maaddawy et al. 2005, Du et al. 2007) and relatively good agreement was found between FE predictions and experimental results.
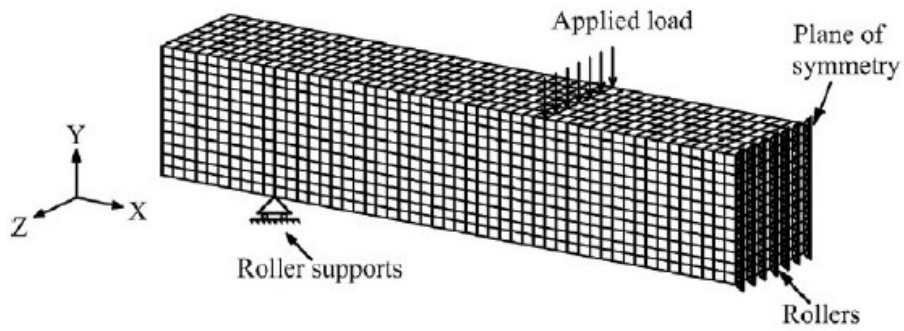
Figure 2-12: 3D finite element model for corroded RC beams (Jnaid and Aboutaha 2016)

Darmawan and Stewart (2007) developed a 3D finite element model (as shown in Figure 2-13) using a commercial FE software ABAQUS to study a typical pre-stressed concrete bridge girder located at a coastal environment. In this model, 8-node solid elements and truss elements were used for concrete and pre-stressing steels, respectively. The truss elements were perfectly embedded in concrete, assuming no bond loss in the analysis. Only geometric change of steels was considered for pitting corrosion, using the geometric model proposed by Val and Melchers (1997). Failure of a wire was assumed to occur when the tensile load at the cross-section of maximum pitting exceeded the yield capacity. Strand failure would only occur when all wires in the strand failed.
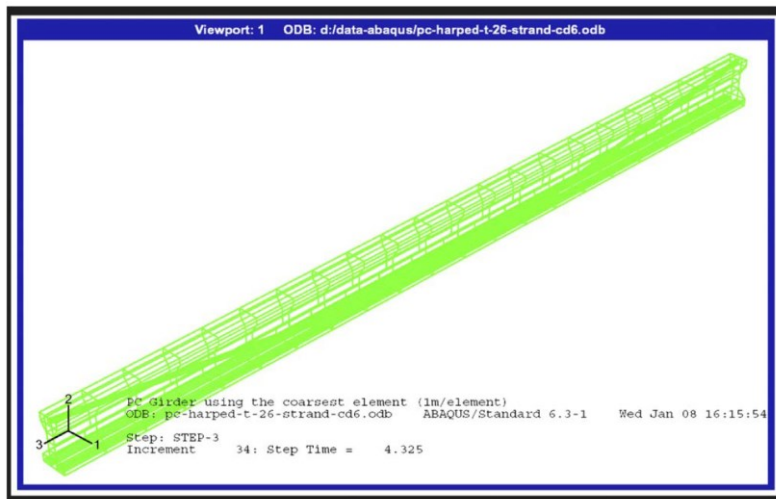
Figure 2-13: 3D finite element model (Darmawan and Stewart 2007)

Pettigrew et al. (2016) developed a 3D finite element model for deteriorated 48-year-old PC bridge girders in a commercial FE software ANSYS, as shown in Figure 2-14. In this model, *SOLID 65* and *SOLID 45* elements were used to model the concrete and bearing plates of the girders, respectively, and *LINK 8* elements were employed to explicitly model the prestressed steel. The flexural models were created using half the nominal deck thickness, a reduced value for concrete compressive strength and modulus of elasticity to take into account the deteriorations. The FE model was reported to be able to predict the flexural behaviour of the deteriorated PC girders in terms of cracking scheme, failure mode and ultimate capacity. Using the same FE software and modelling strategy, Osborn et al. (2012) simulated a series of tested shear PC girders with deteriorations and proved that this method was also capable of predicting the behaviour of deteriorated shear girders.
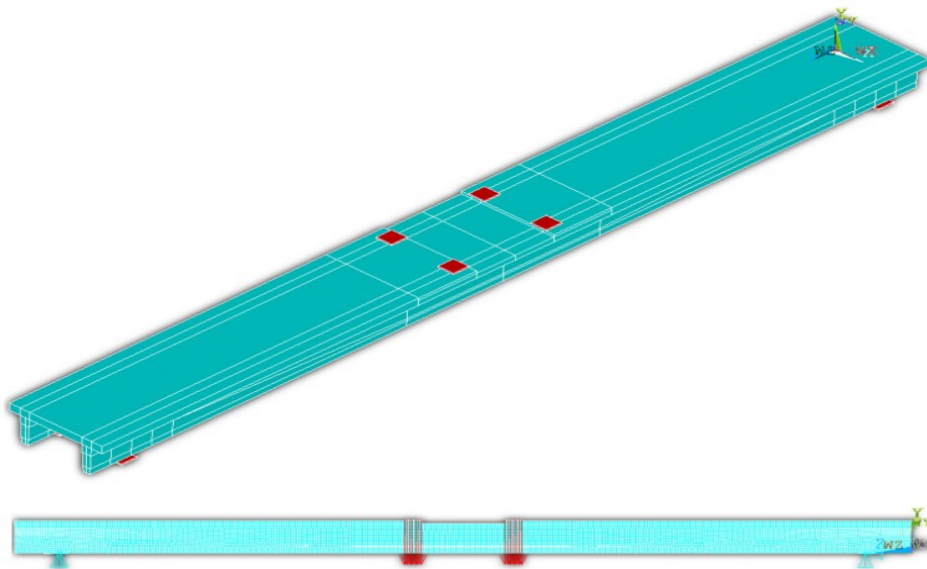
Figure 2-14: 3D finite element model in ANSYS (Pettigrew et al. 2016)

2.5.2   2D FE Models

Coronelli and Gambarova (2004) developed a 2D FE model to evaluate the structural behaviour of RC beams with corroded reinforcement. The corroded beam modelled was simply supported beam, as shown in Figure 2-15. In the model, four-node plane-stress elements with a thickness were used for concrete; two-node truss elements were used for the steel bars; bond-link elements were used to simulate the bond-slip relationship of concrete and the corresponding steel bars. The effect of corrosion was incorporated by

modifying the geometry of the steel bars and concrete, the constitutive laws of steel and concrete materials, and the bond-slip relationship of steel and concrete. Specifically, corrosion-induced cracking in concrete are described by reducing the strength of the concrete elements, and adopting a brittle post-peak behaviour. Spalling of the concrete was simulated by removal of the spalled elements. Lower ultimate strains were introduced to consider the effects of pitting corrosion on bar ductility compared to the virgin steel. The bond loss was modeled by considering a modified stress-slip relation from the one proposed by CEB-FIP Model Code 90 (1993). However, the geometry change for concrete spalling was determined empirically or vaguely in a qualitative sense. It was found from the analysis that corrosion could affect both strength and ductility of the beam and the ductility was closely related to the failure mode. Zandi Hanjari et al. (2011) presented a similar FE modelling approach using 2D FE models to analyze the mechanical behaviour of corroded RC structures. The model was used to simulate experimental tests of other researchers and it was shown that the failure mode change due to uniform and pitting corrosion of steel reinforcement could be reasonably predicted by this method.
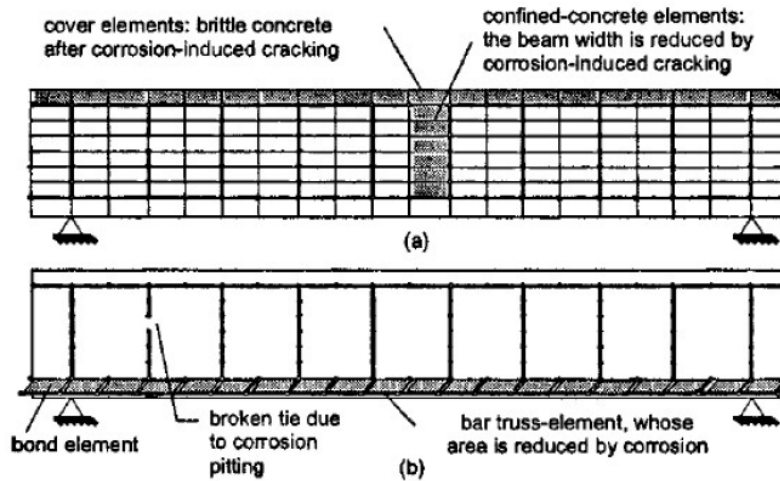
Figure 2-15: 2D finite element model for corroded RC beams (Coronelli and Gambarova 2004)

Kallias and Rafig (2010) developed a 2D nonlinear FE model in DIANA v9.1 to investigate the structural behaviour of a series of corroded RC beams. Corroded beams from two experimental studies, which tested beams with different steel ratios, were simulated using

the 2D FE model (Rodriguez et al. 1996, Du et al. 2007). In this model, concrete was modelled using four-node plane stress elements. All steel re-bars were modelled using one-dimensional truss elements associated with an elastic perfectly plastic material model. Bond between steel and the surrounding concrete was modelled using 2D interface elements without thickness. The effect of corrosion was modelled by reducing the cross-sectional area for uniformly corroded steel, linearly reducing the yield strength of steel with pitting corrosion, reducing bond strength and modifying local bond stress-slip law for bond deterioration and reducing the compressive strength for cracked concrete. It was claimed that the model was able to analyze the existing structures well.

Coronelli et al. (2009b) developed a 2D nonlinear FE model to study the corrosion effects on PC beams with bonded reinforcements (Coronelli 2008). The FE model developed was based on a nonlinear finite element model for corroded RC members (Coronelli and Gambarova 2004). Plane stress 8-node iso-parametric elements were used for the concrete. Truss elements were used for the steel, and two-node contact elements were used for the bond. To take corrosion effects into account, the same material constitutive laws were used for the concrete and the ordinary reinforcement as in the study for RC beams (Coronelli and Gambarova 2004). Additionally, the bond deterioration for both mild steels and strands were considered based on test data in the literature, and their cross-sectional area reduction was considered accordingly.

Guo et al. (2010) developed a 2D nonlinear FE model in a commercial FE software DIANA to assess the time-dependent reliability of existing pre-stressed concrete box-girder bridges. An 8-node composite degenerated shell element in the FE model was used for concrete. Mild steels were embedded in the shell elements and modelled by a reinforcement grid; pre-stressed tendons were modelled by an automatic tendon generation scheme in DIANA. Structural interface elements were used to simulate the bond-slip relationship between steel and concrete. Time-dependent corrosion was considered for both uniform corrosion under concrete carbonation by deriving the diameter of corroded reinforcements as a function of time, and pitting corrosion under chloride attack by estimating the net cross-sectional area of a corroded rebar (Stewart 2009). Yield stress reduction was also considered due to

pitting corrosion, but the ductility of corroded steels, corrosion on concrete, and loss of bond were not considered in this model.

Castel et al. (2011) developed a 2D nonlinear FE model to evaluate the structural response of deteriorated un-bonded post-tensioned beams. The model was developed based on the nonlinear FE model for corroded RC elements (Coronelli and Gambarova 2004), considering breaking of tendons, ductility-reduction for both pre-stressing and mild steel, bond deterioration for mild steel. Specifically, the reduction on ultimate strain of mild steel with pits in the re-bars were modelled using the method proposed by Castel et al. (2000b). Deteriorated bond strength was imposed in the stress-slip law of the contact elements based on the model of Lundgren (2007). For pre-stressing tendons, it was assumed that the pre-stressing loss was proportional to the cross-section loss. In the model, iso-parametric 8 node elements were used for concrete. 2 node trusses were used for the steel bars, and 4 node-contact elements were used for the interface between steel and concrete. The pre-stress of a post-tensioned beam in the FE model was simulated by applying the pre-stressing force on the concrete at the beam ends and an opposite force was imposed on the reinforcement at these locations. The model was validated by simulating the tests of three corroded beams, which were exposed in a marine environment for 40 years, with un-bonded pre-stressed strands. The simulation results agreed well with the test results.

2.5.3   1D FE Models and Analytical Models

François et al. (2006) developed a model based on 1D macro-element method to study the mechanical behaviour of corroded RC structures. Macro-elements were generated according to the cracking map of the beam after taking tension stiffening into account as shown in Figure 2-16. The average bending inertias were calculated based on the transfer length and the element length. The stiffness matrix for one macro-elements was then obtained by substituting the average bending inertias and the element length into the general beam stiffness matrix. The cross-section of the steel reinforcement was reduced in the model to consider corrosion effect; the transfer length between rebar and concrete was expressed as a function of the intensity of the re-bar corrosion to simulate the bond damage due to corrosion. Since this model was based on elastic beam stiffness matrix, it was

supposed to be applied to beams under service load. The coupling effects with shear stresses was neglected. The model was validated by simulating an experimental test on a 17-year-old beam in chloride environment under service load. Furthermore, this method relied on the prior information or assumption of the cracking pattern and thus not considered as an approach for general structural analysis.
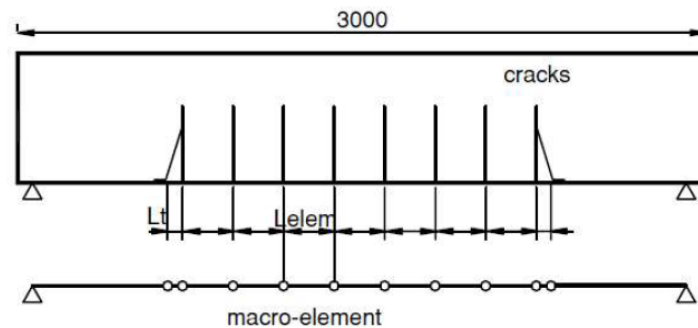
Figure 2-16: Mesh of a RC beam using macro-elements (François et al. 2006)

In addition to numerical models using an FE analysis approach, some empirical or simplified analytical models were also used in the literature to study the corroded RC and PC beams (e.g., Cavell and Waldron 2001, El Maaddawy et al 2005, Azad et al. 2007, Wang 2008, Wang et al. 2017). Wang (2008) proposed a model for the prediction of flexural capacity of the corroded RC beams. They considered the corrosion effects on the yield strength and elastic modulus of reinforcement assuming the unchanged cross-sectional area for steel re-bars. Azad et al. (2007) proposed a two-step, easy-to-apply procedure to predict the residual flexural strength of a corroded beam. They used regression analysis to calculate the flexural strength by taking into account the loss of steel due to corrosion and an applicable correction factor to account for the loss of bond. These analytical approaches are relatively simple and the applicability to general corroded beams is questionable for their over simplification.

It was found that, 2D FE model was used by the researchers more than 3D and 1D FE model. In 3D model, the modelling approach was generally consistent: concrete was usually modelled by 8-node solid elements; steel was modelled by 2-node truss elements; bonding between concrete and steel was modelled by 2-node spring elements (Darmawan

41

and Stewart 2007, Pettigrew et al. 2016, Jnaid and Aboutaha 2016). Whereas in 2D model, concrete was modelled differently by researchers, including 4-node plane stress elements, 8-node iso-parametric elements and 8-node shell elements (Coronelli and Gambarova 2004, Coronelli et al. 2009b, Kallias and Rafig 2010, Guo et al. 2010, Castel et al. 2011). Steel reinforcement and bond behaviour in 2D model were usually modelled by 2-node truss elements and dimensionless contact/link elements, respectively. Both 2D and 3D models were proved to be potentially capable of predicting the behaviour of deteriorated RC and PC girders. There are very limited numerical studies based on 1D FE model due to some limitations such as the dependency on prior information or assumptions (François et al. 2006). Deteriorations due to corrosion were simulated by reducing the cross-sectional area and yield strength for steel, reducing bond strength or modifying bond stress-slip laws to consider bond deterioration, and reducing the compressive strength for concrete.

2.6   Probabilistic Studies on Corroded PC Girders

It is well known that there exist large variabilities in the material properties for both concrete and steel in PC bridge girders, as well as in the bridge loads. By accounting for the pertinent uncertainties, significant research work has been devoted to reliability-based code calibration or performance assessment for newly designed PC bridges (e.g., Tabsh and Nowak 1992, Akgül and Frangopol 2004, Cheng 2013). Most of these works highly relied on over-simplified design equation models for the flexure or shear resistance for simplicity and computational efficiency. The model inaccuracy was either ignored or considered by using a random modelling error term, i.e., the test-to-prediction ratio, which typically required considerable experimental data to evaluate the model performance and a probability distribution fitting. An alternative to this is to use high-fidelity models, such as detailed mechanics-based FE models, for reliability assessment.

With the aging of PC girders, the reliability levels associated with a limit state (e.g., ultimate), or the general probabilistic performance, would evolve with time, especially when there is corrosion or other deteriorations. This implies a time-dependent reliability analysis is generally required for comprehensive probabilistic performance assessment. As such, several researchers have started to study the time-dependent reliability or

probabilistic performance of aged PC girders by considering the deteriorations and their associated uncertainties, in addition to the uncertainties in material properties, geometrical dimensions, and loads. A few representative studies were summarized as follows.

Darmawan and Stewart (2007) performed spatial time-dependent reliability analysis of a typical pre-tensioned PC bridge girder to study the pitting corrosion effects on the strength and serviceability. The authors developed probabilistic models for pitting corrosion and strength capacity of 7-wire strands based on the data from accelerated pitting corrosion tests for maximum pit-depth of pre-stressing wires. The probabilistic model was then combined with non-linear FE analysis, as well as probabilistic models of corrosion initiation and propagation. The uncertainties related to material properties, dimensions, loads and deterioration process, and the spatial variability of pitting corrosion of pre-stressing strands were considered. In addition, the statistical parameters for the corrosion initiation time and corrosion rate for pre-stressing strands were also obtained from Monte Carlo simulation. It was found that the spatial variability of pitting corrosion increased the probabilities exceeding both the strength and serviceability limit-states. It was claimed that the proposed probabilistic approach could provide a more realistic prediction of the actual behaviour of pre-stressed concrete bridge girders suffering corrosion attack. Later, Darmawan (2010) combined the probability analysis with a framework, which was developed for the prediction of flexural strength of corroded PC structures in a chloride environment. A wide range of statistical parameters were considered (e.g., concrete strength, steel yield strength, cover thickness, beam dimensions, in-situ strength factor, model error for flexure and corrosion rate) to determine the effect of corrosion on flexural strength of PC beam. It was indicated that parameters for pre-stressing strands, corrosion rate, yield strength of prestressing steel, model error for flexure, and cover thickness had the most significant effect on the flexural strength of PC beams.

Bin et al. (2010) studied the lifetime performance of existing PC bridges under corrosion attacks. The time-dependent reliability of flexural cracking of PC beams for the service limit state was determined through integrating first order reliability methods (FORM) and the time discretized approach. From the numerical studies, it was concluded that chloride-

induced corrosion in steel reinforcement could reduce the service limit-state reliability of PC bridges significantly.

Peng et al. (2010) also carried out a time-dependent structural reliability analysis to predict probability of damage (i.e., severe cracking) of a typical pre-tensioned PC bridge girder considering several scenarios of future atmospheric CO_2 emission. The uncertainties for material properties, concrete cover thickness, loads were considered. It was shown that for the worst scenario, the probability of corrosion initiation was 460% higher than the best scenario. In addition, the probability of failure was much higher when the deterioration was severe.

Guo et al. (2011) performed a case study of time-dependent reliability analysis for an existing PC box-girder bridge with structural deterioration due to corrosion and increasing traffic loads. The random variables considered in this analysis included material properties (e.g., concrete strength), geometrical dimensions of the girder, corrosion parameters (e.g., threshold chloride concentration, diffusion coefficient, corrosion current density and penetration ratio), and load factors (e.g., dynamic load amplification). It was shown that pitting corrosion due to chloride ingress had more effect on the decrease in the time-dependent reliability indexes compared with the uniform corrosion caused by concrete carbonation.

Aforementioned studies on time-dependent reliability analyses allowed to take into account all aleatory and epistemic uncertainties, including those related to corrosion initiation, propagation, and its effects on the mechanical and geometrical properties. Nevertheless, the uncertainties associated with corrosion highly depend on the environment and/or the stochastic model used to predict the corrosion process and corrosion-affected properties, which in turn affect the probabilistic performance assessment of corroded structures. To understand the effects of corrosion on existing PC beams more realistically, the performance assessment given a corrosion condition is desired. For example, Pandey and Nessim (1996) presented a practical Bayesian approach for updating the reliability of corroded post-tensioned pre-stressed concrete slabs and beams based on inspection data

regarding the number of broken tendons in a randomly selected sample. A systematic incremental inspection procedure was developed to assist planning cost-effective inspection and repair of existing pre-stressed concrete structures. This approach is built based on the information obtained from techniques (e.g., NDE or local destructive testing) regarding the corrosion-affected properties.

CHAPTER 3: NUMERICAL MODELING OF DETERIORATIONS FOR TESTED RC BEAMS

3.1   Introduction

Over the past few decades, considerable research has been conducted to study the effects of various deterioration features due to corrosion on concrete beams/girders. Among those studies, far more work was examining RC beams/girders compared to PC beams/girders. For example, many researchers found the slight reduction of the flexural capacity of beams with exposed reinforcement by experimental tests (e.g., Raoof and Lin 1993, 1995, 1997, Xiong et al. 2000, Sharaf and Soudki 2002, Mousa 2016). Raoof and Lin (1993) found that higher tensile reinforcement ratio could increase the strength loss due to steel exposing by testing a series of beams and this is further verified by Cairns and Zhao (1993). Additionally, it was also found that both the exposure and the un-bonding of the flexural reinforcement might increase the shear capacity of a shear-critical beam (Cairns and Zhao 1993, Cairns 1995, Kotsovos et al. 2015).

Considering their similarity and ready access of well-documented experimental tests of corroded RC beams in the literature, numerical modeling of structural deteriorations for tested RC beams with corrosion defects is first studied in this chapter before analyzing corroded PC girders in upcoming chapters.

In order to incorporate detailed deterioration features (e.g., concrete spalling, steel cross-section loss, bond loss) into finite element (FE) models of RC/PC beams, 2D continuum-based FE modeling approach is taken in this study. Specifically, VecTor2, a nonlinear analysis software for 2D RC membrane structures developed by University of Toronto (Wong et al. 2013), is used. VecTor2 is used to model two sets of tested RC beams selected from the literature, aiming at verifying its modeling and prediction capabilities for deteriorated beams.

3.2   Experiments for Numerical Validation

Since both flexural and shear behaviours could dominate the failure mechanism of deteriorated concrete beams, this study chose one set of flexure-critical RC beams and one

set of shear-critical RC beams with steel re-bar de-bonding. Note that it was important to have the specific deterioration of interest under control during tests; special experimental strategies was adopted in some studies. For example, instead of introducing real corrosion-induced deterioration, Mousa (2016) simulated the un-bonded length due to corrosion by using a plastic tube to cover the reinforcement bars in the tests. Similarly, Kotsovos et al. (2015) used polyvinyl chloride (PVC) pipes to isolate part of steel re-bars from concrete in the de-bonded regions. As such, the experimental program in these two studies were selected here to mainly study the effects of de-bonding. The other geometrical and material deteriorations in concrete and steel, which are deemed relatively easier to be incorporated, are not considered here.

3.2.1 Flexure-critical RC Beams with Un-bonded Steel Re-bars

Mousa (2016) performed an experimental study of a series of six simply supported beams to investigate the impact of bond loss on the flexural behaviour of RC beams (see Figure 3-1). All these beams had the same geometrical dimension of 2250 mm × 120 mm × 200 mm. This series of beams consisted of one beam with no stirrups (i.e., B0), one beam with stirrups and fully bonded longitudinal steel re-bars (i.e., B1), and four beams with stirrups but un-bonded longitudinal steel re-bars, as shown in Figure 3-2. Beams B0 - B5 had the same longitudinal reinforcement layout, i.e., $2\phi16$ at the bottom and $2\phi10$ at the top. Beams B1 - B5 had closed stirrups with $\phi6@150$ mm to provide sufficient shear resistance, as shown in Figure 3-2. The average yield strength of the ribbed bars at the bottom and top was 498 MPa and 427 MPa, respectively. The average yield strength of the plain round steel for stirrups was 300 MPa. The compressive strength of concrete was 67.32 MPa, and its tensile strength was 4.53 MPa. The beams were tested to failure under two force-controlled loads with an increment of 10 kN.
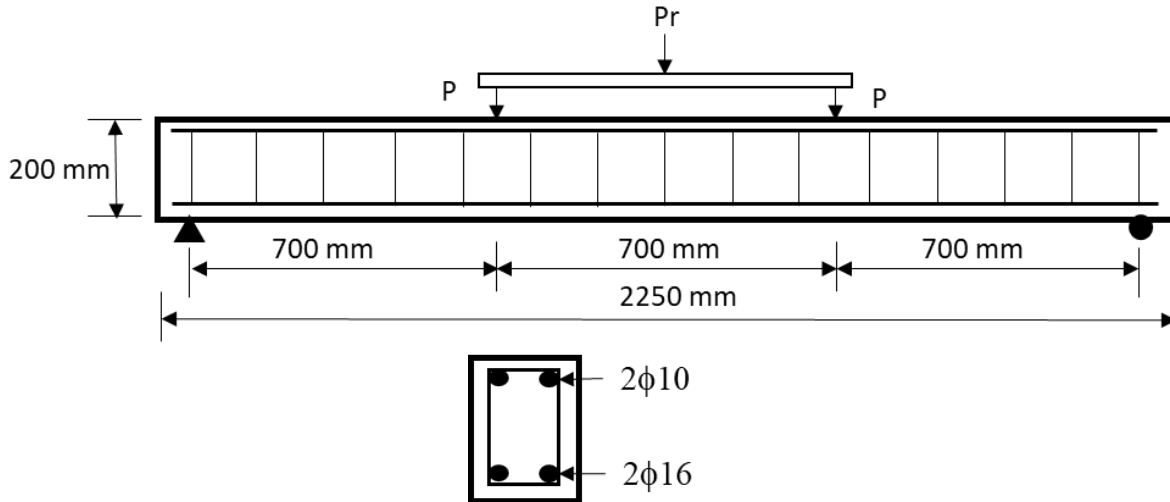
Figure 3-1: Cross-section and beam details

In the tests, the un-bonded length due to corrosion was simulated by using a plastic tube to cover the reinforcement bars. Five different bonding conditions were considered (Figure 3-2), including two control beams B0 and B1, both of which had fully bonded reinforcement at the bottom. B0 with no stirrups was used to ensure this set of beams were flexure-critical by comparing its failure mode with B1 that had stirrups. Beams B2, B3, and B4 had different lengths for the un-bonding region. Specifically, the un-bonded length increased by two stirrup-spacing (i.e., 300 mm) extending from supports to the mid-span for beams B2 to B4. Note that the un-bonding was discrete since bonding (20 mm long) was not eliminated at every intersection between stirrups and bottom steel bars. This set of beams (B0, B1, B2, B3, and B4) are modeled in this study, neglecting the bonding at the intersection points between stirrups and bottom steel bars.
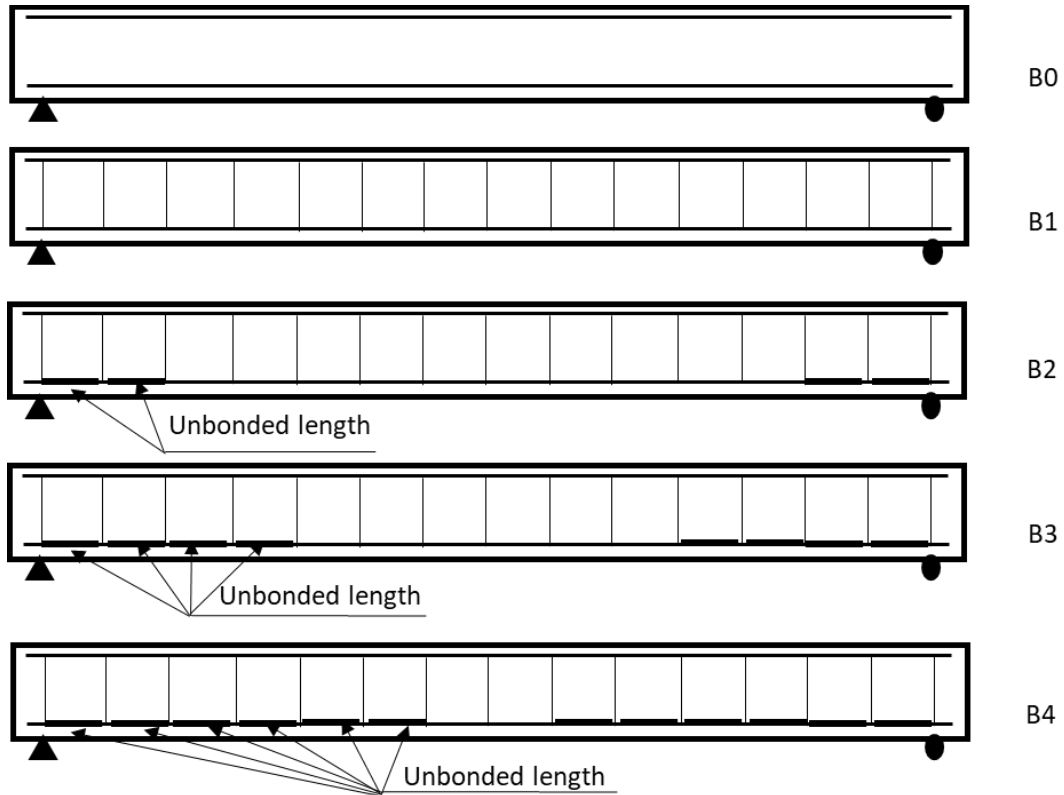
Figure 3-2: Details of the un-bonded zones

3.2.2 Shear-critical RC Beams with Un-bonded Steel Re-bars

Kotsovos et al. (2015) tested two groups of RC beams without stirrups under four-point bending to investigate the effect of un-bonded length and location on the structural behaviour. One group had a rectangular cross-section (150 mm × 300 mm), and the other had a square cross-section (200 mm × 200 mm). Each group consisted of beams subjected to a constant axial force at four different levels, i.e., 0, 50, 100 and 315 kN, respectively. In this study, the test results for beams with a rectangular cross-section and zero axial force applied are studied. All beams were 2300 mm long and simply supported with a clear span of 1950 mm during the two supports, see Figure 3-3. The RC beams were reinforced at the bottom by a layer of three deformed bars (i.e., $3\phi16$). The concrete compressive strength was 28 MPa and the yield strength of steel was 575 MPa.
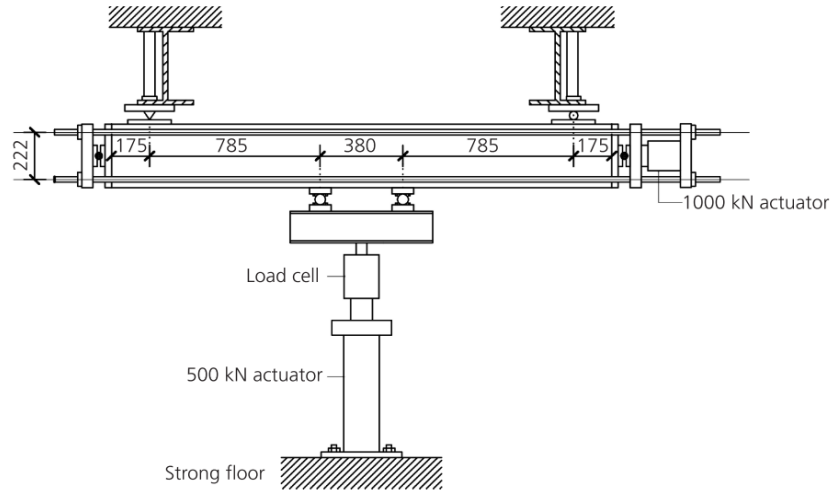
Figure 3-3: Setup for corroded RC beam tests (Kotsovos et al. 2015)

With the main objective to study the effect of de-bonding, the researchers used polyvinyl chloride (PVC) pipes to isolate part of steel bars from concrete in the de-bonded regions. As shown in Figure 3-4, different de-bonding conditions were designed with varying locations or lengths (referred to as NB0, NB1, NB2, and NB3). In order to focus on the effect of bonding loss along the beam while assuming full anchorage of the steel re-bars at the end of the beam, the steel re-bars were welded to the steel plates at the ends of the beams (Kotsovou and Mouzakis 2011, Kotsovou and Mouzakis 2012).
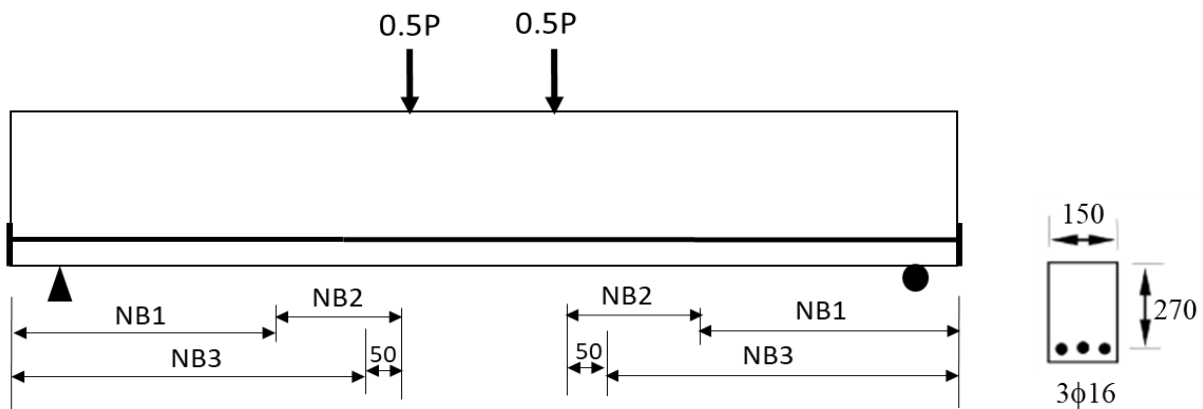
Figure 3-4: Beams with regions within which steel re-bars were un-bonded

3.3   Finite Element Modeling Scheme

The two sets of the beams considered here are both analyzed using a 2D nonlinear finite element software, VecTor2 (Wong et al. 2013). The schematic view of FE models for the

flexure-critical (B) and shear-critical (NB) series of beams considered is shown in Figure 3-5. In the FE model, concrete is modeled by plane-stress rectangular elements with a mesh size of 20 mm × 20 mm and 10 mm × 10 mm for flexural-critical and shear-critical beams, respectively. The steel stirrups in the flexure-critical beams are considered through the smeared approach (note that there were no stirrups in the shear-critical beams considered). All the longitudinal steel bars were modelled using discrete truss bar elements. Without exact stress-strain curves for the concrete and steel used in the tests, the basic (default) constitutive models were used. Specifically, the compressive behaviour of concrete material is modeled by *Hognestad* and *modified Park-Kent* model for pre- and post-peak behaviours, respectively, and tension stiffening and tension softening of concrete is modelled by *Modified Bentz 2003* and *Bilinear*, respectively. The steel material is modeled by *linear strain-hardening* model in VecTor2. The material properties of concrete and reinforcement provided in the literature are used, in addition to empirical or default values in VecTor2 for the unspecified model parameters. The material parameters used are summarized in the following Table 3-1. Note that for the tested shear-critical beams (NB beams), steel plates are modeled with extremely large stiffness at the ends of the beam to provide anchorage of the longitudinal bars.

VecTor2 is based on the Modified Compression Field Theory (MCFT), which is used to predict the load-deformation response of reinforcement concrete elements subjected to in-plane shear and normal stresses (Vecchio and Collins 1986). MCFT uses a smeared rotating approach to model cracked concrete as an orthotropic material. The relationships used in this theory, which are compatibility, equilibrium and stress-strain relationships, are based on average stresses and strains.

Following the test of the shear-critical beams, the load was applied through displacement control with a load step size of 0.5 mm (e.g., increasing the deflection at the middle span at the control node with 0.5 mm per step). Similarly, for flexural-critical beams, the load was applied through force control with an increment of 2.5 kN per load step.

Table 3-1 Material properties used in the FE models

Materials	Symbols	Parameters	Formula	Reference	B Series	NB Series
Concrete	f'_c	Compressive strength	Tested	Mousa 2016, Kotsovos et al. 2015	67.32 MPa	28 MPa
	ε_0	Strain at peak compressive stress	$1.8+0.0075 f'_c$	Wong et al. 2013	0.0023	0.00201
	E_c	Elastic modulus of concrete	$5500\sqrt{f'_c}$	Wong et al. 2013	45 GPa	29 GPa
	f_t	Tensile strength	$0.33\sqrt{f'_c}$	Wong et al. 2013	4.53 MPa	1.75 MPa
	f_u	Ultimate compressive strength	$0.2 f'_c$	Wong et al. 2013	13.46 MPa	5.6 MPa
Bottom steels (Top steels)	f_y	Yield strength	Tested	Mousa 2016, Kotsovos et al. 2015	498 (427) MPa	575 MPa
	E_s	Elastic modulus of steel	Empirical	-	200 GPa	200 GPa
	f_u	Ultimate strength	Empirical	-	600 MPa	700 MPa
	ε_y	Yield strain	f_y / E_s	Wong et al. 2013	0.00249 (0.00241)	0.00288
	E_{sh}	Strain hardening modulus	$0.01 E_s$	Wong et al. 2013	2000 MPa	2000 MPa
	d	Diameter	Tested	Mousa 2016, Kotsovos et al. 2015	16 (10) mm	16 mm
Stirrups	f_y	Yield strength	Tested	Mousa 2016	300 MPa	-
	E_s	Elastic modulus of steel	Empirical	-	200 GPa	-
	f_u	Ultimate strength	Empirical	-	500 MPa	-
	ε_y	Yield strain	f_y / E_s	Wong et al. 2013	0.0015	-
	E_{sh}	Strain hardening modulus	$0.01 E_s$	Wong et al. 2013	2000 MPa	-
	d	Diameter	Tested	Mousa 2016	6 mm	-

In order to simulate the de-bonding between steel re-bars and the surrounding concrete, *Link elements* were created to represent the bonding interface along the un-bonded length of reinforcement for all the tested beams. *Link element* in Vector2 (Ngo and Scordelis 1967) is a dimensionless element linking two nodes in the same location, e.g., one associated with the concrete element and the other associated with the steel reinforcement element. The link between the two nodes can be conceptualized as two orthogonal springs since it can displace in both the longitudinal and transverse directions of the beam. The bond type used was *un-bonded bars or tendons* in VecTor2 to simulate the complete bond loss between concrete and steel.

(a)

(b)
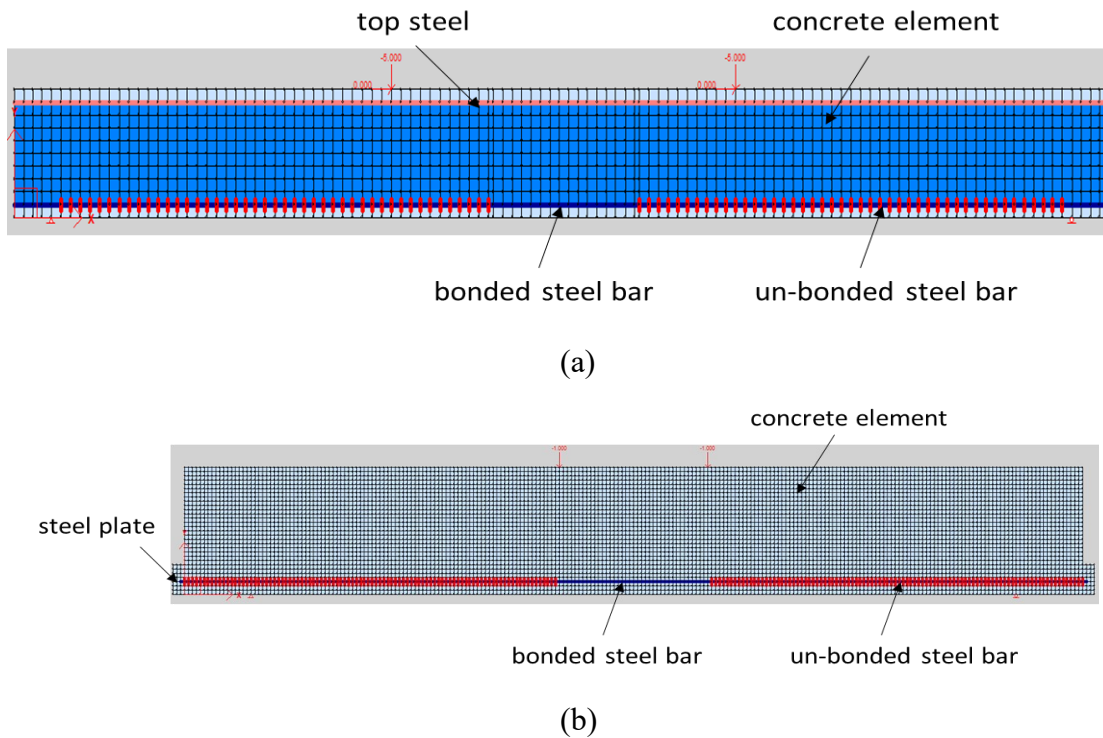
Figure 3-5: Schematic view of FE models for (a) B, and (b) NB series of beams

3.4 Simulation Results Compared with Test Results

3.4.1 Flexure-critical RC Beams with Un-bonded Steel Re-bars

Figure 3-6 and Figure 3-7 show the comparison between experimental and FE model predictions in terms of load-displacement curves and failure patterns, respectively, for flexure-critical beams (i.e., B series). For this series of tests, the load-displacement

behaviours are reasonably well captured. The capacities of the beams are slightly underestimated, which could be attributed to the non-calibrated material models used due to the lack of sufficient information on the material behaviours. Figure 3-7 shows that the failure patterns provided by FE prediction are able to capture the failure modes and crack propagations of the tested beams. The cracks usually started close to the ends of the bond loss, and then spread along the bond length of the steel. It is observed from the failure patterns that the cracks reduced in number but increased in width as the length of de-bonding increased. This is especially obvious in B4 in that only four, but fairly wide, main cracks appeared in the midspan of the beam.

Seen from the effects of the un-bonded steel re-bars in the experimental and simulated results, the models capture all the trends mentioned above fairly well qualitatively. Specifically, it is found that as the un-bonding length increased, the stiffness of the beams decreased, and the deflection of the beams increased in general. However, the capacity almost remained unchanged, with only moderate reduction when the un-bonding length was up to 70% of span for B4.

(a)　　　　　　　　　　　　　　(b)
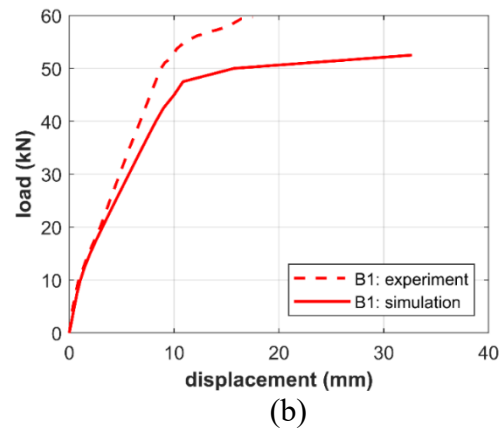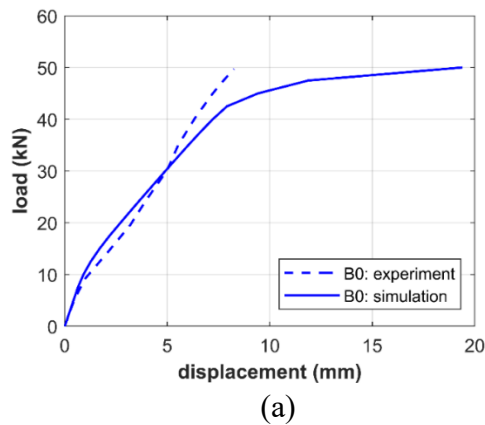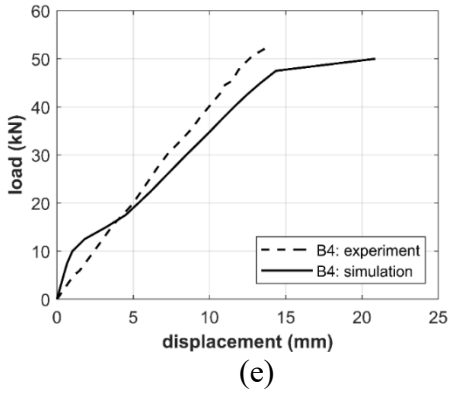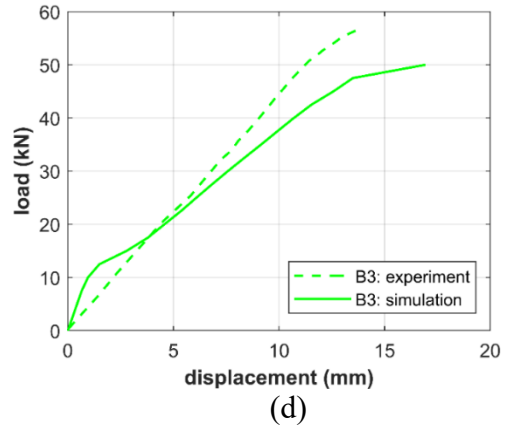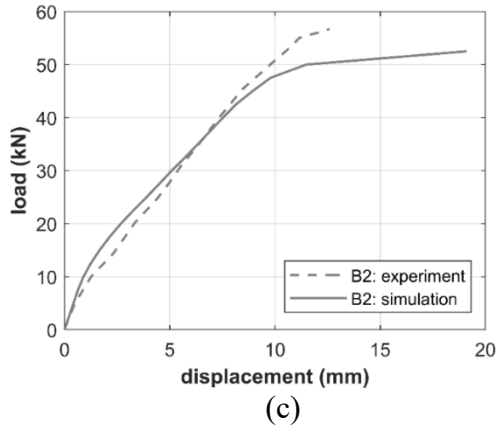
Figure 3-6: Load-displacement comparisons between experimental (Mousa 2016) and FE model predictions for B series of beams: (a) B0, (b) B1, (c) B2, (d) B3, and (e) B4

(a)

(b)

(c)

(d)

(e)
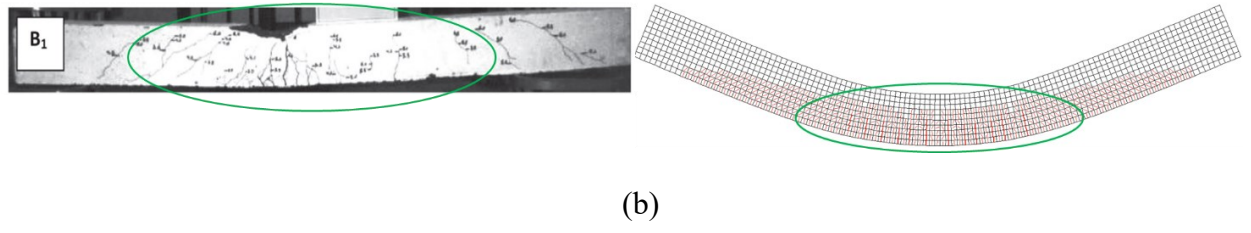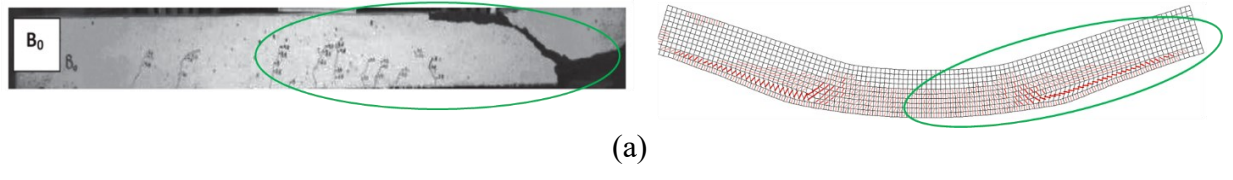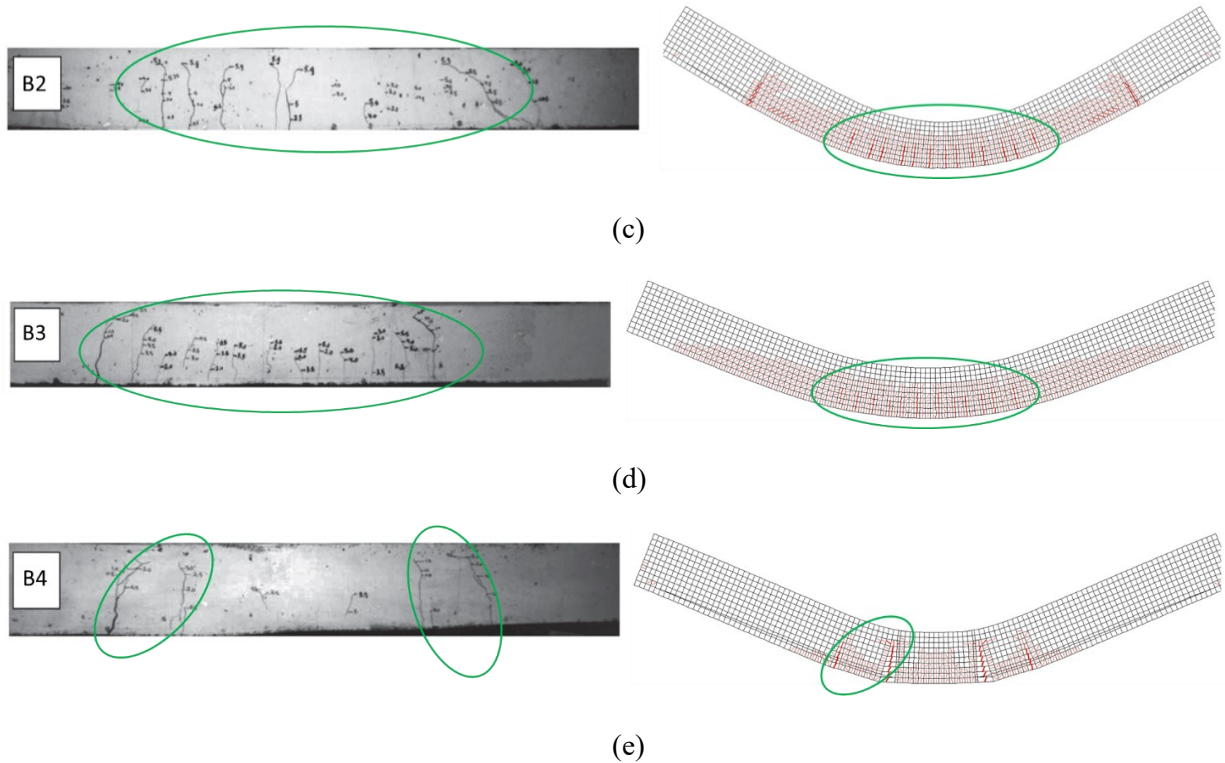
Figure 3-7: Failure pattern comparisons between experimental (Mousa 2016) and FE model predictions for B series of beams: (a) B0, (b) B1, (c) B2, (d) B3, and (e) B4

3.4.2   Shear-critical RC Beams with Un-bonded Steel Re-bars

Figure 3-8 shows the comparison of load-displacement curves of NB series of beams between experimental and FE model predictions. It shows a good correlation between the simulation and test for NB0 and NB2. The stiffness' of the beams decrease after the concrete cracking at the dividing point of bond and deboned region. Regarding the failure patterns, as shown in Figure 3-9, FE analysis results match well with test results and the simulated crack propagations agree with the tests reasonably well for NB1, NB2, and NB3.

Figure 3-10 (a) and (b) show the experimental and simulation results for the load-displacement curves of the beams, respectively to see the general trend of the effects of the un-bonded steel reinforcement. It is concluded that when the de-bonding length increases from the supports to the loading points within the shear span, the shear capacity will increase (see NB0, NB1 and NB3). This trend is captured well by the simulation results.

However, NB2, which is not de-bonded from support, had nearly no difference from NB0. To summarize, the FE model is able to capture the general trend qualitatively.
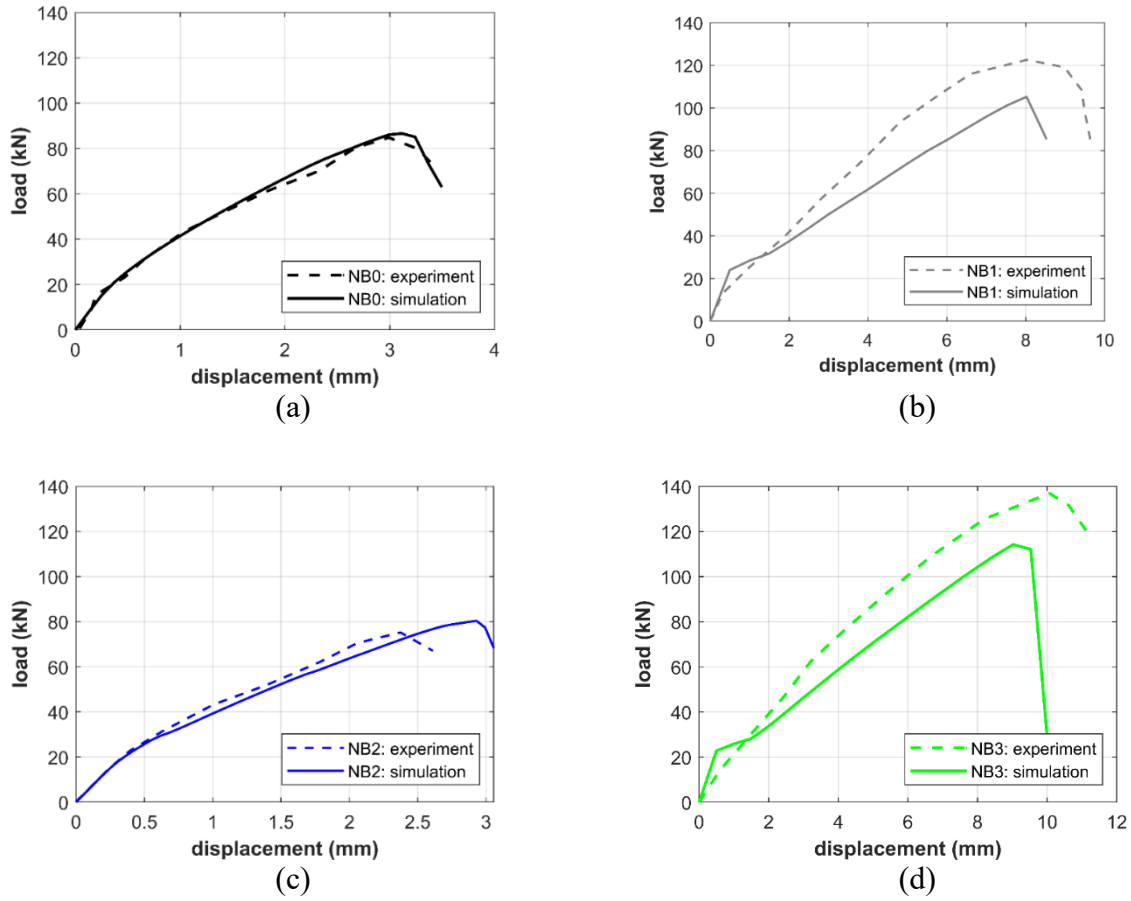
Figure 3-8: Load-displacement comparisons for NB series of beams between experimental and FE model predictions: (a) NB0, (b) NB1, (c) NB2, and (d) NB3

(c)
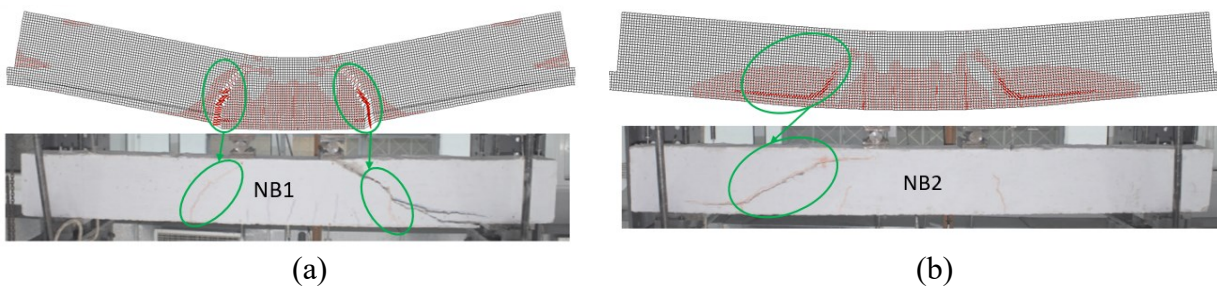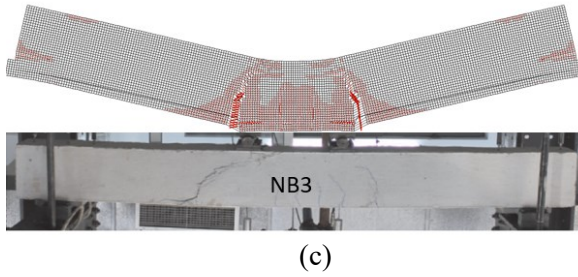
Figure 3-9: Failure pattern comparisons for NB series of beams between experimental (Kotsovos et al. 2015) and FE model predictions: (a) NB1, (b) NB2, and (c) NB3

(a)   (b)
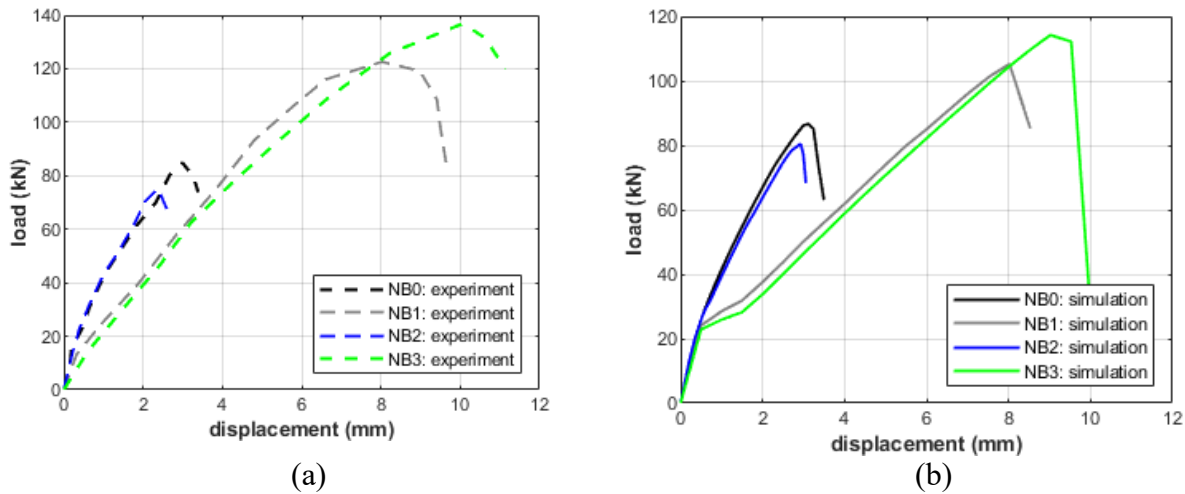
Figure 3-10: Load-displacement curves for all beams considered: (a) experimental predictions, and (b) FE model predictions

3.5   Summary and Discussion

The objective of this chapter is to evaluate the predictability of 2D FE -models developed in VecTor2 for RC beams with various deteriorations, with a focus on steel de-bonding in both flexure-critical and shear-critical beams. Two series of tested beams (i.e., one set of flexural-critical beams and one set of shear-critical beams) with de-bonded steels are selected from literature to study numerically.

It is observed that for flexural-critical beams (e.g., NB series beams considered), only moderate reduction in the capacity is observed when length of un-bonded region increases from end supports towards the mid-span, although the stiffness decreases. Meanwhile, the cracks decreased in number but increased in width with the increasing length of steel re-

bar de-bonding. However for shear-critical beams (e.g., NB series beams with no stirrups considered), as the un-bonded length increases from the supports towards the loading points within the shear span, the load carrying capacity of the beam increases and the beam can become more ductile. The 2D FE models developed is able to capture the load-displacement behaviours and failure patterns for both flexural and shear-critical beams reasonably well. To sum up, the modelling and prediction capabilities of 2D continuum-based FE model in VecTor2 is generally validated by both flexural and shear-critical deteriorated beams.

CHAPTER 4: INVESTIGATION OF CORRODED PC BRIDGE GIRDERS: FLEXURE

4.1 Introduction

Pre-stressed concrete (PC) highway bridges represent an integral part of the transportation network in Canada. Their functionality and safety has been playing a significant role towards the socio-economic development. However, the degraded structural performance of highway bridges due to aging is a common threat to the transportation infrastructure in the cold climate of North America.

To study structural deteriorations for PC girders (or beams) due to aging effect such as corrosion, considerable experimental (i.e., non-destructive and destructive) and/or analytical studies exist with different focuses and limitations in the literature. Destructive testing is more informative with detailed quantification of the structural performance and numerical analysis of PC girders corroded in laboratory conditions or natural environment. Compared with artificially corroded beam/girders (e.g., Zhang et al. 2017a, Zhang et al. 2017b, Rinaldi et al. 2010, Li et al. 2010), PC girders salvaged from the real-world bridges can more realistically represent the structural deterioration. As surveyed from the public literature, a limited number of aged PC girders (ranging from 27 to 48 years old) from real-world bridges were tested. Among these work, the degraded flexure and/or shear performance were of great concern. Examples are flexural tests (e.g., Shenoy and Frantz 1991, Labia et al. 1997, Pape and Melchers 2013, Dasar et al. 2016, Pettigrew et al. 2016), shear tests (e.g., Cullington and Raggett 1991, Osborn et al. 2012, Murray et al. 2017), and other tests focusing on both flexure and shear (e.g., Lau et al. 2010). It was found that the common aging effects (e.g., corrosion and pre-stress loss) led to the premature failure of the girders with reduction in both load bearing and deformation capacities. Note that in addition to corrosion of steel reinforcements, the pre-stress loss in strands, which can be 20% - 40% for PC girders of 40 years-old or so (e.g., Halsey and Miller 1996, Czaderski and Motavalli 2006), also contributes to the performance degradation.

The recent removal of a highway bridge (1990 - 2017) near Barrhead in central Alberta offered a great opportunity to investigate the behaviour of aged PC girders experimentally

and analytically. Numerical studies of the PC girders are conducted as complementary to experimental study. In this chapter, pre-test simulation was performed using different modeling approaches before the test of a visually intact bridge girder. After the flexural tests and the material coupon tests, based on updated material model and steel arrangement information, a two-dimensional (2D) FE model is developed and the simulation results are compared with the experimental test results. Parametric study with a full range of deterioration types (i.e. steel area loss, concrete spalling, concrete material deterioration, de-bonding, pre-stress loss, and intermediate bond loss) and corrosion degrees is then implemented based on the 2D FE model in order to study the effects of corrosion and pre-stress loss. The effects of different deteriorations on PC girders learned from the parametric study can help to identify the possible causes for the performance degradation of other interior PC girders with severe deteriorations salvaged from the same bridge. Additionally, the insights into the structural behaviour of aged PC girders with various defects are potentially beneficial for bridge inspectors and evaluators, in that the parametric study can shed lights on the behaviour of similar aged PC girders.

4.2   Pre-test Simulation

4.2.1   General Information

Nine girders were salvaged from an abandoned bridge (1990 - 2017) near Barrhead in central Alberta (see Figure 4-1 a). Four out of seven interior girders were tested to failure in the I. F. Morrison Structures Laboratory at University of Alberta to study their residual performance. The interior bridge girders are of type SM-510, 11 m long with a solid cross-section at both ends as the rigid-end diagrams and a three-cell hollow cross-section in the middle as shown in Figure 4-1 (b). The three-cell hollow cross-section is 1206 mm in width and 510 mm in depth, and each of the three voids is circular with a diameter of 300 mm as provided in blueprint. The concrete, made of lightweight coarse aggregate and sand fines, is semi-light weight with a mass density of 1920 kg/m^3, and the specified (nominal) concrete compressive strength is 35 MPa according to the drawings. There are 20 pre-stressed seven-wire low-relaxation strands and 7 M10 steel re-bars (i.e., 5 G1012 and 2 G1013) of Grade 400 as shown in the cross-section in Figure 4-1 (b). The diameter of the

7-wire strands is 12.7 mm with a nominal area of 98.7 mm^2 and the ultimate tensile strength is 1860 MPa. The initial pre-tensioning force and the design pre-tensioning load after loss are 129 kN and 107 kN per strand, respectively. The transverse reinforcement of Grade 400 consists of three series of stirrups, i.e., U-type G1001 at the top uniformly spaced at 250 mm along the entire girder, U-type G1003 at the bottom and G1004 hooks with varying spacing along the girder. Before the load testing, numerical simulation through finite element analysis is performed to predict the behaviour of the PC bridge girder assuming as-built condition. Note that all geometrical and material information used is the nominal values from the drawings for the pre-test simulation.

(a)
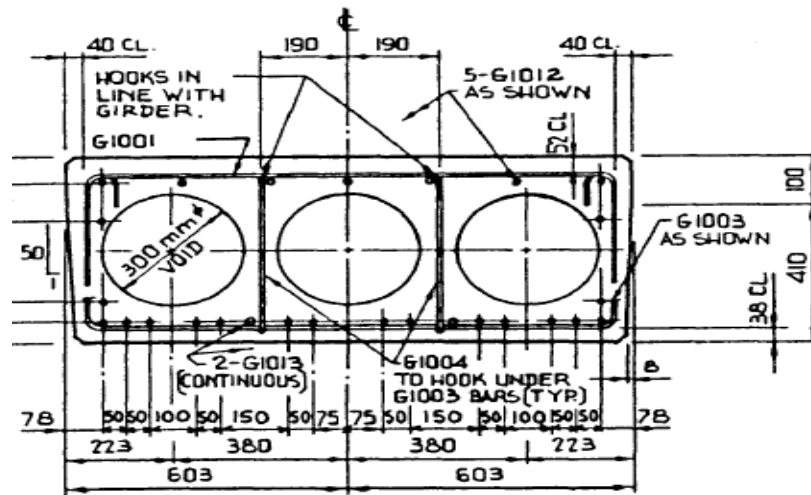
(b)

Figure 4-1: (a) The abandoned bridge near Barrhead, and (b) a representative cross-section of a interior bridge girder (courtesy of Alberta Transportation)

4.2.2   Finite Element Modeling

Finite element (FE) modeling has been used extensively to predict the performance of concrete structures. FE models of various levels of sophistication can assist the understanding of the structural behaviour and failure mechanism. These models include 3D models using continuum elements with complex tri-axial constitutive material models, 2D models using quadrilateral elements with 2D material models for plane stress or plane strain problems, 1D models using the fibre-based beam-column elements. Among these modeling approaches, 2D models are attractive to researchers for a good balance of accuracy and efficiency. As such, 2D model is selected for the simulation of the bridge girder. For the purpose of cross-checking, 1D model is also used here as the fibre beam-column element in OpenSees (Open System for Earthquake Engineering Simulation) proves to be very accurate and efficient for frame-type structures with flexure-dominated behaviour.

4.2.2.1   2D Continuum FE Model in VecTor2

VecTor2 is a nonlinear analysis software for 2D RC membrane structures, and the modeling capability of VecTor2 based on the Modified Compression Field Theory (MCFT) was validated in terms of predicting/calculating the load-carrying capacity, the load-deformation response, and the failure mode by previous researchers (Vecchio and Collins 1988, Aquino and Erdem 2007).

In the FE model developed using VecTor2, a plane-stress condition is assumed for the concrete girder and concrete is modeled by 4-node plane-stress rectangular elements, as shown in Figure 4-2 (a). According to convergence analysis with different mesh refinement, a mesh size of approximately 40 mm × 40 mm is selected for its good balance of computational efficiency and accuracy. The plane-stress elements are assigned with different thicknesses for the ten layers in order to simulate the three voids in the girder cross-section (see Figure 4-2 b). The longitudinal reinforcements (i.e., mild steel and pre-stressing strands) are simulated by 2-node truss bar elements, which are able to deform axially only without flexural stiffness. The transverse steels are considered through the smeared approach (i.e., without explicit modeling of the stirrups) based on the transverse

reinforcement ratios. Due to the different stirrup spacing along the girder, seven regions with four different smeared reinforcement ratios are considered. Note that in pre-test simulation, no rigid-end diagram is considered (i.e., a constant section along the entire length of the girder) since the length of the rigid end zone is unknown before testing. Following the test plan, the girder is simply supported with a clear span of 10,800 mm. The gravity load is applied as the first load step, in which the pre-stress is also taken into account. It is followed by the displacement-controlled static analysis with two concentrated loads (0.5P each) applied at the middle of the girder with a pure bending span of 1,500 mm, as shown in Figure 4-2 (a).

(a)

(b)
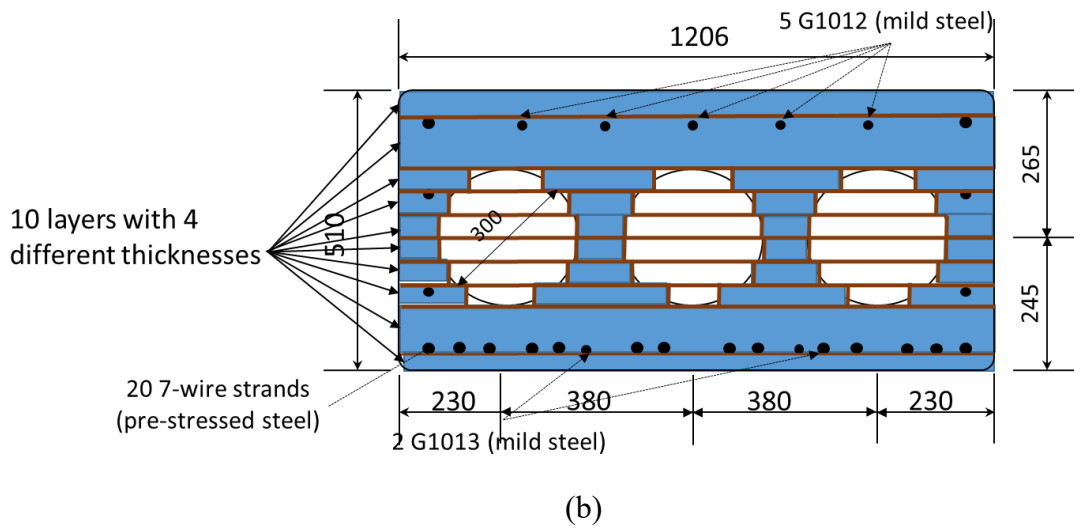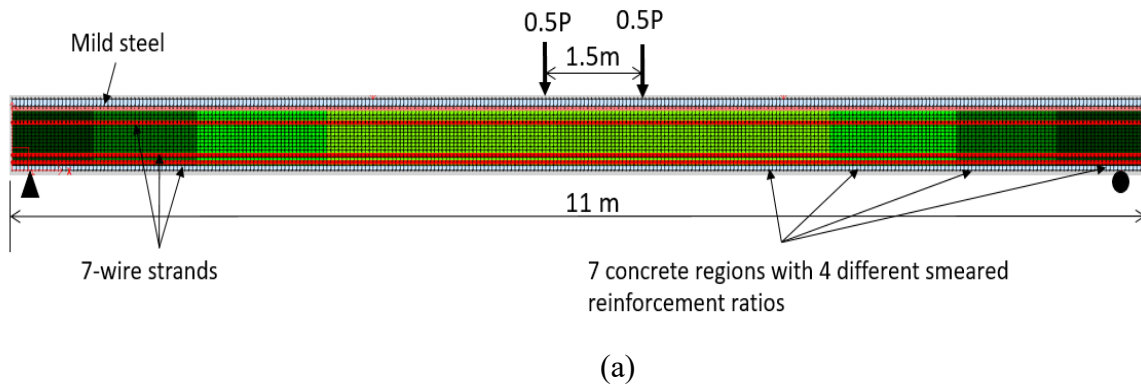
Figure 4-2: 2D FE modeling scheme of the bridge girder in VecTor2: (a) elevation view of the FE model of the simply supported bridge girder, and (b) cross-section in the middle span of the girder

The compressive behaviour of the material model used for concrete in VecTor2 is shown in Figure 4-3. The *Hognestad model*, which is a parabola symmetric about the strain corresponding to the compressive strength f'_c, is used for pre-peak behaviour of concrete. The pre-peak stress-strain curve is described by the following relationship as shown in Eq. (4-1):

$$\sigma = f'_c \left[2\frac{\varepsilon}{\varepsilon_0} - \left(\frac{\varepsilon}{\varepsilon_0}\right)^2 \right] \tag{4-1}$$

Modified Park-Kent model is used for post-peak behaviour of concrete. The slope of the descending branch of the curve is *Zm*, which is a function of the concrete cylinder strength, concrete compressive strain corresponding to the cylinder strength, and principal stresses acting transversely to the considered direction. *Modified Bentz* formulation is used for the tension stiffening that takes into account the percentage of reinforcement and bond characteristics.
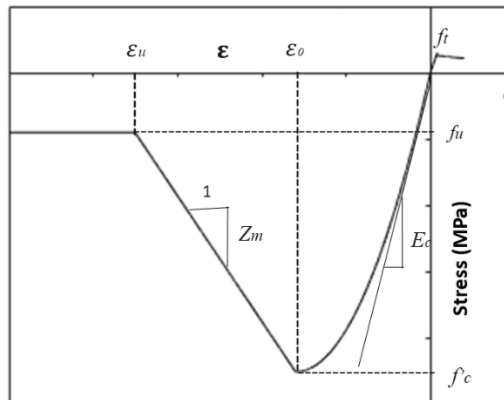
Figure 4-3: Compressive behaviour of the material model used for concrete in VecTor2

Ductile Steel Reinforcement in VecTor2 is used for mild steels. Corresponding material stress-strain behaviour for the steel in tension and compression is shown in Figure 4-4. The steel is assumed to be a bilinear material, with the initial slope defined by the modulus of

elasticity E_s, and the post-yield slope defined by the strain hardening modulus E_{sh}. The pre-stressed steels are modeled using *prestressing steel* in VecTor2, as shown in Figure 4-5.
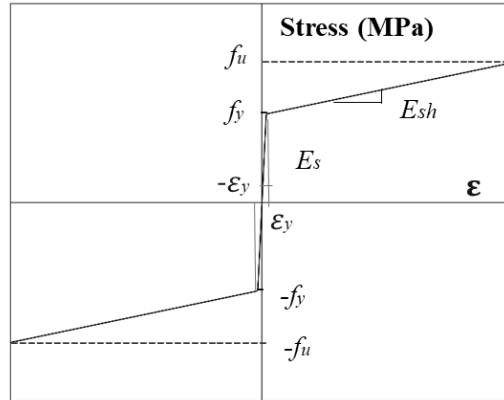
Figure 4-4: *Ductile Steel Reinforcement* response in VecTor2
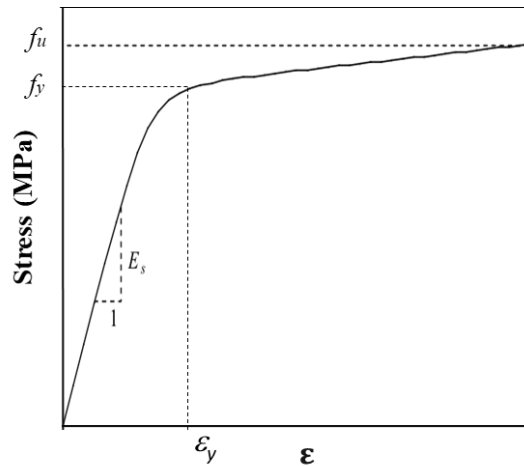
Figure 4-5: *prestressing steel* stress-strain response in VecTor2

Material properties of concrete and steel used in pre-test simulation are provided values in the blueprint, as summarized in in Table 4-1, together with other material model parameter values obtained from the literature.

Table 4-1 Material properties in pre-test simulation

Material	Symbols	Parameters	Formula	Value
Concrete	f'_c	Compressive strength	Provided	35 MPa
	ε_0	Strain at peak compressive stress	$1.8+0.0075f'_c$	0.00206
	E_c	Elastic modulus of concrete	$5500\sqrt{f'_c}$	29580 MPa
	f_t	Tensile strength	$0.33\sqrt{f'_c}$	1.95 MPa
	f_u	Ultimate compressive strength	$0.2f'_c$	7 MPa
Mild steel	f_y	Yield strength	Provided	400 MPa
	E_s	Elastic modulus of steel	Empirical	200000 MPa
	f_u	Ultimate strength	Empirical	600 MPa
	ε_y	Yield strain	f_y/E_s	0.002
	ε_{sh}	Hardening Strain	$\varepsilon_{sh}=\varepsilon_y$	0.002
	E_{sh}	Strain hardening modulus	$0.01E_s$	2000 MPa
	d	Diameter	M10	11.2 mm
7-wire strands	f_y	Yield strength	Empirical	1676.5 MPa
	E_s	Elastic modulus of steel	Empirical	196500 MPa
	f_u	Ultimate strength	provided	1860 MPa
	ε_y	Yield strain	f_y/E_s	0.0085
	f_{pi}	Initial tension load	Provided	129 kN/strand
	f_p	Design load	Provided	107 kN/strand
	d	Diameter	Provided	12.7 mm

4.2.2.2 1D Fibre-based FE Model in OpenSees

OpenSees is an open-source FE software framework for simulating the seismic response of structural and geotechnical systems. It has been widely used throughout the world mainly for research purposes. In the model developed using OpenSees, the PC girder is represented using 16 displacement-based fibre beam-column elements according to mesh sensitivity analysis; each element has 5 integration points, which are assigned with fibre sections, as shown in Figure 4-6. The cross-section is discretized into concrete fibres (10 mm × 10 mm) and steel fibres to represent the mild steel and pre-stressed tendons. Note that only uni-axial material models (e.g., realistic stress-strain relationships) need to be assigned to each material fibre.
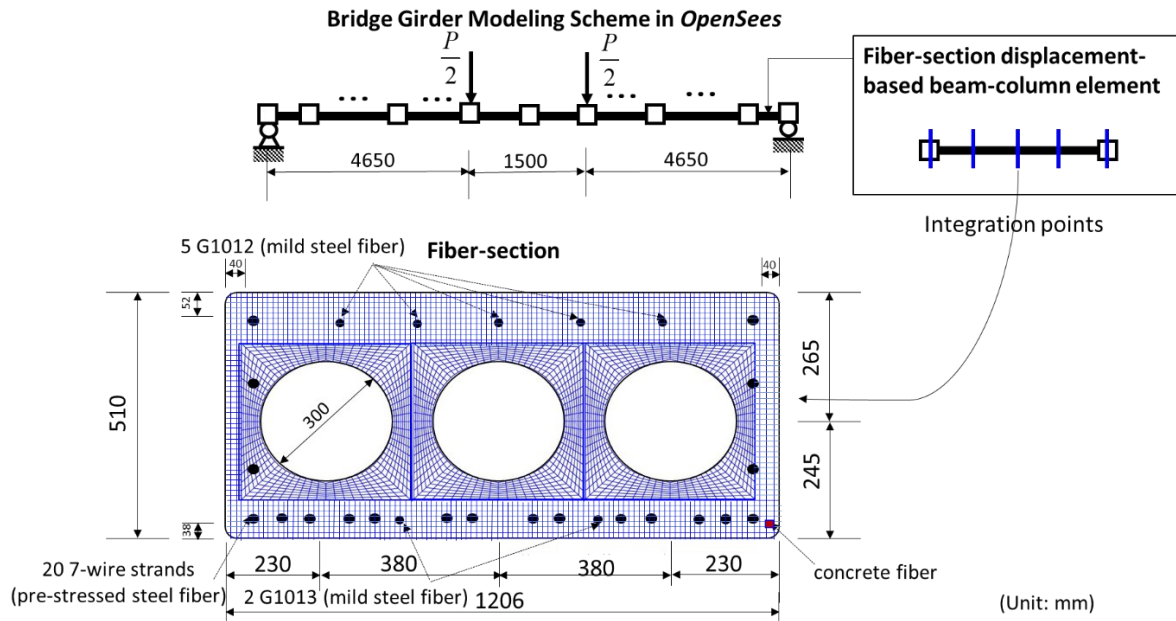
Figure 4-6: 1D FE modeling scheme of the bridge girder in OpenSees

The material for cover concrete is modeled by *Concrete01* (see Figure 4-7 a), which is a uniaxial Kent-Scott-Park concrete material model with degraded linear unloading/reloading stiffness according to the work of Karsan-Jirsa and no tensile strength. The material for core concrete is modeled by *Concrete02* (see Figure 4-7 b). It is a uniaxial concrete material model with a linear elastic behaviour until cracking strength reached in tension and with a linear tension stiffening; it has a parabolic pre-peak behaviour and linear softening to the ultimate strain with a residual compressive strength in compression. Note that the pre-peak behaviour is similar to the Hognestad model in VecTor2 but the confinement effect for the core concrete due to stirrups is considered based on Mander et al. (1984). The compressive strength and ultimate strain of confined concrete can be calculated as a function of the confinement (transverse reinforcing steel). The parameter values are consistent with the values in Table 4-1. The mild steel is modeled using *Steel01* in OpenSees (see Figure 4-7 c), which is a uniaxial bilinear steel material with kinematic hardening and optional isotropic hardening. The 7-wire strands are modeled by *Steel02* (see Figure 4-7 d) to construct a uniaxial Giuffre-Menegotto-Pinto steel material with isotropic strain hardening, in which an initial stress can be assigned to simulate the pre-stressing force. Additionally, the *MinMax* material in OpenSees is used to make sure the

failure of steel when the ultimate stress is reached. The minimum and maximum strains are assigned as the ultimate strain of the steel, which are calculated using the hardening modulus E_{sh} and the yield strain f_y. It is worth noting that the material behaviours of concrete and reinforcing steel in OpenSees and VecTor2 are not exactly the same, but close with the same basic material properties.
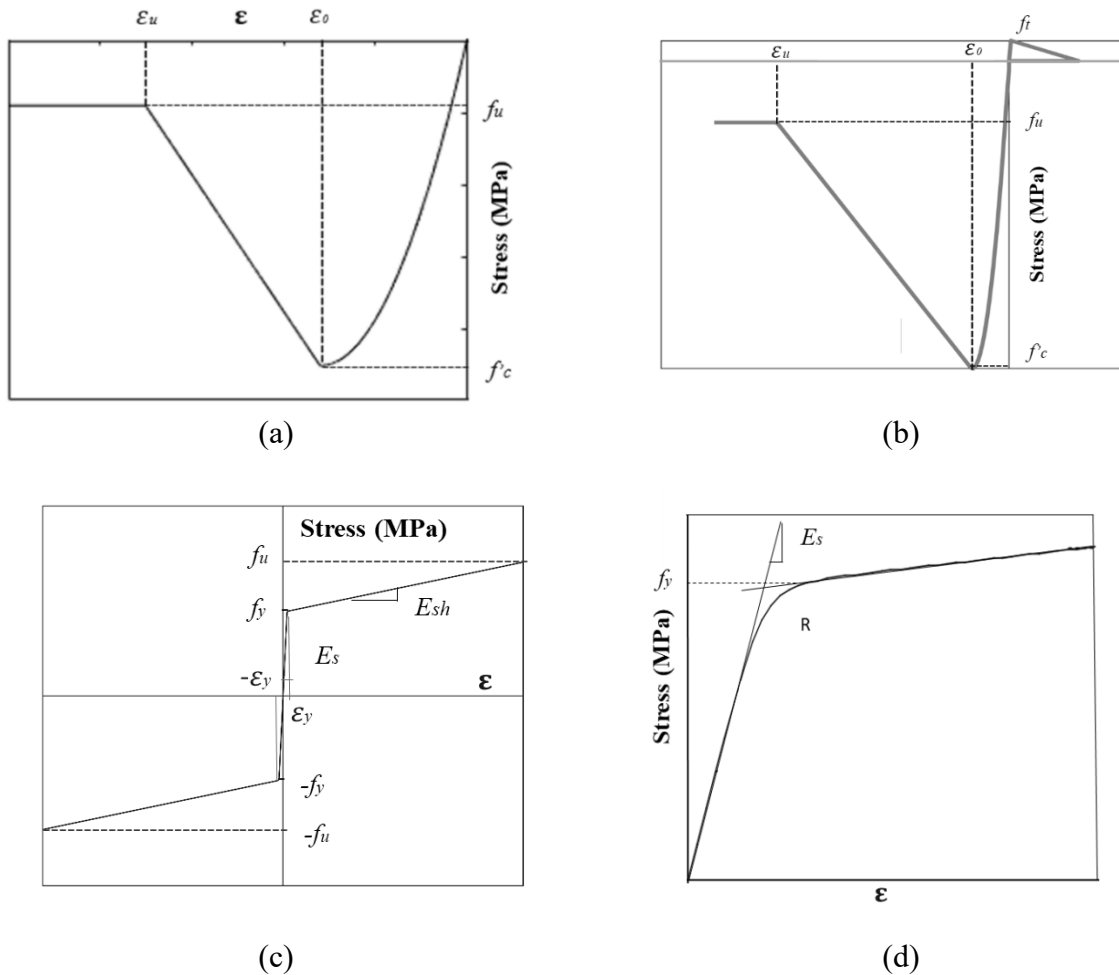
Figure 4-7: Uniaxial material behaviour for (a) *Concrete01*, (b) *Concret02*, (c) *Steel01*, and (d) *Steel02* in OpenSees

Similar to the model in VecTor2, the girder is simply supported with a clear span of 10,800 mm. The gravity load is applied as the first load step, followed by the two concentrated displacement-controlled static loads applied at the middle of the girder with a bending span of 1,500 mm.

4.2.3 Pre-Test Simulation Results

The models use the design pre-stressing force after relaxation (107 kN) instead of the initial tensioning force (129 kN) for the 7-wire strands. The comparison of load-displacement curves obtained using 1D and 2D models are shown in Figure 4-8. Note the load is the total load (i.e., summation of the two point-loads), and the displacement is vertical deflection of the girder in the mid span. It is found that the initial stiffness of two models are the same but the camber of VecTor2 model is slightly larger than that of OpenSees. Both models predict the load carrying capacity of the girder around 470 kN when pre-stressing force is 107 kN per strand. However, the girder is predicted to be much more ductile in OpenSees than that in VecTor2. This is because the 1D model in OpenSees ignored shear effect thus was not able to capture the damage due to shear.
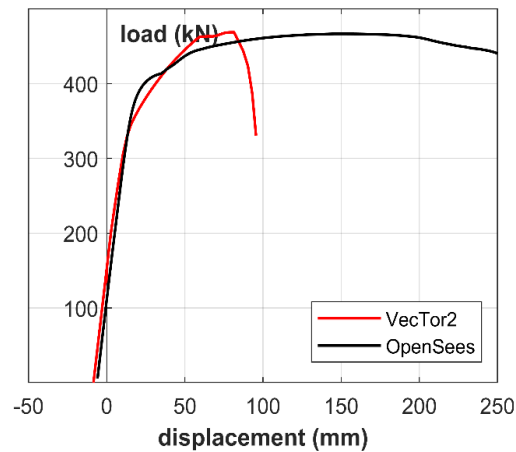
Figure 4-8: Comparisons of load-displacement curved predicted by 2D and 1D models

Critical stages are indicated in the load-displacement curve predicted from VecTor2 (see Figure 4-9 a), where P_s and P_u are corresponding to the service and ultimate truck loads calculated according to the Bridge Load Evaluation Manual (Alberta Government 2016) and the Canadian Highway Bridge Design Code (CSA S6-14), and P_f is the load when the girder fails. The cracking patterns predicted at each critical stage are also shown in Figure 4-9. It can be observed that when load applied is at P_s, there is only subtle deformation and no cracks can be observed (Figure 4-9 b). When the load applied reaches P_u (Figure 4-9 c), some flexural cracks form on the tension side in middle span. When the load applied

reaches P_f (Figure 4-9 d), the flexural cracks propagate further and become wider; additionally, shear cracks start to form in the shear span.

(a)

(b)

(c)

(d)
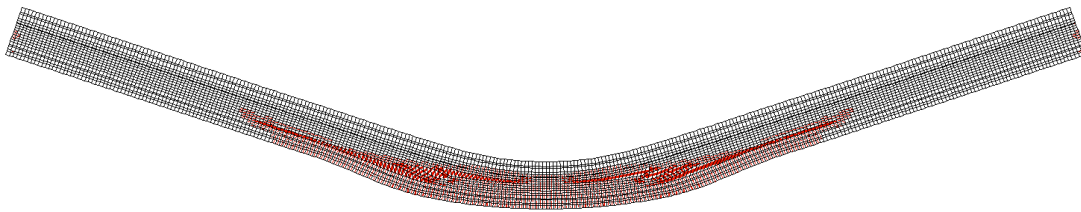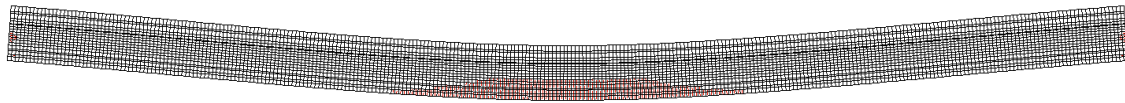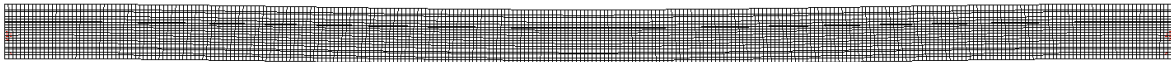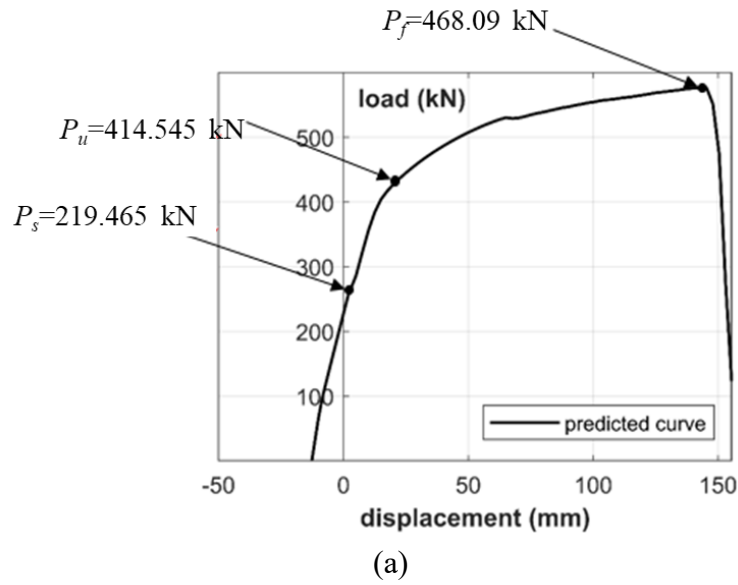
Figure 4-9: (a) Load-displacement curve predicted in VecTor2 with critical stages indicated, (b) cracking pattern at P_s, (c) cracking pattern at P_u, and (d) cracking pattern at P_f

Critical stages corresponding to and are also indicated in the load-displacement curve predicted from OpenSees as shown in Figure 4-10 (a). The stress-strain responses of critical

71

fibres are presented for 7-wire strands (Figure 4-10 b), the bottom concrete fibre (Figure 4-10 c), and the top concrete fibre (Figure 4-10 d) to provide better insight into the structural behaviour of the girder. It can be concluded from these fibre responses that the girder is in a fairly good condition when the load applied is at P_s. When the load applied reaches P_u, the concrete on the tension side has been cracked, and the mild steel and 7-wire strands have not yielded.

(a)

(b)
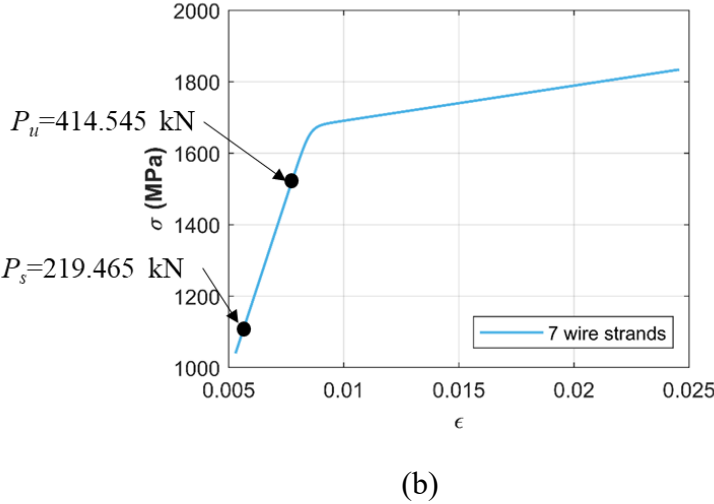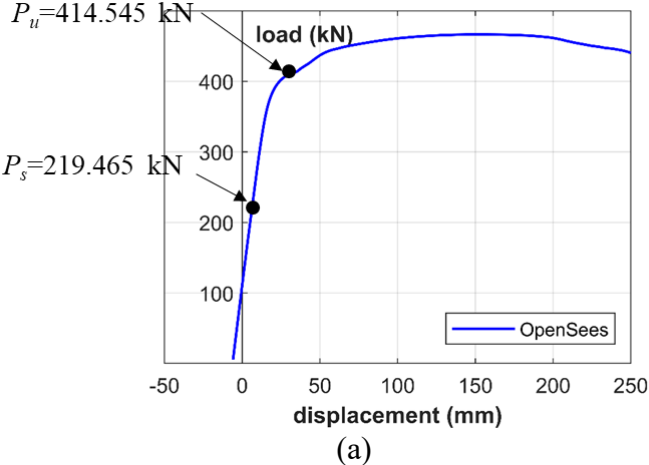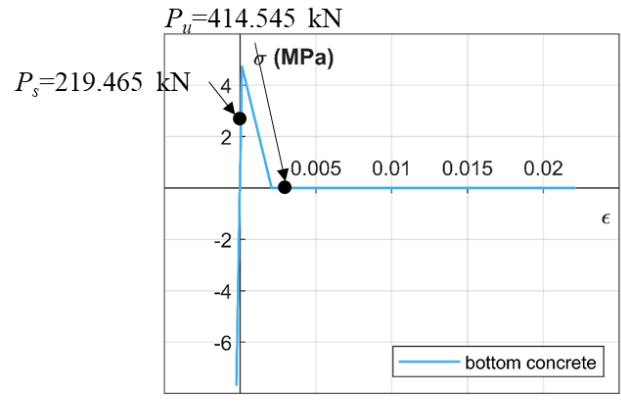
(c)
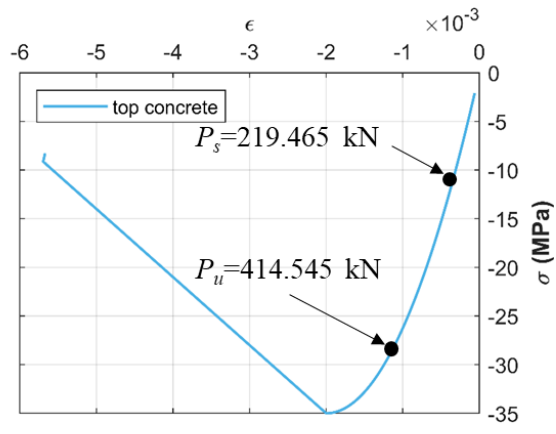
(d)

Figure 4-10: (a) Load-displacement curve predicted in OpenSees with critical stages indicated, (b) fibre response of 7-wire strands, (c) fibre response of the bottom concrete, and (d) fibre response of the top concrete

4.3   Post-test Simulation

4.3.1   General Test Information

A visually intact interior PC girder salvaged from the bridge, denoted as girder #1, was first tested to failure through four-point bending. The girder was simply supported on neoprene pads with a clear span of 10,800 mm subjected to two concentrated loads (0.5P each), which are applied with a pure bending span of 1,500 mm, as shown in Figure 4-11.

73

The girder was loaded to failure with two unloading-reloading cycles occurring at the designed loads corresponding to the serviceability and ultimate limit-states, respectively.
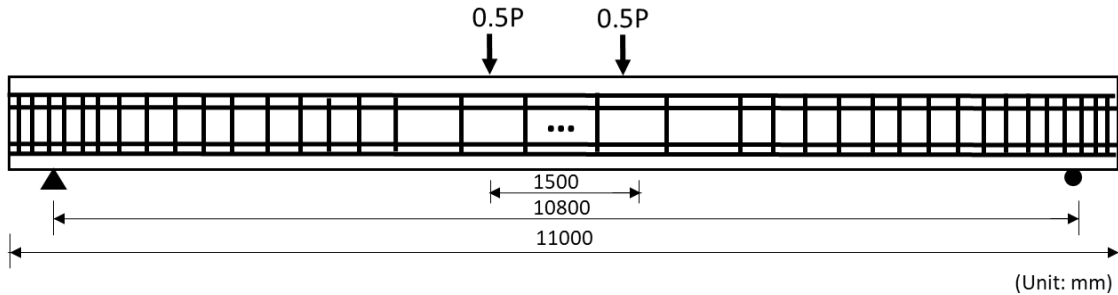
Figure 4-11: Schematic view of the tested interior bridge girder #1

After the test, the girder #1 was cut and the cross-section arrangement of stirrups were measured to obtain the accurate information of the girder. It is found that the arrangement of transverse steels is generally consistent with that provided in the blueprints. However, the measured dimensions of the cross-sections are found to be a little larger than provided values and the rigid-end diagrams are 260 mm long on each end. The three-cell hollow cross-section is 1,219 mm wide and 515 mm deep as measured in the laboratory, and each of the three voids is approximately circular with a diameter of 305 mm, as shown in Figure 4-12. The longitudinal steels in the cross-section agree well with the blueprints. But what is worth mentioning is that an extra layer of 4 extra M25 re-bars of Grade 400 are observed in the tested girder, in addition to the re-bars provided in the blueprints.
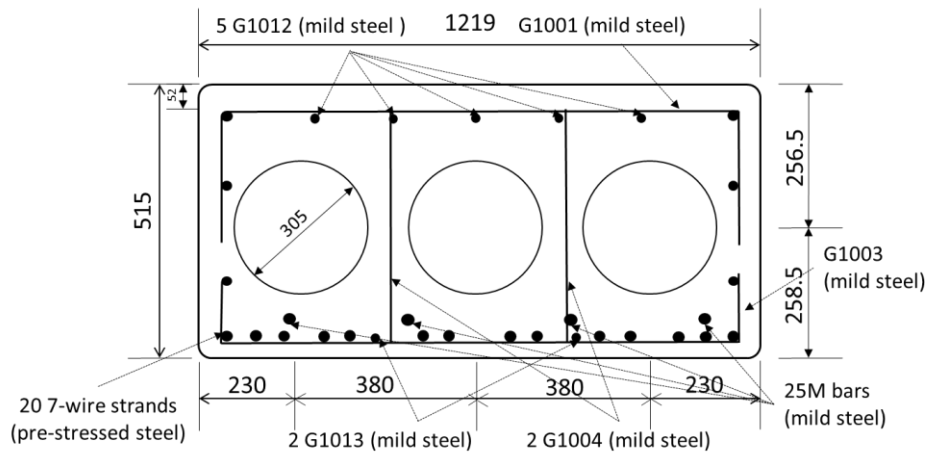
Figure 4-12: Updated representative cross-section in the middle span of interior PC girders

4.3.1.1 Material Behaviours

The material behaviours obtained from the material coupon tests are used here to evaluate the material models utilized in the pre-test simulation, including the compressive stress-strain curves for concrete, the tensile stress-strain curves for 7-wire strands, mild steels, and stirrups, as shown in Figure 4-13 (a) – (d), respectively.

It is found that concrete models used in the pre-test FE models have much lower compressive strength and larger ultimate strain, which are very different from the material test results. This can cause underestimation of load-carrying capacity and overestimation of the deflection at failure. Steels are generally well represented in terms of the yield strength and the elastic modulus, except the post-yield behaviour (e.g., post-yield hardening ratio, ultimate strain). The four M25 re-bars, as unexpected longitudinal reinforcements, were not included in the pre-test simulation and thus the capacity was under-estimated.
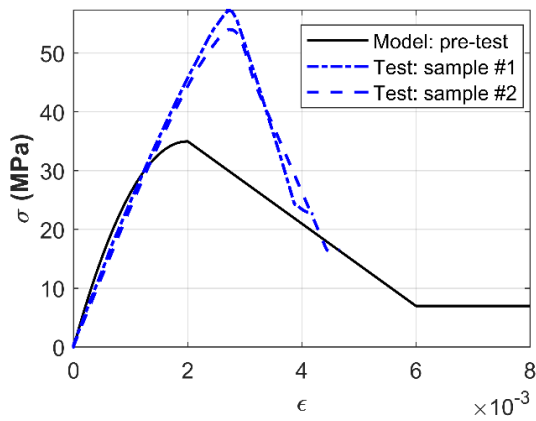
(a)
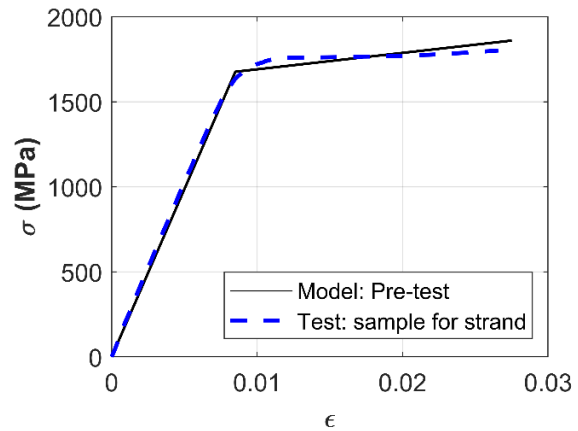
(b)
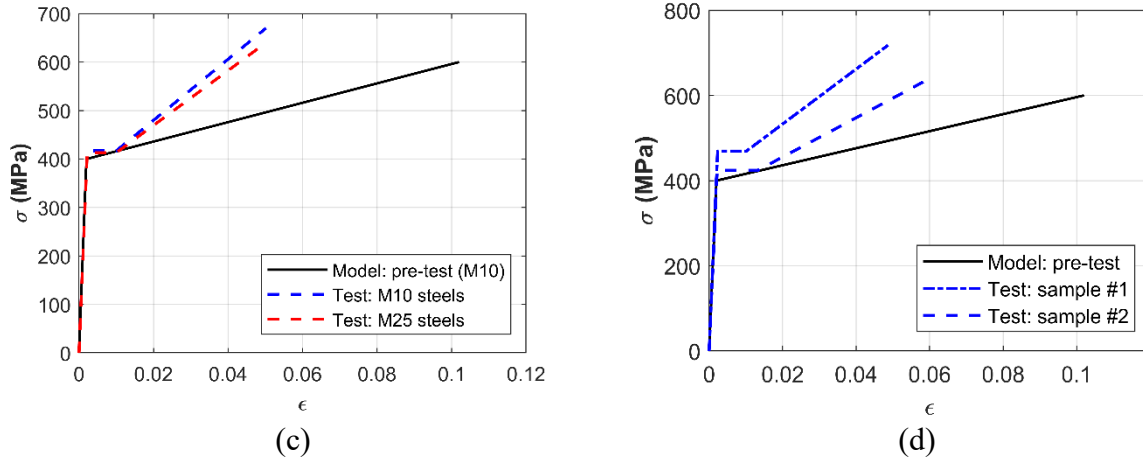
Figure 4-13: Comparison of tested material behaviours with the models used in pre-test simulation: (a) concrete, (b) 7-wire strands, (c) mild steels, and (d) stirrups

4.3.2   Finite Element Modeling

4.3.2.1   2D Continuum FE Model in VecTor2

Based on the new material properties from the tests and the accurate dimensions of the cross-section, the 2D FE model is updated accordingly. In the updated 2D model implemented in VecTor2 (shown in Figure 4-14), concrete is modeled by plane-stress rectangular elements with an average mesh size of 40 mm × 40 mm. Since plane-stress condition is assumed for the concrete girder, the elements are assigned with different thicknesses for the ten layers in order to simulate the three voids in the girder cross-section, as shown in Figure 4-14 (b). Different from the model for pre-test simulation, 260 mm long rigid-end diagrams with a solid cross-section are considered at both ends of the girder as measured in the test.

Similar to the model for pre-test simulation, the longitudinal reinforcements are simulated by 2-node truss bar elements and the only difference is the addition of the extra layer of longitudinal M25 bars. The stirrups are smeared with different transverse reinforcement ratios assigned to the concrete elements due to the different stirrup spacing along the girder and the four different thicknesses (see Figure 4-14 a). The load and boundary conditions are consistent with the test setup and the pre-test model (i.e., simply supported with a span of 10,800 mm and two loads in the middle with a pure bending span of 1,500 mm)

76
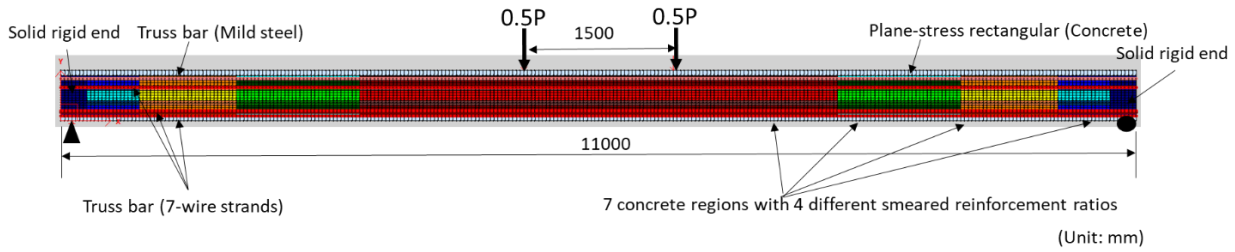
(a)
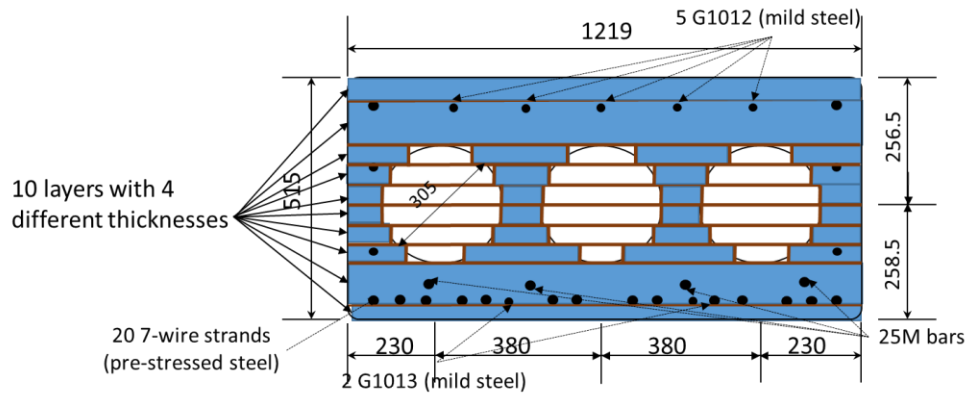
(b)

Figure 4-14: 2D FE modeling scheme of the bridge girder in VecTor2: (a) elevation view of the FE model of the simply supported bridge girder, and (b) cross-section in the middle span of the girder

Material properties of concrete and steel reinforcement, provided from the material tests for girder #1, are used to define the material models. For the concrete material, the pre-peak and post-peak behaviour in compression is represented by the *Popovics (High strength)* model and the *modified Park-Kent* model, respectively in VecTor2. The properties obtained from two concrete cylinders tests are fairly close, so the average behaviour is used in the FE model. As such, the material model parameters used include the concrete compressive strength $f'_c = 55.5$ MPa, the corresponding compressive strain $\varepsilon_0 = 0.00286$, and the elastic modulus $E_c = 25500$ MPa. Figure 4-15 (a) shows a comparison between the compressive stress-strain curve characterized by the used material models and stress-strain curves from the tests. A good correlation between them is observed, which validates the material models used for concrete in terms of compression. The tensile behaviour of concrete is characterized by a linear branch before cracking, and the *modified Bentz-2003* model is used to consider the tension-stiffening in concrete after cracking. The

cracking stress is determined as $0.33\sqrt{f_c'(\text{MPa})}$ as recommended in VecTor2 manual (Wong et al. 2013). The values for other model parameters are shown in Table 4-2 according to the material tests.

The longitudinal mild steel is modeled by *Ductile Steel Reinforcement* model (in VecTor2), which has a linear branch with a slope characterized by the elastic modulus E_s, a yield plateau at the yield strength f_y, and a linear strain hardening branch with $E_{sh} = bE_s$ (b = the post-yield stiffness ratio). The parameters used in this model are determined according to the mild steel coupon tests: $f_y = 415$ MPa as the average yield strength of mild steels (for G1012, G1013, and M25), the corresponding yield strain = 0.0021, and the elastic modulus $E_s = 200,000$ MPa. As shown in Figure 4-15 (b), the material models used for mild steels in the FE model correlate well with the coupon tests in terms of the stress-strain curves. Similar material models are used for stirrups with material properties obtained from coupon tests. Note that there are two batches of transverse reinforcements extracted from the girder and they behaved very differently. The lower set of properties are used here due to negligible sensitivity of the flexure test results with respect to the smeared transverse reinforcement, as shown in Figure 4-15 (c).

The pre-stressed steel is modeled as *Prestressing Steel* (in VecTor2), which consists of an initial linear-elastic branch, followed by a smooth transition curve to a linear strain-hardening branch. The yield stress $f_y = 1677$ MPa, the yield strain = 0.0085, and the ultimate stress = 1860 MPa are obtained from the material coupon test, which allows the model to represent the true material behaviour as evidenced from the material test as shown in Figure 4-15 (d). To summarize, all model parameters for the material properties are presented in Table 4-2.

The pre-stressing force is applied before performing static analysis using displacement-control following the loading protocol except the two unloading-reloading cycles. Note that the true pre-stress is unavailable for the tested girder, and thus the remaining pre-stress level is considered as a primary variable to study.

Table 4-2 Material properties in the FE model

Concrete		Steel				
			longitudinal			transverse
parameter		parameter	M10	7-wire strands	M25	stirrups
f'_c (MPa)	55.5	f_y (MPa)	417	1676.5	413	424
f_t (MPa)	2.46	f_u (MPa)	670	1860	640	636
f_u (Mpa)	11.1	ε_y	0.0021	0.0085	0.0022	0.0022
E_c (Mpa)	25500	E_s (MPa)	198000	196500	203000	196000
ε_0	0.00286	E_{sh} (MPa)	6290	9657	5080	4610
ε_u	0.0048	Pre-stress force (kN)	-	107	-	-

(a)

(b)

(c)

(d)

Figure 4-15: Stress-strain comparison between the material model and coupon tests for: (a) concrete in compression, (b) mild steel in tension, (c) stirrups, and (d) 7-wire strands in tension

4.3.2.2   1D Fibre-based FE Model in OpenSees

The post-test simulation using 1D FE model is also conducted in OpenSees, same as the pre-test simulation, the PC girder is modeled by 16 displacement-based fibre beam-column elements, each of which has 5 integration points, assigned with fibre cross-sections, as shown in Figure 4-16. The cross-section is discretized into 10 mm × 10 mm concrete fibres and steel fibres to represent the longitudinal reinforcement. All the material models used in the model are the same as what were used before, except the corresponding material properties.
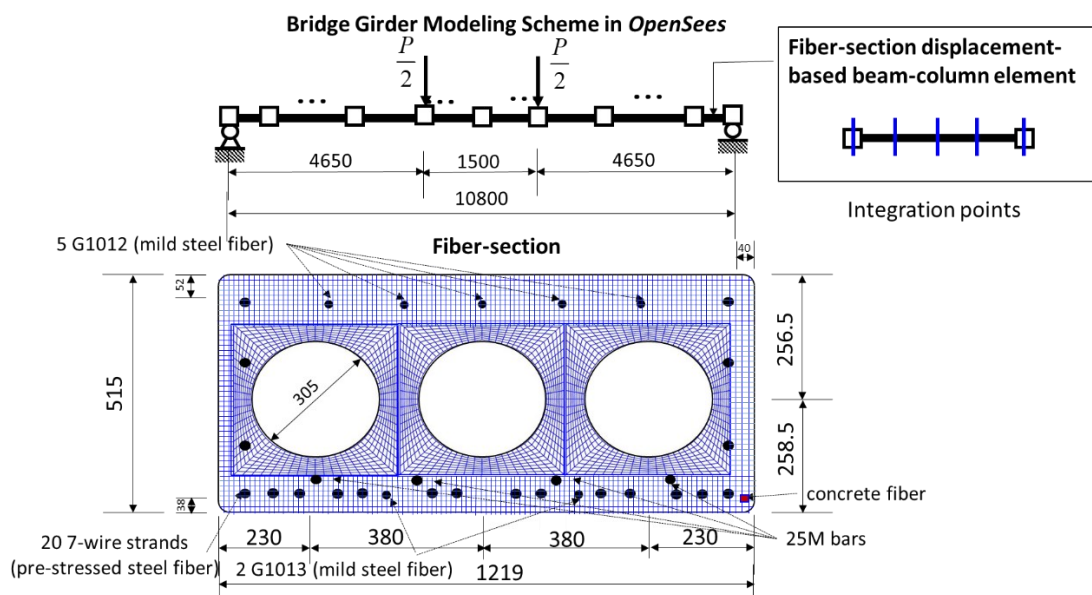
Figure 4-16: 1D FE modeling scheme of the bridge girder in OpenSees

4.3.3   Simulation Results

4.3.3.1   2D Continuum FE Model in VecTor2

The FE model developed here is used to predict the behaviour of the girder #1 under four-point bending. Since the girder #1 is visually intact for bridge inspectors, it is considered as in a pristine condition without corrosion-affected deterioration in the FE model. Two pre-stress levels are considered, namely, the initial pre-tensioning force = 129 kN, and the designed pre-tensioning force = 107 kN after considering pre-stress loss. The corresponding load-displacement (i.e., mid span) curves predicted from the 2D FE analysis (FEA) are shown in Figure 4-17 (a), with comparison to the experimental results. Figure

4-17 (a) also indicates the three critical stages during the loading, i.e., the bottom concrete cracking, the steel yielding, and the top concrete crushing. Accordingly, the cracking patterns are shown in Figure 4-17 (b), (c), and (d), which show the crack formation and growth until failure due to top concrete crushing during the loading process. It is indicated from the model that at point 1, cracks start to initiate on the bottom of the girder as shown in Figure 4-17 (b). After that, the stiffness goes down due to cracking until point 2, around which steels in tension start to yield and some cracks formed in the shear span as shown in Figure 4-17 (c). When the load reaches point 3, the cracks propagate further and become wider, and concrete in compression crushed (Figure 4-17 d), in turn leading to the failure of the girder.

The comparison of the load-displacement curves shows that the 2D FE model predicts the loading behaviour reasonably well. Specifically, the predicted load-carrying capacity is 661 kN, which is only slightly (3.8%) higher than the tested capacity (637 kN). However, the model with almost accurate material and geometry properties over predicts the cracking load, the stiffness (e.g., pre-cracking and post-cracking), even when the lower pre-stressing force is used.

(a)

(b)

(c)

(d)
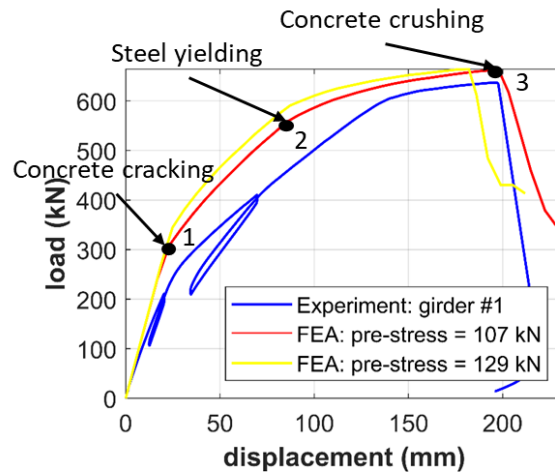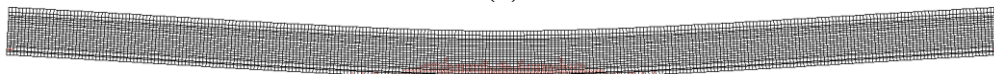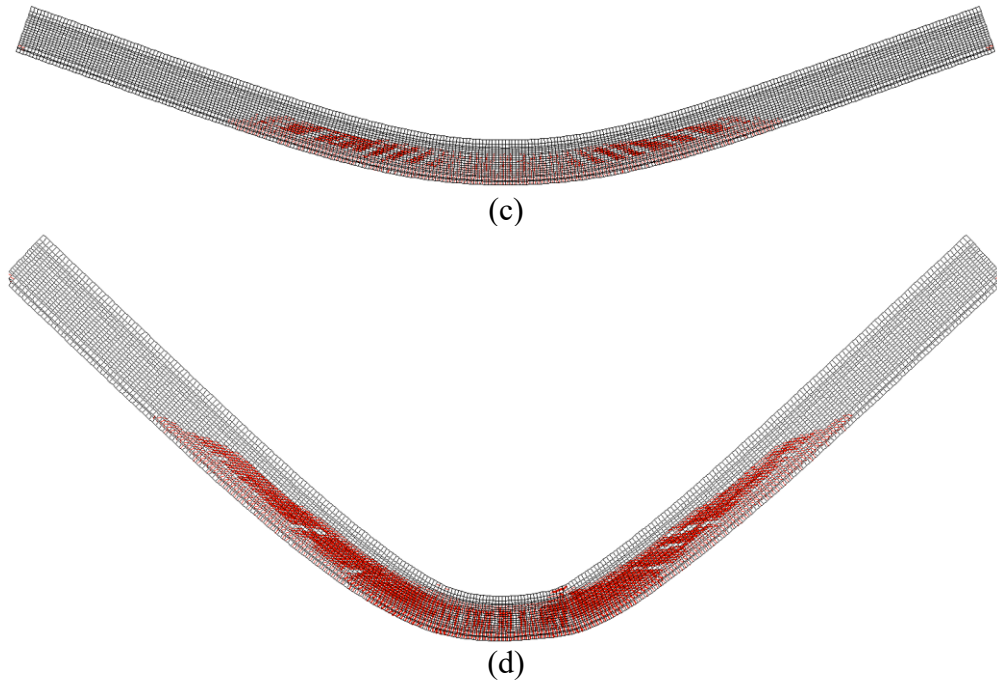
Figure 4-17: (a) Comparison of load-displacement curves between the 2D FE prediction and experiments, (b) cracking pattern at point 1, (c) cracking pattern at point 2, and (d) cracking pattern at point 3

All aforementioned characteristics that are not captured well in the FE model are closely related to the unknown pre-stressing force in the strands. In view of the uncertainty in the remaining pre-stress in the strands, the pre-stressing force used in the model is unsettled. According the literature (Labia et al. 1997, Dasar et al. 2016, Pettigrew et al. 2016), it is likely for the strands to have additional pre-stress loss due to corrosion or other aging effects after 28 years' service. As such, different levels of pre-stress loss are considered in the model to explore the cause of such deviation as a preliminary forensic analysis.

Keeping other material properties the same in the FE model, additional pre-stressing force loss of 20%, 30% and 40% with respect to the designed pre-tensioning force (107 kN) are considered, respectively. The load-displacement curves are presented in Figure 4-18 in comparison with the experimental results. It is observed that when the pre-stress loss increases (i.e., from 0% to 40%), cracking initiates earlier and a lower post-cracking stiffness is observed, which pushes the load-displacement curve closer to the experimental one. In addition, a slight decrease in the predicted load-carrying capacity is observed. As compared to the test data, 30% ~ 40% pre-stress loss leads to a fairly good match between

the FE-predicted and experimental results, in terms of the overall behaviour of the girder. Such a preliminary forensic analysis implies that the additional pre-stress loss due to aging is a possible cause for the large deviation between the FE and experimental predictions, but further investigation (e.g., experimental determination of the pre-stressing force) is needed.
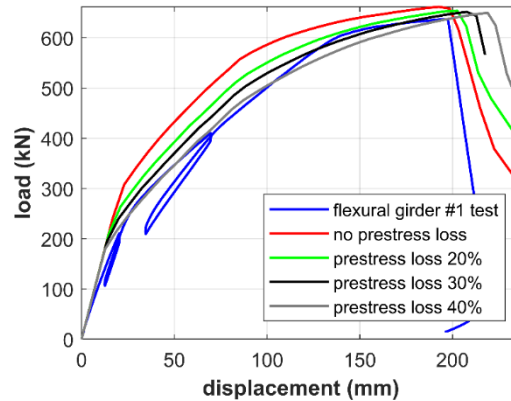
Figure 4-18: Load displacement curves predicted from the 2D FE model considering different levels of pre-stress loss

4.3.3.2   1D Fibre-based FE Model in OpenSees

The load displacement curves predicted by OpenSees with critical stages indicated are compared with test results in Figure 4-19. It shows that the initial stiffness is overestimated but the load at cracking point are around the same. After that, when the load is around 500 kN, M10 steels start to yield, followed by M25 rebars and 7-wire strands. After yielding of all steels in tension, the stiffness goes down to almost the same stiffness with the test. As the loading increases, concrete in compression starts to crush and compression steels yield. The FE prediction matches well with the test in terms of the overall load-displacement behaviours and the ultimate load carrying capacity. Similar to the previous section, different levels of pre-stress loss are studied using the 1D FE model, and the predicted load-displacement curves are shown in Figure 4-19. It is observed that as the additional pre-stress loss increases, post-cracking stiffness decreases and the capacity slightly decreases. Compared to the test, 30% ~ 40% pre-stress loss leads to a fairly good match as well. This observation is consistent with study using the 2D FE model.
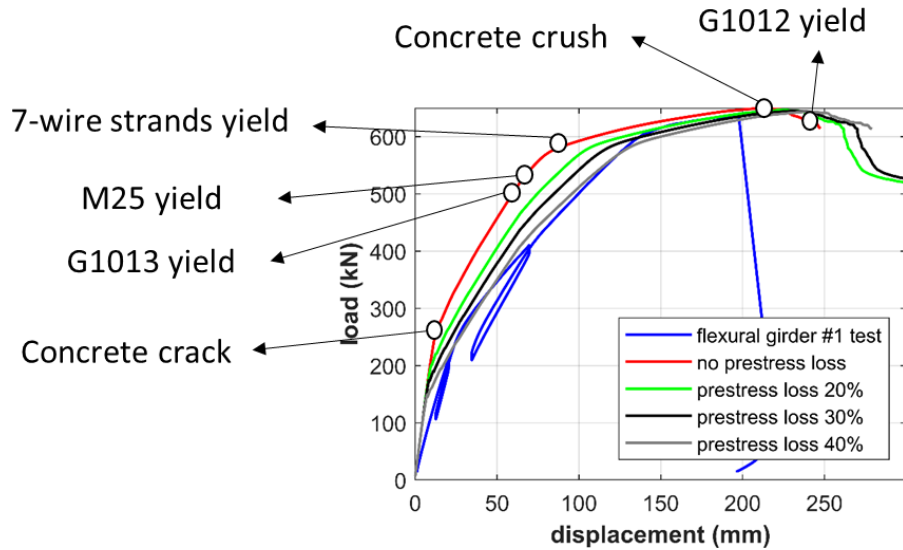
Figure 4-19: Load displacement curves predicted from the 1D FE model considering different levels of pre-stress loss with critical stages indicated

Response of representative fibres in the 1D model are presented in Figure 4-20, including the fibres from the top concrete in compression, 7-wire strands, the compressive, and tensile mild steels. The responses indicate that concrete crushed in compressive zone and all the longitudinal steel yielded when the girder fails.
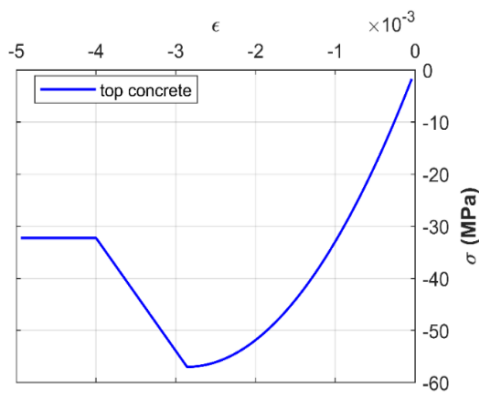
(a)
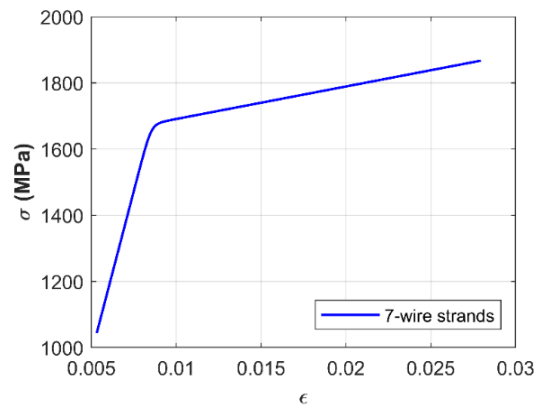
(b)
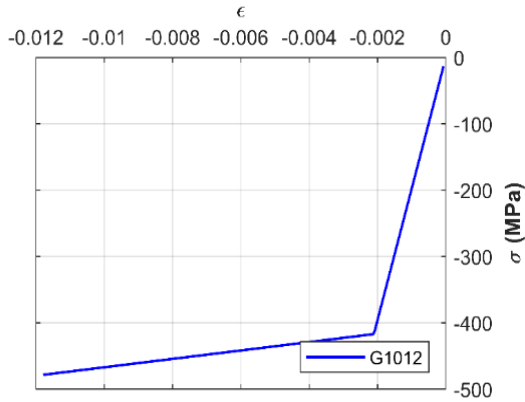
(c)
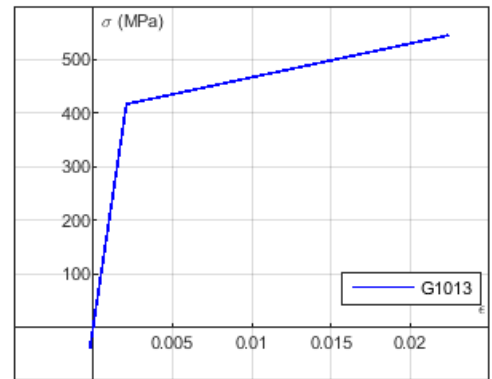
(d)
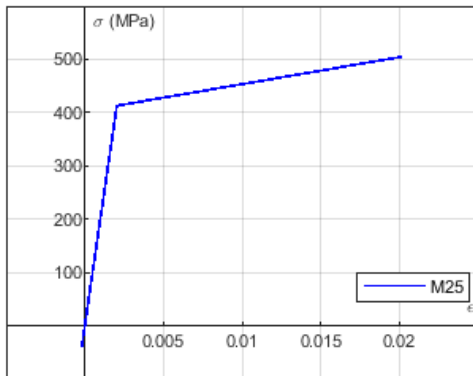
(e)

Figure 4-20: Fibre responses in the 1D FE model for (a) top concrete, (b) 7-wire strands, (c) mild steel in compression, (d) mild steel in tension, and (e) M25

4.4 Parametric Study for PC Girders with Deterioration

The comparison between the FE prediction based on the 2D FE models developed for PC girder and the experimental data confirms the predictability of the model to a reasonable degree. However, as learned from the preliminary forensic analysis of the tested girder #1, pre-stress loss (e.g., due to aging effect or corrosion) has a non-negligible influence on structural behaviour. Moreover, many other possible deteriorations due to corrosion are observed from other girders salvaged from the same bridge. They can affect the structural performance of PC girders to various degrees, which is of great concern for bridge inspectors and evaluators. To learn more about the corrosion-affected deterioration effects

on PC girders, and to predict the residual performance of PC girders with different deteriorations using developed FE model, a comprehensive parametric study is conducted.

4.4.1   Parametrical Design

PC bridge girders are generally exposed to various environmental conditions during their service life period and prone to chemical attacks from chlorides, sulfates, or alkali-silica reaction (Enright and Frangopol 1998) in addition to other deterioration factors. Among those aging factors, chloride corrosion of steel bars is one of the major causes of deterioration in RC and PC structures (Harries 2009). In particular, in cold-climate regions like in Canada, the concrete structures suffer from the de-icing salts, which accelerate the deterioration of highway bridges (Vu and Stewart 2000). In such environment, the effects of both mild steel and pre-stressed steel under corrosion on structural deterioration are studied here. For example, the corrosion can lead to changes in both geometric and mechanical properties, such as cross-section loss (local or uniform) of reinforcements, the ductility reduction of both ordinary and pre-stressing steels (Cairns et al. 2005, Castel et al. 2000, Darmawan and Stewart 2007). Other than those corrosion features, the pre-stress loss is also considered in this study. This is because, in addition to other non-corrosion related pre-stress loss, corrosion can also lead to pre-stressing force reduction in several ways (e.g., cross-section loss, weakening of anchorage due to corrosion).

Moreover, when steels are corroded, the rust formed can occupy six times of the volume of original steel, leading to concrete cover cracking, delamination and even spalling (Broomfiel 2007, Li et al 2008). When the section spalls, concrete cover to protect the reinforcement is lost entirely and thus this geometric change is also considered in this study. Deduction of cross-section of reinforcement, cracking, and spalling of concrete cover can further result in the deterioration of the bond strength between steels and the surrounding concrete (Li and Yuan 2013). This degradation could lead to incompatible strain between steels and concrete (Dekoster et al. 2003), and could even result in anchorage failure, in turn affecting the load-carrying capacity. Therefore, it is necessary to consider the effects of bonding degradation and corresponding anchorage failure when investigating structural residual performance under corrosion (Mangat and Elgarf 1999, Castel et al. 2000).

In addition, corrosion could also affect the degradation of some material properties for steel and concrete, such as the ductility of steels and compressive strength of concrete surrounding the reinforcement. In this study, the parametric analyses are conducted based on 2D model for the tested bridge girder, with the loading condition the same as the flexural test for girder #1. The corrosion-affected properties are related to a commonly used measure of corrosion level, i.e., corrosion degree, which is defined as the mass loss ratio of steel as follows:

$$\eta = \frac{M'}{M} \tag{4-2}$$

where η is the corrosion degree, M' is steel mass loss due to corrosion and M is the original steel mass. In all the cases studied, the corrosion degrees investigated are 5%, 10%, 15%, 20%, 30%, 40%, and 50%.

4.4.1.1 Steel Section Loss

Since the studied girder has considerable amount of mild steels and pre-stressing strands, the effect of their cross-section area loss due to corrosion on the behaviour of PC girders are investigated. Cross-section area loss in stirrups is also studied to see the effects of transverse steels on corroded PC girders under flexure loading conditions. Pre-stressing force loss of strands is considered to be proportional to the cross-section area loss of 7-wire strands as indicated by Castel et al. (2010), as indicated in Eq. (4-3):

$$\Delta F_{pre} = \sigma_{sp} \Delta A_{sp} \tag{4-3}$$

where ΔF_{pre} is reduction in pre-stressing force; ΔA_{sp} is pre-stressing steel cross-section area reduction; and σ_{sp} = pre-stress in the tendons.

4.4.1.2 Material Degradation

Cracked concrete, due to corrosion, exhibits reduced performance compared to undamaged concrete. A reduced value of the compressive strength is calculated for the concrete cover, as suggested by Coronelli and Gambarova (2004):

$$f_c^* = \frac{f_c'}{1+K\left(n_{bars}w_{cr}/b_0\right)/\varepsilon_o} \qquad (4\text{-}4)$$

where K is the coefficient related to bar roughness and diameter, e.g., for medium-diameter ribbed bars $K = 0.1$ Cape (1999); ε_o is the strain at the peak compressive stress f_c', where n_{bars} is the number of the bars in the top layer (bars on the compression side), and w_{cr} is the total crack width according to Molina et al. (1993):

$$w_{cr} = 2\pi\left(v_{rs}-1\right)\left(R-R\sqrt{1-\eta}\right) \qquad (4\text{-}5)$$

where v_{rs} is the ratio of volumetric expansion of the oxides with respect to the virgin material (e.g., the value of $v_{rs} = 2$) and R is the radius of the steel bar in the virgin state, and η is the corrosion degree.

Besides, the ultimate stress and ductility reduction of mild steels due to corrosion are calculated based on corrosion degree as indicated by Zhang et al (2006):

$$f_{uc} = \frac{1-1.119\eta}{1-\eta}f_{u0} \qquad (4\text{-}6)$$

$$\varepsilon_{uc} = e^{-2.501\eta}\varepsilon_{u0} \qquad (4\text{-}7)$$

where f_{uc} is the ultimate stress of the corroded steel, f_{u0} is the ultimate stress in the virgin state, ε_{uc} is ultimate strain of the corroded steel, and ε_{u0} is the ultimate strain in the virgin state.

4.4.1.3 Cover Spalling and Steel De-Bonding in Span

Bottom concrete cover spalling is a common phenomenon for aged PC girders, as for the other girders salvaged in the abandoned bridge studied here. To investigate the effects of

concrete spalling due to corrosion with different lengths and in different locations, 17 cases in total are studied (see Figure 4-21). Five different spalling lengths (i.e. 10%, 20%, 30%, 50%, and 100% of the whole span) are considered. For a given spalling length, various locations are considered, which can be non-symmetrically or symmetrically located in the span of the girder. These cases are labeled in a consistent manner: the second letter (e.g., S or N) indicates whether the spalling is symmetrically (i.e., there are two spots) or non-symmetrically (i.e., only one spot) located in the span. The digits between "L" and "S" / "N" indicate the length percentage of each spalling spot over the span, and the last digit indicates the case number. For example, L10N1 denotes the beam with one concrete spalling with a spalling length = 10% of the whole span (case 1). The width of the spalling area is the same as the width of the girder and the spalling depth is the same as the concrete bottom cover depth.

As the concrete cover spalling naturally exposes the steel reinforcements, the bonding of steel with the surrounding concrete deteriorates. The extreme case, de-bonding of the very bottom layer of longitudinal steels, which consists of 4 mild steels and 14 7-wire strands, is considered to have no bond remain between steel and concrete. Similar to concrete spalling cases, the de-bonding effect is also studied in terms of de-bonding locations and lengths. Note that here only in-span de-bonding is considered and perfect anchorage at the ends is assumed to avoid the effects of anchorage failure, and end anchorage bond loss is considered later.

(a)   (b)

(c)   (d)

Figure 4-21: Parametric analysis cases to study the corrosion-induced bottom concrete cover spalling and steel de-bonding for (a) L10 series, (b) L20 series, (c) L30 series and (d) L50 & L100S1 series

4.4.1.4 *Bond Loss in the End Anchorage*

According to the survey on inspection of corroded bridge girders, deterioration caused by corrosion can be very severe at the ends of the girder, where the anchorage bonding between reinforcement steel and concrete might get impaired. As a result, intermediate bond loss in addition to de-bonding is studied to take into account the corrosion-induced anchorage deterioration. Some cases are selected (i.e., L20S1, L30S1, L20N1, L30N1, L50, and L100) from previously designed ones, which are located in shear span symmetrically or non-symmetrically, and further extended in length to the ends of the girder in this study, as shown in Figure 4-22.
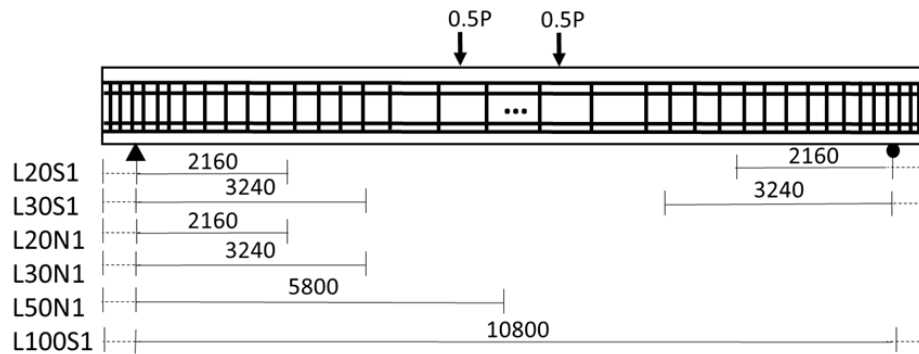
Figure 4-22: Parametric analysis cases for corrosion-affected anchorage bond loss

Different from complete bond loss, intermediate bond loss is related to the corrosion degree. Kivel et al (2015) adopted the bond-slip model from Eligehausen et al. (1983) to consider intermediate bond degradation due to corrosion by concluding forty-two corroded pullout specimens test results from other researchers as shown in Eq. (4-8) and Eq. (4-9). The

90

corroded bond-slip curves corresponding to various corrosion degrees are shown in Figure 4-23.

$$\frac{\tau_{R,\eta}}{\tau_{R,0}} = 1.2e^{-7.6\eta} \tag{4-8}$$

$$\frac{\tau_{f,\eta}}{\tau_{R,\eta}} = \begin{cases} 0.26 + 13\eta & 0\% \le \eta < 3\% \\ 0.65 & 3\% \le \eta < 13\% \\ 0.65 - 0.06(100\eta - 13) & 13\% \le \eta < 20\% \\ 0.23 & 20\% \le \eta \end{cases} \tag{4-9}$$

Here $\tau_{R,\eta}$ is the rupture stress remained after corrosion, $\tau_{R,0}$ is the original rupture stress before corrosion, and $\tau_{f,\eta}$ represents the remaining ultimate frictional stress. Note that the slips corresponding to all critical points on the original bonding stress-slip curve are barely affected by corrosion.
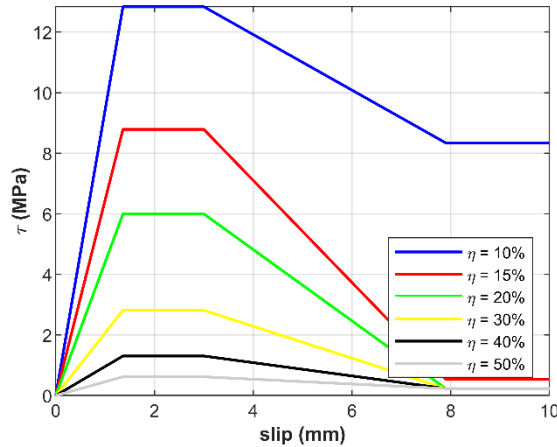
Figure 4-23: Bond-slip relationships under various corrosion degrees

4.4.2   Deterioration Implementation in FE model

The corrosion-affected geometric (e.g., steel section loss) and material (e.g., concrete and steel material properties degradations, pre-stress loss) can be implemented by modifying the material parameters in the FE model. However, corrosion-induced topological changes, such as concrete spalling and bond loss, need special treatment. The concrete spalling is

modeled by deactivating the concrete elements (as indicated by white) in the spalling area, as shown in Figure 4-24 (a).

In order to simulate the bonding loss between steel re-bars and the surrounding concrete, *Link elements* are created to represent the bonding interface along the un-bonded length of reinforcement (see Figure 4-24 b for example). *Link element* in Vector2 (Ngo and Scordelis 1967) is a dimensionless element linking two nodes in the same location, e.g., one associated with the concrete element and the other associated with the steel reinforcement element. The link between the two nodes can be conceptualized as two orthogonal springs in both the longitudinal and transverse directions of the beam. The bond type used is *un-bonded bars or strands* in VecTor2 to simulate the complete bond loss (i.e., de-bonding) between concrete and steel. Regarding intermediate bond loss, *Eligehausen bond-slip* model (1983) for *imbedded bars with custom input* in VecTor2 is used in order to define the corrosion-affected stress-slip relationship, which allows customization of critical parameters of stress-slip curve according to the corroded bond-slip model mentioned earlier.

spalled concrete

(a)

de-bonded steel

(b)
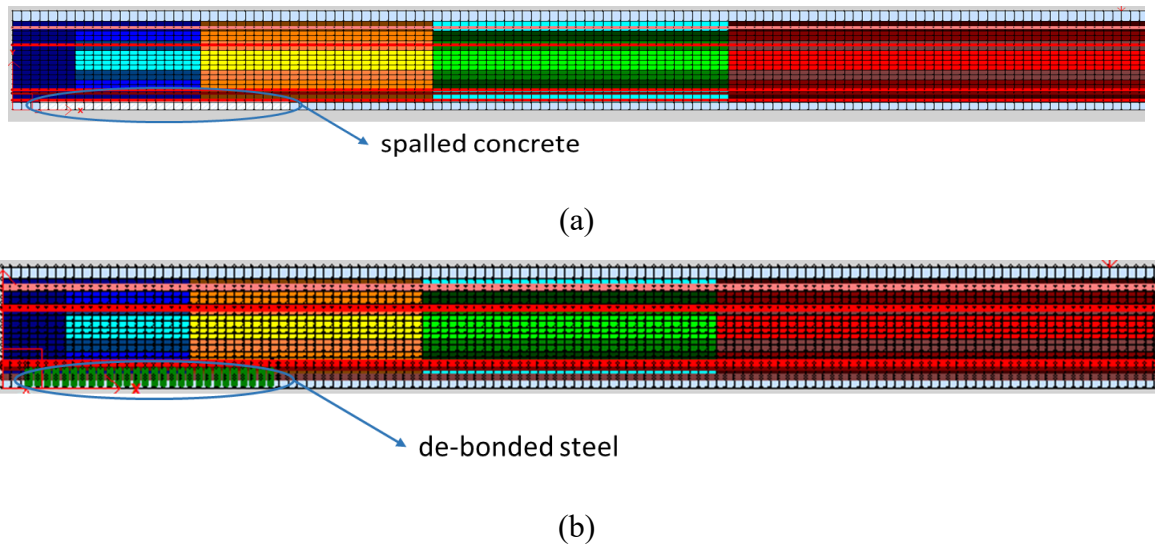
Figure 4-24: Modeling approach of (a) concrete spalling, and (b) corrosion-affected bonding of steel

4.4.3   Parametric Study Results

4.4.3.1   Steel Cross-section Loss

Figure 4-25 shows the comparisons of load-displacement curves of PC girders with steel cross-section loss or pre-stress loss at increasing corrosion levels. This study of a wider range pre-stress loss further verifies the effects learned when simulating behaviour of PC bridge girder #1, which are earlier crack initiation and post-cracking stiffness reduction (see Figure 4-25 a). As indicated by Figure 4-25 (b), corrosion-induced mild steel (e.g., G1012, G1013 and M25) cross-section loss decreases the post-cracking stiffness and the load carrying capacity slightly. Similarly, when pre-stressing steel strands gets corroded, see Figure 4-25 (c), the post-cracking stiffness and load-carrying capacity decrease significantly, and more importantly, earlier initiation of cracking is observed. This is because of pre-stress force loss in the stands resulting from corrosion-induced cross-section area loss in strands. The comparison between the effects of corroded mild steels and strands on structural deterioration shows that the corroded strands affect more than corroded mild steels. The combined effects of the corrosion-induced cross-section loss in both mild steels and strands are shown in Figure 4-25 (d). Figure 4-25 (e) shows that nearly no effect of corrosion-induced cross-section loss in stirrups at low corrosion degrees (e.g., < 30% for girder #1), but the load-carrying capacity decreases if the corrosion degree is high (e.g., > 40% for girder #1). A further investigation shows that when the corrosion degree reaches a critical value of 33% for this PC girder, failure mode changes, as indicated by the failure crack pattern shown in Figure 4-26. When corrosion degree is lower than 30%, there are mainly vertical cracks in the constant moment span and some inclined cracks in shear span (see Figure 4-26 a); however, when corrosion degree is higher than 30% (see Figure 4-26 b), only few flexural cracks form near the midspan and inclined cracks spread on almost whole shear span, leading to shear failure of the girder. This failure mode change results in early failure of the girder along with a significant decrease on load carrying capacity.

Generally speaking, corrosion of strands affects more than the mild steels and it is even worse when both corroded: the capacity decrease is at most 10% for mild steel, 25% for

pre-stressed steel, and can be up to 40% for the combination case, as shown in Figure 4-27.

(a)

(b)

(c)

(d)

(e)
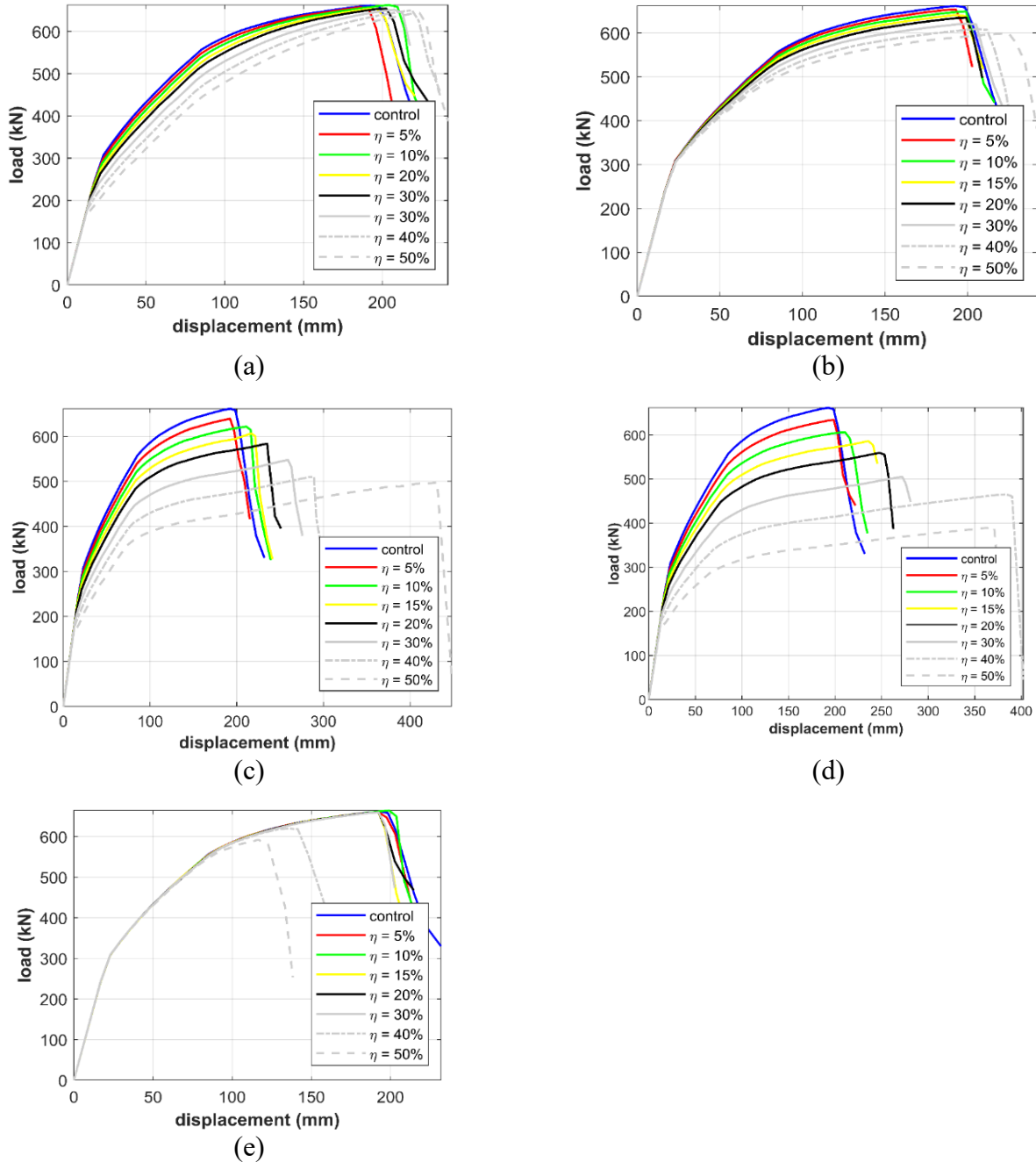
Figure 4-25: Comparison of load-displacement curves of PC girders with corrosion-induced (a) pre-stress loss, (b) mild steel section loss, (c) 7-wire strands section loss, (d) all tension steel section loss, and (e) stirrups section loss

(a)

(b)
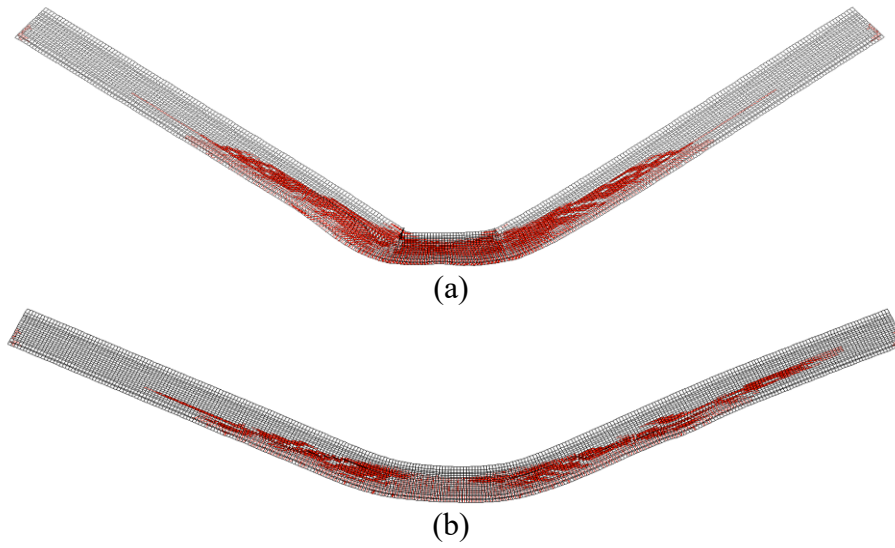
Figure 4-26: Representative failure crack pattern when (a) corrosion-induced cross-section loss in stirrups <= 30%, and (b) corrosion-induced cross-section loss in stirrups >= 40%
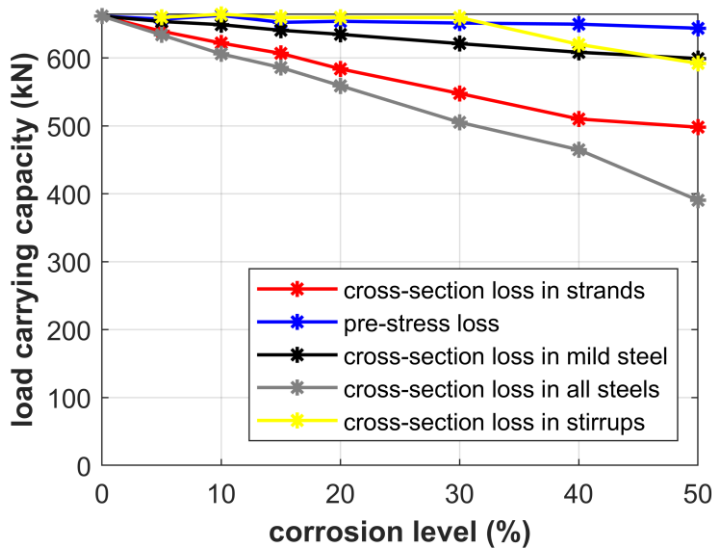
Figure 4-27: Load carrying capacities with respect to increasing corrosion degrees in various deterioration features

4.4.3.2   Material Degradation

Figure 4-28 shows the comparisons of load-displacement curves of PC girders with material property degradation due to corrosion of different levels. The material degradation considered consists of the compressive strength (f'_c) of the top cover concrete and the

ultimate strain of mild steels. Figure 4-28 (a) shows that before the corrosion degree reaches 30%, the girder fails earlier as corrosion degree increases, in turn the load carrying capacity decreases. This is because the failure of this girder is controlled by the crushing of the top concrete. However, when the corrosion degree exceeds 30%, post-cracking stiffness decreases due to the early crush of concrete top cover before the yielding of the steels. In contrast, the material degradation (i.e., the decreased ultimate strain ε_u) due to corrosion barely affects the girder behaviour, since the corrosion effect on the ultimate strain is relatively small such that the top concrete crushes earlier than the steel fractures (i.e., reaching the ultimate strain).
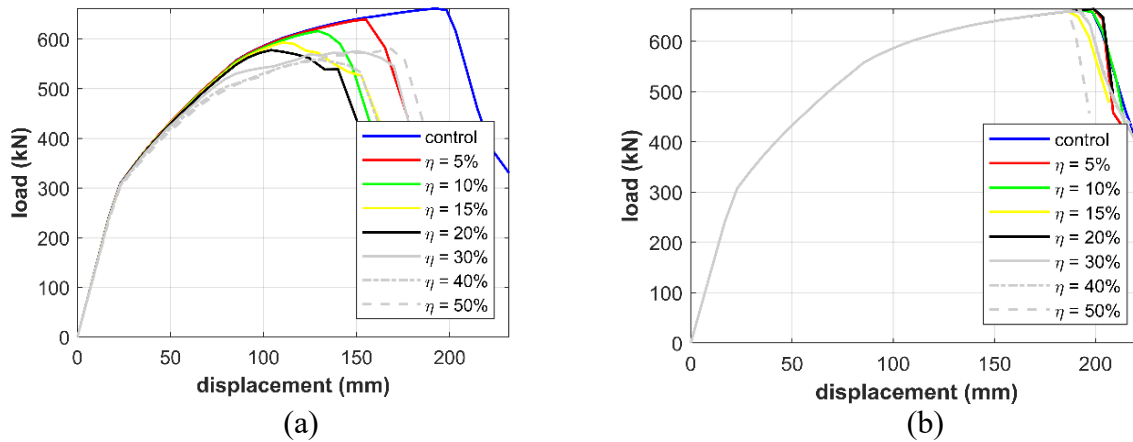
Figure 4-28: Comparison of load-displacement curves of PC girders with corrosion-induced reduction in (a) the compressive strength f'_c of the top concrete cover, and (b) the ultimate strain of the mild steel

4.4.3.3   Concrete Cover Spalling and Steel De-Bonding in Span

Figure 4-29 summarizes the load-displacement curves of PC girders with bottom concrete cover spalling in the fives series considered (i.e., L10, L20, L30, L50 and L100) with different spalling sizes and locations. Overall, the influence of concrete cover spalling can be negligible for the load-carrying capacity, and it only reduces the stiffness very slightly due to the geometry change of girder cross-section when spalling length is relatively long (i.e., longer than 30% of span). Figure 4-30 shows the load-displacement curves of PC girders with the bottom layer of steel reinforcement de-bonded but without loss of end anchorage. In general, there is negligible effect other than a slight decrease on load carrying

capacity and post-cracking stiffness, when the de-bonding length is longer than 30% of the span.

(a)   (b)

(c)   (d)
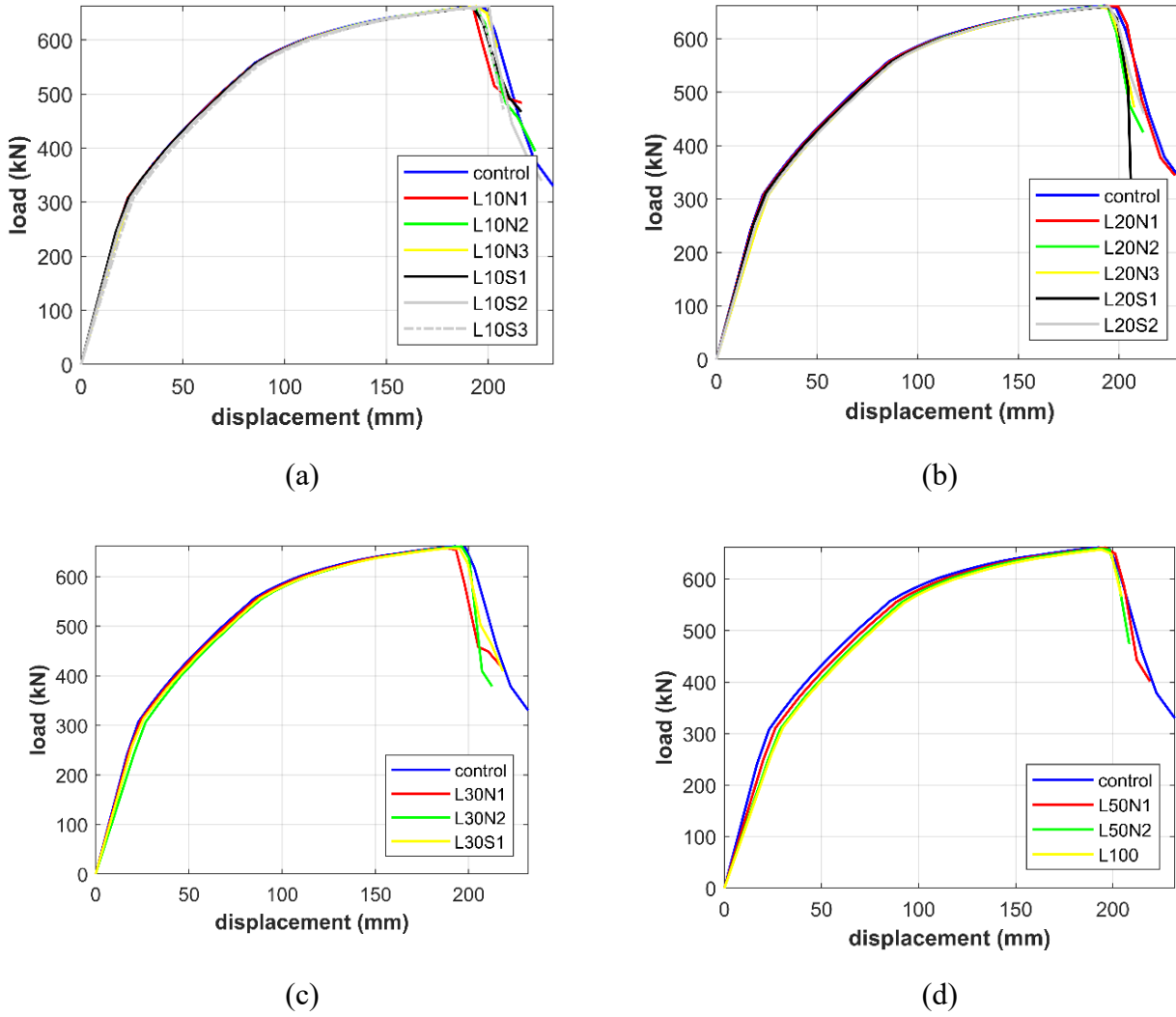
Figure 4-29: Comparison of load-displacement curves of PC girders with corrosion-affected bottom concrete cover spalling for (a) L10 series, (b) L20 series, (c) L30 series, and (d) L50 & L100 series
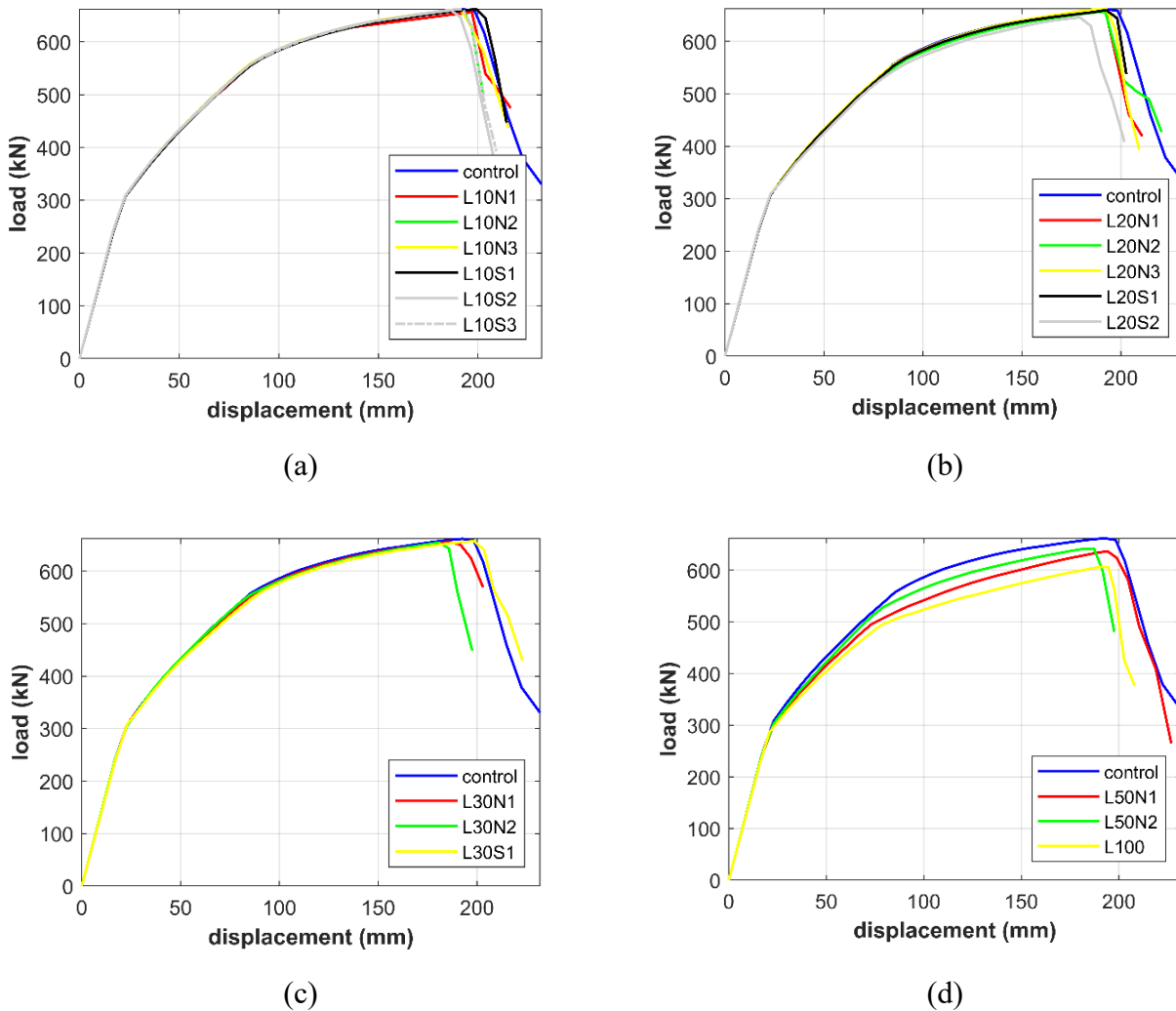
Figure 4-30: Comparison of load-displacement curves of PC girders with corrosion-affected steel reinforcement de-bonding for (a) L10 series, (b) L20 series, (c) L30 series and (d) L50 & L100 series

4.4.3.4   Bond Loss in the End Anchorage

Figure 4-31 summarizes the comparison of load-displacement curves of PC girders with corrosion-affected bond loss in the end anchorage. Various levels of bond loss and different corrosion-affected zones close to the end anchorage are considered. The effect of bond loss in the end anchorage on the girder behaviour depends on both the corrosion degree and the corrosion-affected length. When the corrosion-affected length measured from the end to the middle of the girder is short (e.g., for L20S1, L30S1, L20N1 and L30N1), no corrosion effect is observed for low the corrosion degrees (ranging from 0% to 30%), but significant

corrosion effect (e.g., drastic drop) on the ultimate load and ultimate displacement is found as shown in Figure 4-31 (a) - (d). When the corrosion-affected length measured from the end to the middle of the girder is long (e.g., for L50N1, and L100), as shown in Figure 4-31 (e) - (f), similar trend but more severe effect is observed on the structural deterioration due to corrosion. In addition, with the loss of load-bearing capacity, the girder tends to behave more ductile.
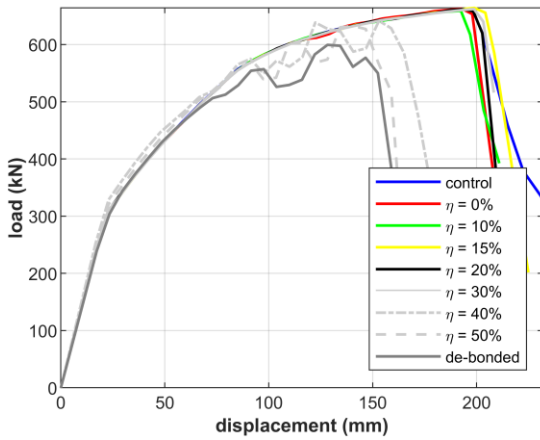
(a)
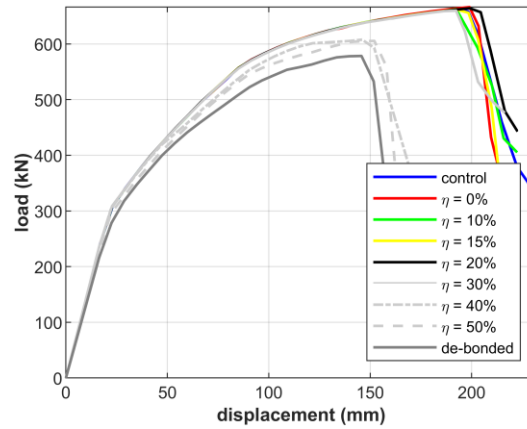
(b)
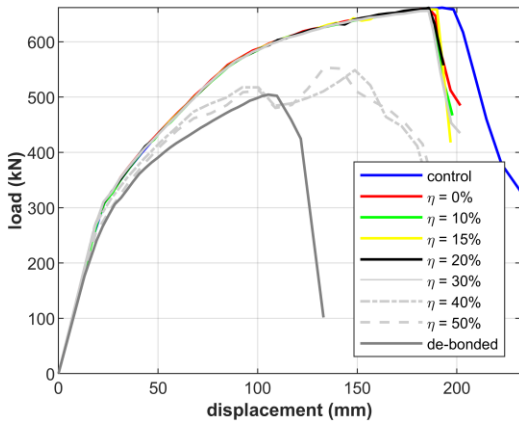
(c)
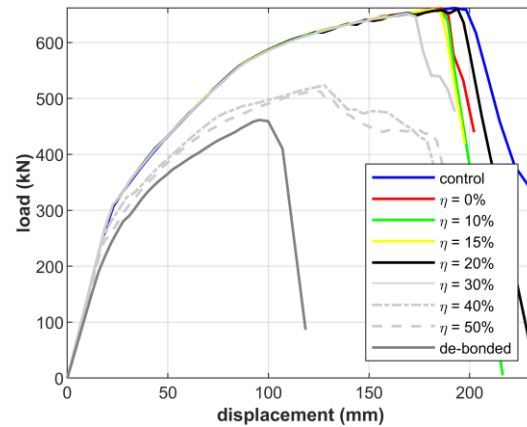
(d)
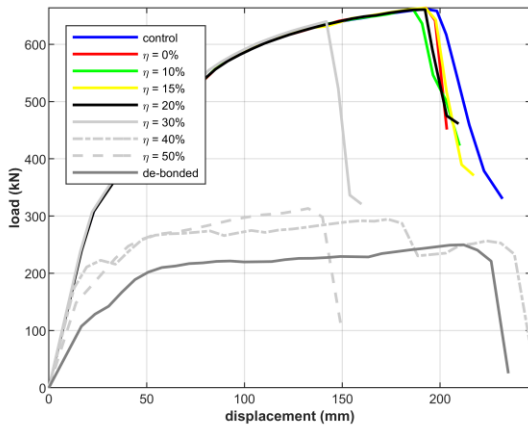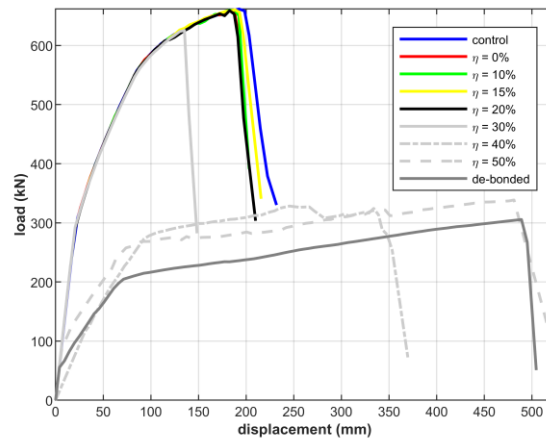
(e)   (f)

Figure 4-31: Comparison of load-displacement curves of PC girders with corrosion-affected end anchorage bond loss for (a) L20S1, (b) L20N1, (c) L30S1, (d) L30N1, (e) L50N1, and (f) L100

4.5   Other Girders Tested

4.5.1   Experimental Test and Preliminary Prediction for Girder #2

All girders removed from the bridge were visually inspected before the tests and girder #1 was considered as the one in the best condition. Additionally, an interior PC girder with the most severe deterioration (denoted as girder #2) was tested to determine the structural behaviour and further study the effect of deteriorations. The tested data was used to infer the deterioration states in the PC girder according to the parametric study performed earlier. Salvaged from the same bridge, girder #2 has the same dimensions with girder #1 that has least deterioration based on visual inspection. Before the flexural test, concrete spalling was observed at both bottom and top of the girder as shown in Figure 4-32 (a). The dimensions of spalling areas were measured before the test and indicated by the blue zones sketched in Figure 4-32 (b). In most of spalled zones, the depth exceeded the concrete cover depth and the bottom layer of reinforcements are exposed with some cross-section area deduction due to corrosion. The flexural test followed the same setup as the test of girder #1; as a result, the FE modelling strategy for girder #2 is the same as that for girder #1, as shown in Figure 4-33. Similarly, material models and properties used in the FE model are the same as the ones used for girder #1 since they are from the same bridge. Nevertheless, the measured concrete spalling is incorporated into the FE model for girder #2.

(a)
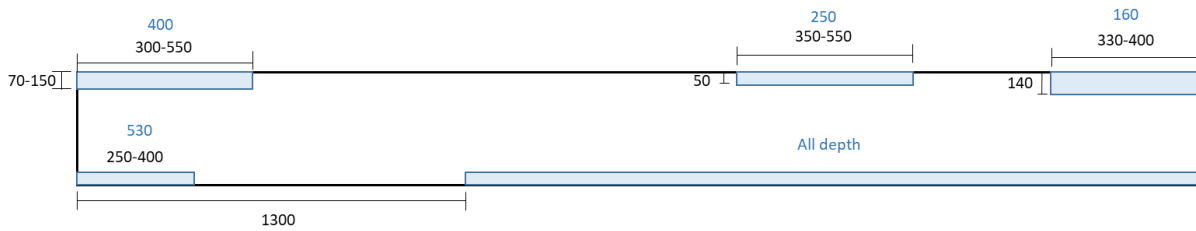
(b)

Figure 4-32: (a) Picture of girder #2, and (b) sketch of concrete spalling condition of girder #2
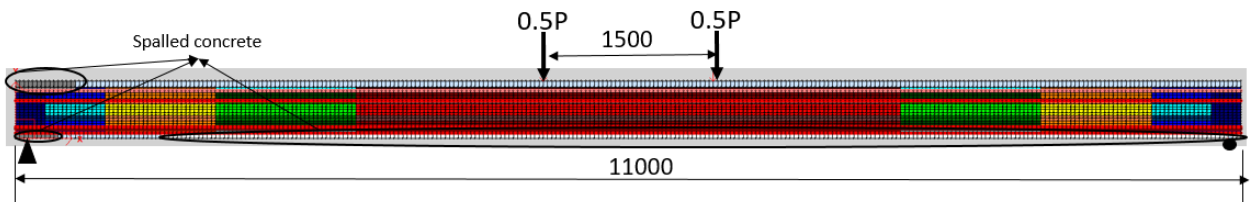
Figure 4-33: Modelling scheme of girder #2

Figure 4-34 (a) compares the tested load-displacement curve of girder #2 with that of girder #1. It shows that the general trend of girder #2 agrees well with girder #1. However, both initial stiffness and post-cracking stiffness of girder #2 are lower than those of girder #1, and it failed earlier than girder #1 because of strand rupture. As such, the load-carrying capacity of girder #2 (490.67 kN) is much lower than that of girder #1 (636.68 kN).

The tested load-displacement curve of girder #2 is also compared with the one predicted from the 2D FE model considering the additional pre-stress force loss (e.g., 30% and 40%) as discovered for girder #1, as shown in Figure 4-34 (b). The load-displacement curves exhibit better correlation with the tested one, compared with the case ignoring the additional pre-stress loss. However, the post-cracking stiffness is still higher than the tested one, even though the predetermined concrete spalling has been taken into account. Additionally, the FE-predicted strength is much higher than the tested one, and such discrepancy can not be explained by the pre-stress loss as learned earlier. This implies that more deteriorations other than pre-stress loss could have occurred to girder #2, which was observed to have the most severe deterioration. Thus, further analyses considering more deterioration features are needed to provide more insight into the girder behaviour.
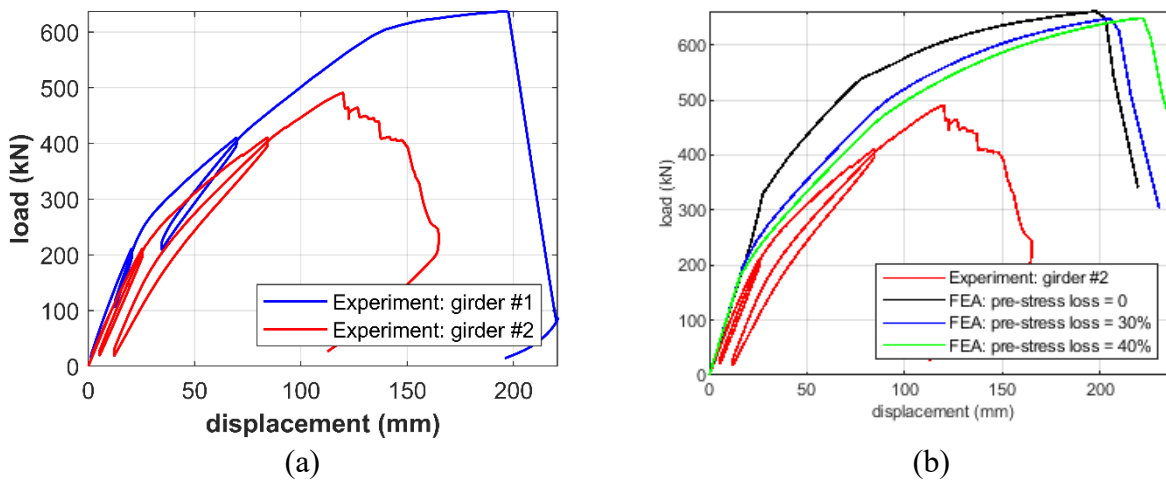
Figure 4-34: Comparison of the tested load-displacement curve for girder #2 with (a) tested one for girder #1, and (b) FE-predicted ones considering different levels of pre-stress loss

4.5.2 Possible Deteriorations Analysis for Girder #2

In order to understand the deteriorated structural behaviour of girder #2 better and infer the deterioration states in girder #2 that could not be visually inspected, more possible factors are considered with reference to the parametric study presented earlier.

During the test, the girder failed due to the fracture of strand wires (see Figure 4-35) in an early stage. Thus, it can be inferred that the ultimate strain (i.e., fracture strain) changed

due to corrosion (Li et al. 2012, Zhang et al. 2017). It is also learnt that the fracture strain of corroded strand is one of the deterioration features, which can be incorporated into the FE model for girder #2 to under the behaviour of other similar bridge girders (e.g., girder #3).

Figure 4-35: Picture of girder #2 after test with ruptured strand wires

Note that a large amount of concrete cover spalling exposed longitudinal steels on both tension and compressive side, resulting in the corrosion of the reinforcement. According to the parametric study, spalling of bottom concrete has negligible effect on structure behaviour, and the degradation of compressive strength of the remaining top concrete (cover) affect the post-cracking stiffness little. On the contrary, the post-cracking stiffness can be affected by the cross-section area loss in the mild steel or strands, bond deterioration, and the pre-stress force loss. Consequently, without detailed information on these aspects (e.g., from non-destructive testing), numerical analyses were performed to infer the possible deterioration levels by considering one at a time. The following four cases are studied.

Case 1: To explain the earlier failure of girder #2 and the post-cracking stiffness, the fracture strain of 0.0066 and the cross-section area loss of 15% for the strands is considered. As shown in Figure 4-36 (a), both the earlier failure of girder #2 and the post-cracking stiffness can be captured with these extra deteriorations, in addition to the 40% pre-stress loss inferred from girder #1 and concrete spalling observed.

Case 2: Similarly, as shown in Figure 4-36 (b), both the earlier failure of girder #2 and the post-cracking stiffness can be explained with the extra deteriorations in the fracture strain of 0.0066 for the mild steel area loss of 20%.

Case 3: Since almost all bottom concrete cover is spalled for girder #2 and the longitudinal steels are observed to be corroded, bond between concrete and steels is very likely to deteriorate. As a result, intermediate bond loss is assumed for the steels on the bottom layer through the whole girder in this case. As learned from the parametric analysis, the intermediate bond loss can also play a significant role on the post-cracking stiffness. It is found that together with the deterioration in the fracture strain (0.0066) for the strands, an intermediate bond loss corresponding to a corrosion degree of 40% can also explain the deteriorated structural behaviour well, as shown in Figure 4-36 (c).

Case 4: Since girder #1 is believed to have 30% ~ 40% pre-stress loss and such loss can be more severe for girder #2. Additional pre-stress loss is considered in this case, and it is found that an additional 10% pre-stress loss, a total of 50% pre-stress loss with the deterioration in the fracture strain (0.0066), can help explain the post-cracking stiffness (see Figure 4-36 d).

The aforementioned studies indicate that the current deteriorated structural behaviour can be explained by any of one of the above cases, or the combination of different deterioration features. Note that identification of the damage source is challenging as in structural health monitoring, where only a global damage measure can be determined (e.g., stiffness change). However, the study of possible sources of damage helps to provide guidance on inspection or non-destructive testing of similar girders.
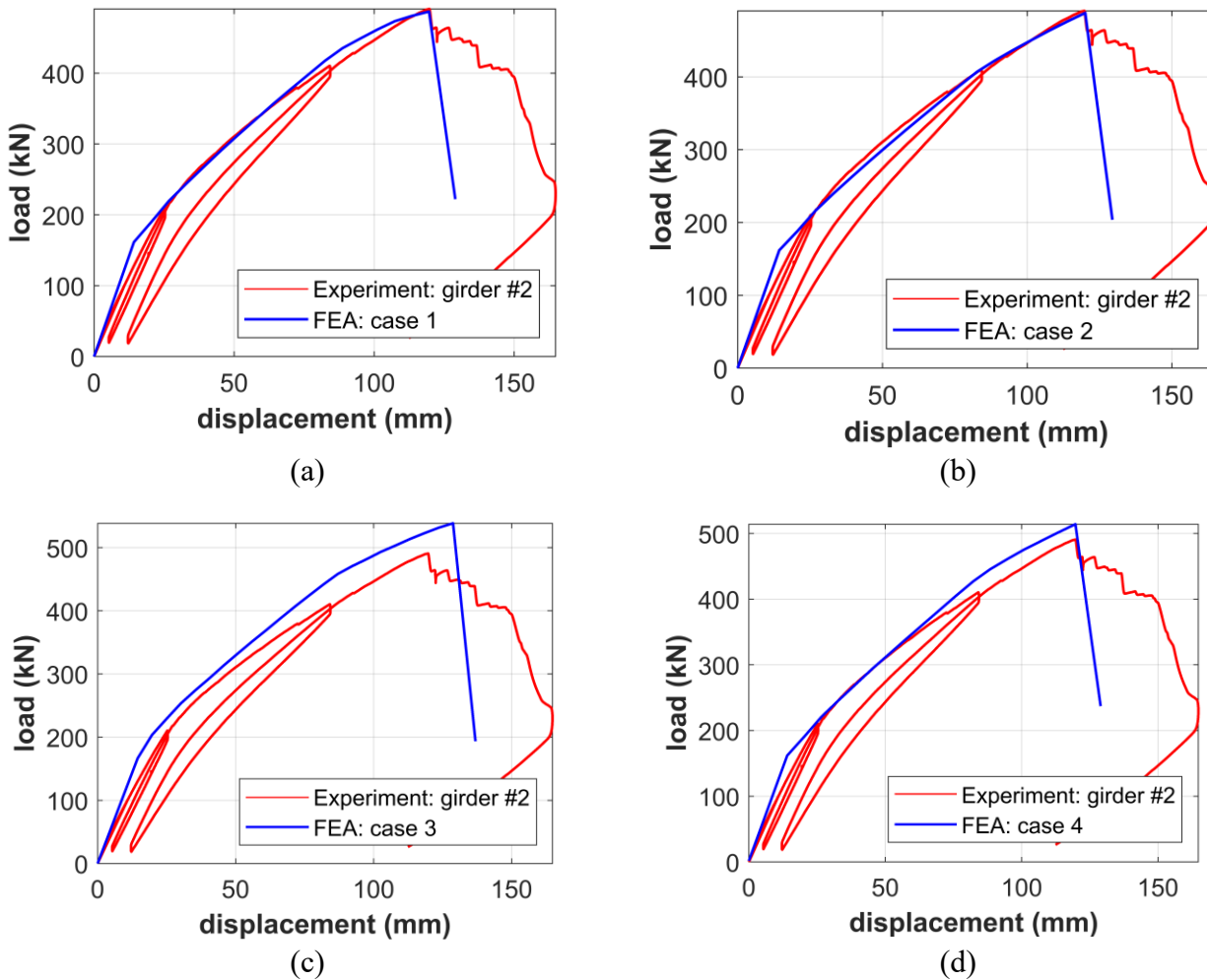
Figure 4-36: Load-displacement curve comparison for girder #2 between the test results and the simulation results with possible deteriorations: (a) case 1, (b) case 2, (c) case 3, and (d) case 4

4.5.3 Preliminary Analysis of Girder #3

The third girder removed from the same bridge for testing is observed to have closer deteriorations to girder #2, but with a slightly better condition as judged visually. Even though no significant concrete spalling was observed on girder #3, longitudinal cracks on the tension side were visible. Under the similar testing condition to girder #1 and girder #2, the girder failed at 546 kN when top concrete crushed in the midspan.

The tested load-displacement curve for girder #3 is compared with the FE-predicted curves by assuming intact girder condition, girder #1 condition, and girder #2 condition assuming case 3 (see Figure 4-37 a). It shows that the load-carrying capacity and stiffness of girder

#3 is much lower than the intact girder and the FE prediction assuming girder #1 condition. In contrast, FE prediction assuming girder #2 condition provides a good loading behaviour, i.e., capturing both initial stiffness and post-cracking stiffness of girder #3, except the ultimate strength and displacement of girder #3. This is because the earlier facture of strand wires in girder #2. Further analysis based on the FE model assuming girder #2 condition, except considering no fracture strain reduction in the strands, confirms this, as shown in Figure 4-37 (b).

(a)

(b)
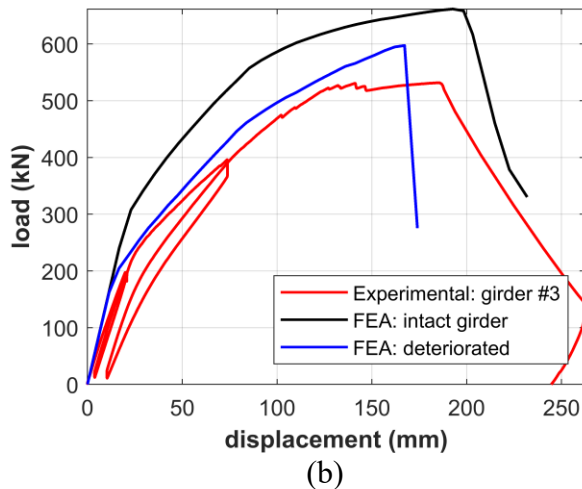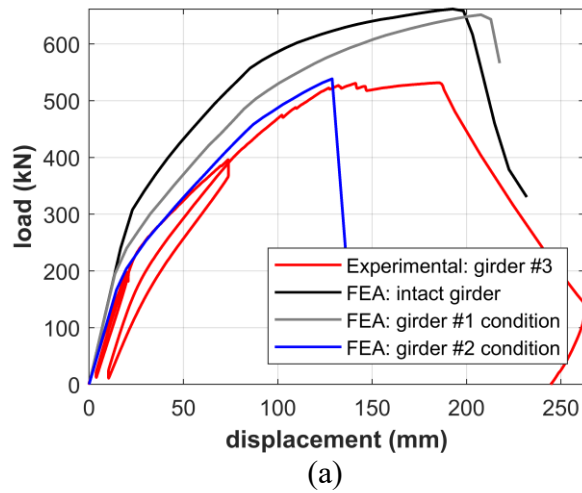
Figure 4-37: Load-displacement comparison for girder #3 between the test and FEA results assuming various conditions: (a) girder #1 and girder #2 conditions, and (b) girder #2 condition except no fracture strain reduction

106

4.6   Summary and Discussion

Both pre-test and post-test simulations were performed in this chapter for the visually "intact" girder #1 under the flexure loading condition (i.e., four-point bending). It was found that pre-test simulations (both 1D and 2D FE models) under predicted the girder strength significantly, and one of the primary reasons was the unexpected M25 bars in this girder. With detailed material information provided from the coupon tests and well calibrated material models, both the 1D and 2D FE models for the truly intact bridge girder failed to predict the structural behaviour of girder #1: the post-cracking stiffness was over-predicted significantly. A preliminary computational forensic analysis confirmed that an additional 30% ~ 40% pre-stress loss in the pre-stressing strands could explain the deteriorated structural behaviour of girder #1, the visually "intact" PC girder salvaged from a 27-year-old bridge in Alberta.

Based on the 2D model developed for the PC girder, a comprehensive parametric study was performed to investigate the structural deterioration due to corrosion-related damage, including steel cross-section area loss (in mild streel, strands, and stirrups), concrete spalling, top concrete cover material degradation, steel de-bonding, pre-stress loss, and intermediate bond loss including the end anchorage of steel reinforcements. It reveals that corrosion-induced cross-section area deduction of steels (particularly the pre-stressing strands), and the bond loss in end anchorage could decrease the stiffness and flexural load-carrying capacity of the PC girder significantly. In contrast, the spalling and in-span de-bonding (assuming full anchorage at ends) have little effect on structural behaviour. The parametric analysis can help engineers better understand the structural behaviour of deteriorated PC girders.

With reference to the behaviour of girder #1 and the parametric studies, the possible causes of structural deterioration in girder #2, which had most severe deteriorations as judged visually, were investigated. It was found that the deteriorated behaviour of girder #2 could be explained successfully, though the specific corrosion damage is un-identifiable. These preliminary forensic analysis can potentially provide guidance for bridge inspectors and evaluators, especially on non-destructive testing of similar bridge girders.

CHAPTER 5: INVESTIGATION OF CORRODED PC BRIDGE GIRDERS: SHEAR

5.1 Introduction

In addition to the flexural behaviour, the shear behaviour of corroded bridge girders is also of great concern for bridge administrators and engineers since shear failure is usually brittle without obvious signs, leading to catastrophic consequences.

To study the behaviour of deteriorated shear girders due to corrosion or other aging effect, limited experimental and analytical studies were conducted by researchers compared to the flexural behaviour. Xia et al (2011) investigated the shear performance of RC beams with corrosion in both longitudinal and transverse reinforcement by experimental tests. It was found that the stiffness and shear capacity decreased as the corrosion level increased and the failure of shear beam can be characterized by stirrup failure instead of concrete crushing when the corrosion level became severer. Kotsovos et al. (2015) studied the shear capacity of RC beams focusing on the effect of bond loss between longitudinal reinforcement and concrete. It was reported that the shear capacity could increase when the area of complete bond loss within the shear span was long and the failure mode can change from shear to flexural when the de-bonding is throughout the whole span. Juarez et al (2011) fabricated and tested RC beams with artificially corroded stirrups to study the corrosion effects on the ultimate shear strength. It was claimed that moderate and severe levels of deterioration could affect the ultimate shear strength more.

Compared with investigation on RC shear beams in the laboratory conditions, the studies on the aged girders salvaged from real-world bridges can contain more realistic corrosion-induced deteriorations. Murray et al (2017) conducted destructive tests on two 45-year-old bridge girders to study the shear strength. It was found that the girders performed well in general after 45 years service and different levels of corrosion at the ends did not affect the shear strength much except bond-slip observed. By contrast, Floyd et al. (2016) claimed that corrosion at the ends of a girder could cause spalling and bond loss and Osborn et al. (2012) performed shear tests on two girders removed from a 42-year-old bridge and found that corrosion deterioration could affect the shear capacity.

In order to investigate the residual shear strength of PC bridge girders after years of service, the tested flexural bridge girders with different levels of deteriorations were cut to short girders to study experimentally. In this research, a 2D FE model is established to simulate the behaviour of the shear girder. A comprehensive parametric study is then carried out based on the validated 2D FE model for the shear girder to investigate the influence of various types of deterioration on the shear behaviour of PC girders due to corrosion. The effects of different deteriorations on shear PC girders obtained from the study are then used to identify the possible causes of the degraded behaviour of other shear girders with severe deteriorations.

5.2   Simulation of Shear Girder #1

5.2.1   General Information

After the flexural test of girder #1, one end (denoted as shear girder #1) was cut for the shear testing. Note that it was assumed in a fairly good condition since the damage caused by the flexural test on the girder mainly occurred in the midspan The shear girder #1 is a beam segment of 3950 mm long beam, and the cross-section details are all the same as the original flexural girder #1 as shown in Figure 5-1, except the rigid end diagram (260 mm long). The shear girder is 36% long of the original girder #1, and the transverse reinforcements include: U-type G1001 spaced uniformly at 250 mm along the whole girder at top, U-type G1003 at the bottom, and G1004 hooks with an increasing spacing (e.g., 150 mm, 200 mm, 250 mm, and 350 mm) from the solid end to the other end of the shear girder #1.
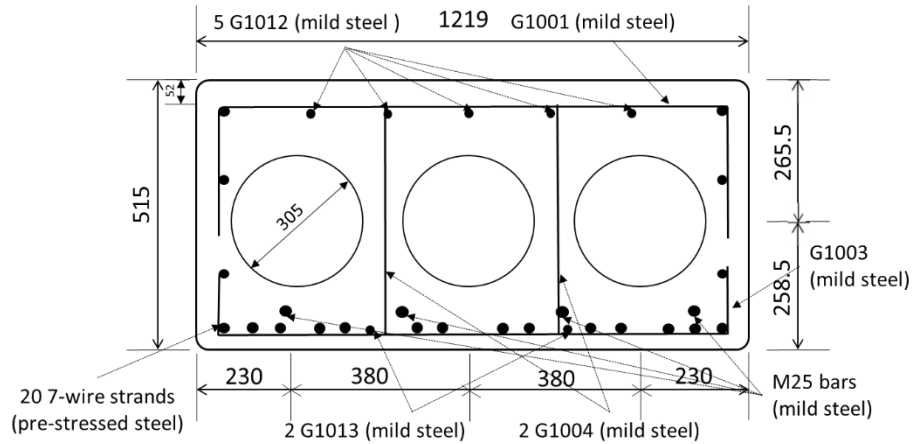
Figure 5-1: A representative cross-section for the shear girder #1

In the test, the shear girder was simply supported with a clear span equal to 3800 mm and subjected to a single point load 1000 mm away from the support, as shown in Figure 5-2. The load was displacement controlled and increased monotonically to the girder failure. Cable transducers were installed to measure the deflections of the girder as indicated in Figure 5-2.
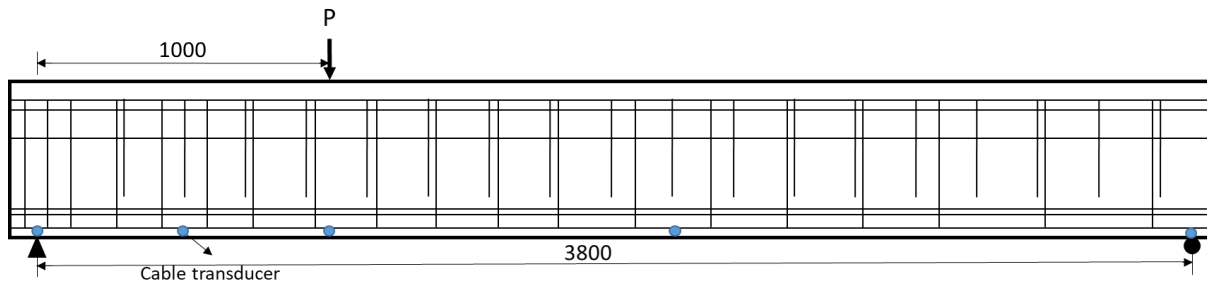
Figure 5-2: Sketch of the test setup for the shear girder #1

5.2.2 Finite Element Modeling

Same as the FE model for the flexural girder, concrete is modeled by 4-node plane-stress rectangular elements with an average mesh size of approximately 40 mm × 40 mm, and ten layers with four different thicknesses are assigned to the plane-stress elements to simulate the three voids in the hollow cross-section (see Figure 5-3 b). The longitudinal reinforcements (i.e., mild steel and pre-stressing strands) are simulated by 2-node truss bar elements. However, different from the FE model for the flexural girder where stirrups are

smeared in concrete elements, stirrups are modeled explicitly for the shear girder using 2-node truss bar elements in VecTor2. This is to represent the amount and position of the stirrups accurately, which could play an important role on the shear behaviour of the girder. The modeling scheme of the shear girder is shown in Figure 5-3.
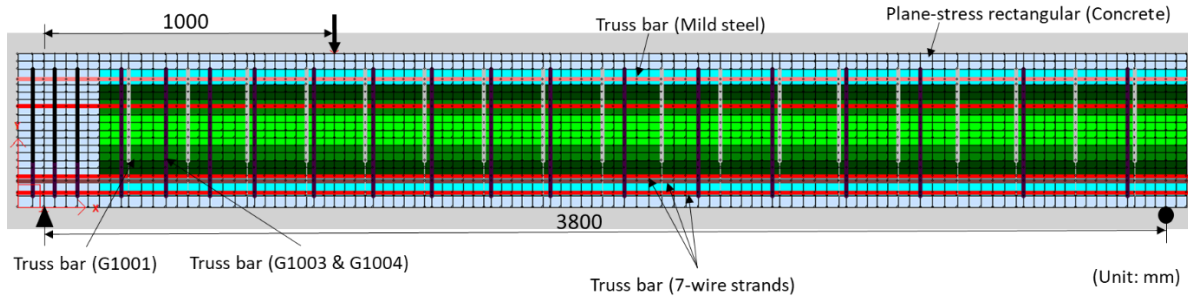
(a)
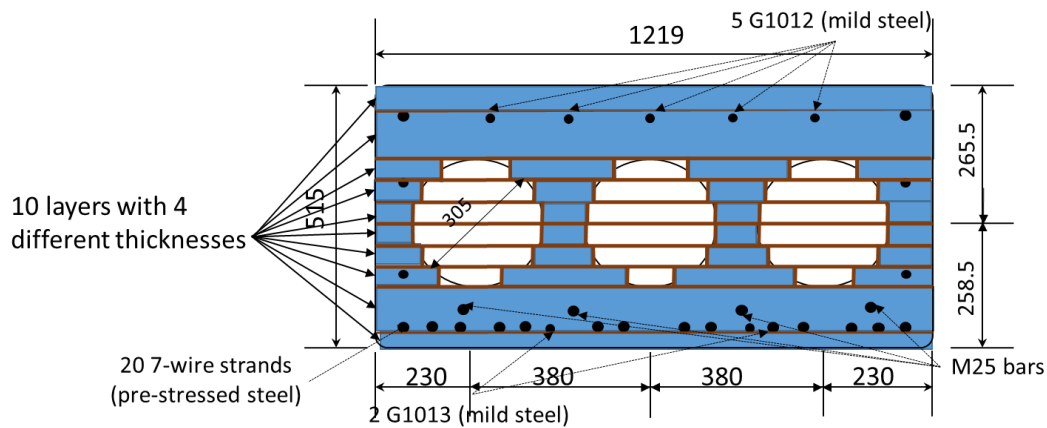
(b)

Figure 5-3: 2D FE modeling scheme of the bridge girder in VecTor2: (a) elevation view of the FE model of the simply supported shear girder #1, and (b) cross-section

The material properties of concrete and steel reinforcements from the tests are used for the FE model of shear girder #1, which are summarized in Table 5-1. The material models used in the FE model for shear girder are also consistent with the flexural model: *Popovics (High strength)* model and the *modified Park-Kent* model for pre-peak and post-peak behaviour of concrete material respectively; *Ductile Steel Reinforcement* model for mild steels and *Prestressing Steel* for 7-wire strands. The comparisons of material stress-strain curves in the model and from tests are shown in Figure 4-13 in chapter 4.

Table 5-1 Material properties in the FE model for shear girder #1

Concrete		Steel				
			longitudinal			transverse
parameter		parameter	M10	7-wire strands	M25	stirrups
f'_c (MPa)	55.5	f_y (MPa)	417	1676.5	413	424
f_t (MPa)	2.46	f_u (MPa)	670	1860	640	636
f_u (Mpa)	11.1	ε_y	0.0021	0.0085	0.0022	0.0022
E_c (Mpa)	25500	E_s (MPa)	198000	196500	203000	196000
ε_o	0.00286	E_{sh} (MPa)	6290	9657	5080	4610
ε_u	0.0048	Pre-stress force (kN)	-	107	-	-

5.2.3 Simulation Results

As inferred from the study of the flexure girder, there is an additional 30% ~ 40% prestress loss. For the purpose of comparison, the shear girder in the pristine condition (i.e., no additional prestress loss) is modeled. The load-displacement curve obtained from the 2D FE model is shown in Figure 5-4 (a) with critical points indicated. At point 1, the stiffness of the shear girder degraded due to inclined cracks that formed in the shear span between the loading point and the support, followed by vertical cracks on the bottom of the girder as shown in Figure 5-4 (b). After that, the stiffness of the girder continued to degrade along with the widening of the inclined cracks, and at the same time, more vertical cracks propagated under the loading point. When the applied load reached 1798.7 kN (i.e., at point 2), failure occurred to the shear girder with a drop in the load bearing capacity. It was shown that there were both flexural cracks and wide inclined cracks in the shear span, which caused the failure of the shear girder (see Figure 5-4 c). A similar phenomenon was observed for the tested shear girder, where a big inclined crack formed in shear span, leading to the failure of the girder (see Figure 5-4 d).
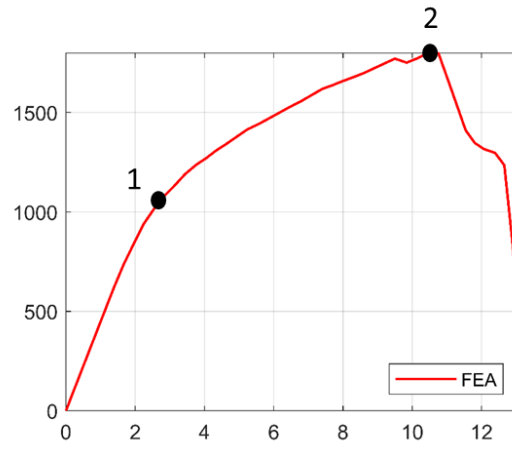
(a)
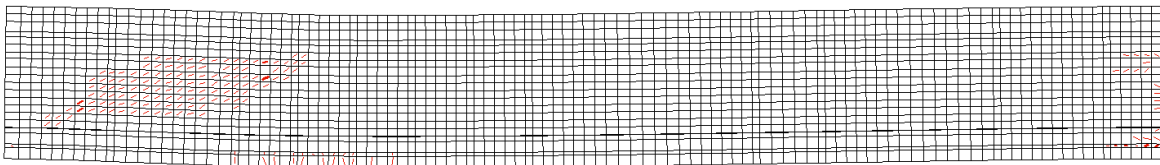
(b)
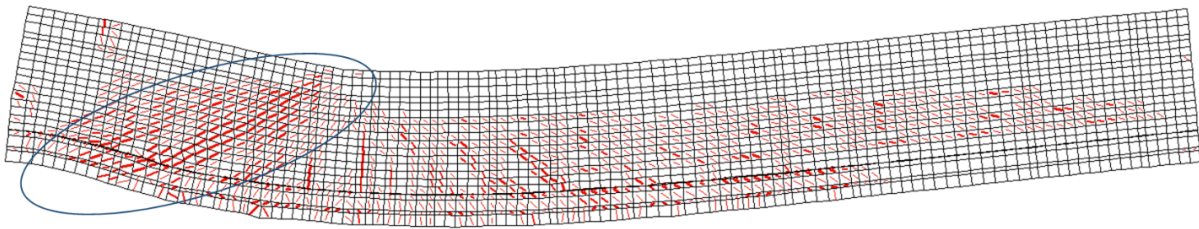
(c)

(d)

Figure 5-4: (a) Load-displacement curve predicted from 2D FE model with critical points indicated, (b) cracking pattern at point 1, (c) cracking (failure) pattern at point 2, and (d) failure pattern in the test

Figure 5-5 (a) shows the comparison between the FE-predicted and the experimental load-displacement curves, along with the analytical straight line to indicate the initial stiffness. The analytical prediction as indicated by the straight line is obtained based on unit load method assuming linear elastic material properties. It is found that the initial stiffness obtained from the FE model is approximately the same with the analytical estimation; however, there is a large discrepancy between the initial stiffness predicted by the FE model and the one obtained by the shear test. Nevertheless, the general behaviour of the load-displacement curve predicted from the FE model is similar to the test results, and the failure displacement is reasonably captured. However, the predicted load-carrying capacity (1798.7 kN) for the shear girder is much higher than the tested capacity (1406.1 kN) when assuming no additional prestress loss. Similar to the flexure girder, a possible reason could be the unknown pre-stress force in the shear girder #1. Thus, different levels (i.e., 0%, 20%, 30%, and 40%) of pre-stress loss are also considered to see their effect on the shear girder, and the load-displacement curves are compared in Figure 5-5 (b). It is observed that as the pre-stress loss increases, the load-carrying capacity of the beam decreases, and the case with 40% pre-stress loss leads to close FE prediction to the shear test result. This additional prestress loss level is consistent with the prestress loss level inferred from the flexure test.

114

This preliminary forensic study further confirms that the deviation between the FE prediction assuming pristine condition for the girder and test result can be caused by the deterioration such as prestress loss. Thus, it can be inferred that there is an additional 40% prestress loss in the girders tested.
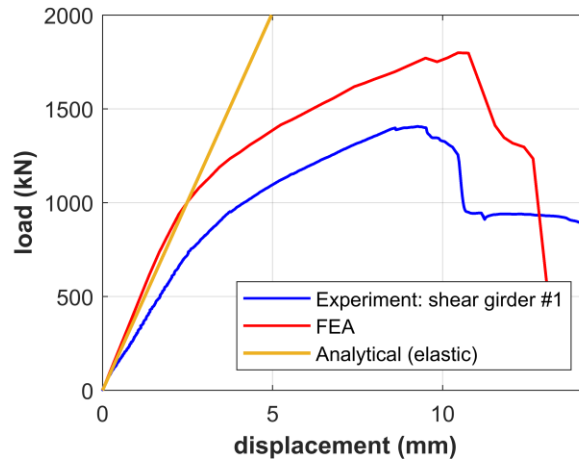
(a)
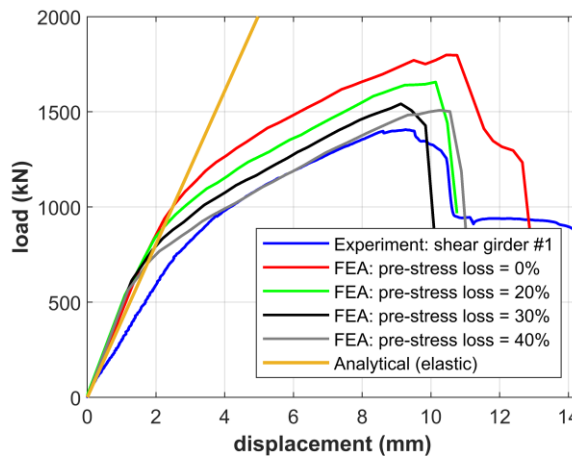
(b)

Figure 5-5: Comparison of load-displacement curves between the experiment and FE predictions (a) assuming pristine shear girder, and (b) considering different levels of pre-stress loss

5.3   Parametric Study for PC Girders with Deterioration

To study the effect of corrosion-induced deteriorations on the shear behaviour of aged PC girders, similar parametric analysis is performed for the shear girder. Note that in the test

of shear girder #1, the point load P was applied at 1000 mm away from the support (i.e., with the shear span depth ratio of 2.0 approximately), and the strut mechanism was observed in the test. The loading point for the shear tests was changed to be 1,500 mm away from the support to represent a truly shear failure mechanism, and thus the parametric analysis is performed using the FE model developed for shear girder #1, but with a different loading point (i.e., 1,500 mm away from the support).

5.3.1   Parametric Design

The corrosion features considered in the parametric analysis for the shear PC girder are similar to those considered for the flexural girder, including steel cross-section area loss, concrete spalling, tensile steel de-bonding, and intermediate bond loss including the end anchorage of steel reinforcements. All the parameters investigated are related to the corrosion degree, and the same corrosion degrees are considered as the flexure girder, i.e.,

η = 5%, 10%, 15%, 20%, 30%, 40%, and 50%.

5.3.1.1   Steel Section Loss

Since the studied girder has considerable amount of mild steels and pre-stressing strands, the effect of their cross-section area loss due to corrosion on the behaviour of PC girders are investigated. More importantly, cross-section area loss due to corrosion in stirrups is studied to see the effects of transverse steels on corroded PC girders under shear loading conditions. Pre-stressing force loss of strands is considered to be proportional to the cross-section area loss of 7-wire strands in the similar way as the parametric study of the flexure girder.

5.3.1.2   Cover Spalling and Steel De-Bonding in Span

To investigate the effects of concrete spalling due to corrosion in different length and locations, 7 cases are studied (see Figure 5-6). Four different spalling lengths (i.e. 10%, 30%, 50%, and 100% of the whole span) are considered. For a given spalling length, various locations are considered, which can be non-symmetrically or symmetrically located in the span of the girder. These cases are labeled in a consistent manner: the second letter (e.g., N) indicates whether the spalling is non-symmetrically (i.e., only one spot)

located in the span. The digits between "L" and "N" indicate the length percentage of each spalling spot over the span, and the last digit indicates the case number. For example, L10N1 denotes the beam with one concrete spalling with a spalling length = 10% of the whole span (case 1). The width of the spalling area is the same as the width of the girder and the spalling depth is the same as the concrete bottom cover depth.

As the concrete cover spalling naturally exposes the steel reinforcements, the bonding of steel with the surrounding concrete deteriorates. The extreme case, de-bonding of the very bottom layer of longitudinal steels, which consists of 4 mild steels and 14 7-wire strands, is considered to have no bond remain between steel and concrete. Similar to concrete spalling cases, the de-bonding effect is also studied in terms of de-bonding locations and lengths. Note that here only in-span de-bonding is considered and perfect anchorage at the ends is assumed to avoid the effects of anchorage failure, and end anchorage bond loss is considered later.

Figure 5-6 Parametric analysis cases to study the corrosion-induced bottom concrete cover spalling and steel de-bonding for the shear girder: (a) L10 series, (b) L30 series, (c) L50 series, and (d) L100 series

5.3.1.3   Bond Loss in the End Anchorage

Similar to the parametric analysis of the flexure girder, intermediate bond loss in addition to de-bonding is studied to take into account the corrosion-induced anchorage deterioration.

Some cases are selected (i.e., L10N1, L10N2, L30N1, L30N2, L50N1, L50N2, and L100) from previously designed ones, which are further extended in length to the ends of the girder in this study, as shown in Figure 5-7. The bond loss with various corrosion degrees is studied (i.e., $\eta = 10\%$, 20%, 30%, 40% and 50%), and the corroded bond-slip relationship is determined by bond-slip model from Eligehausen et al. (1983) as mentioned in Chapter 4.

(a)

(b)
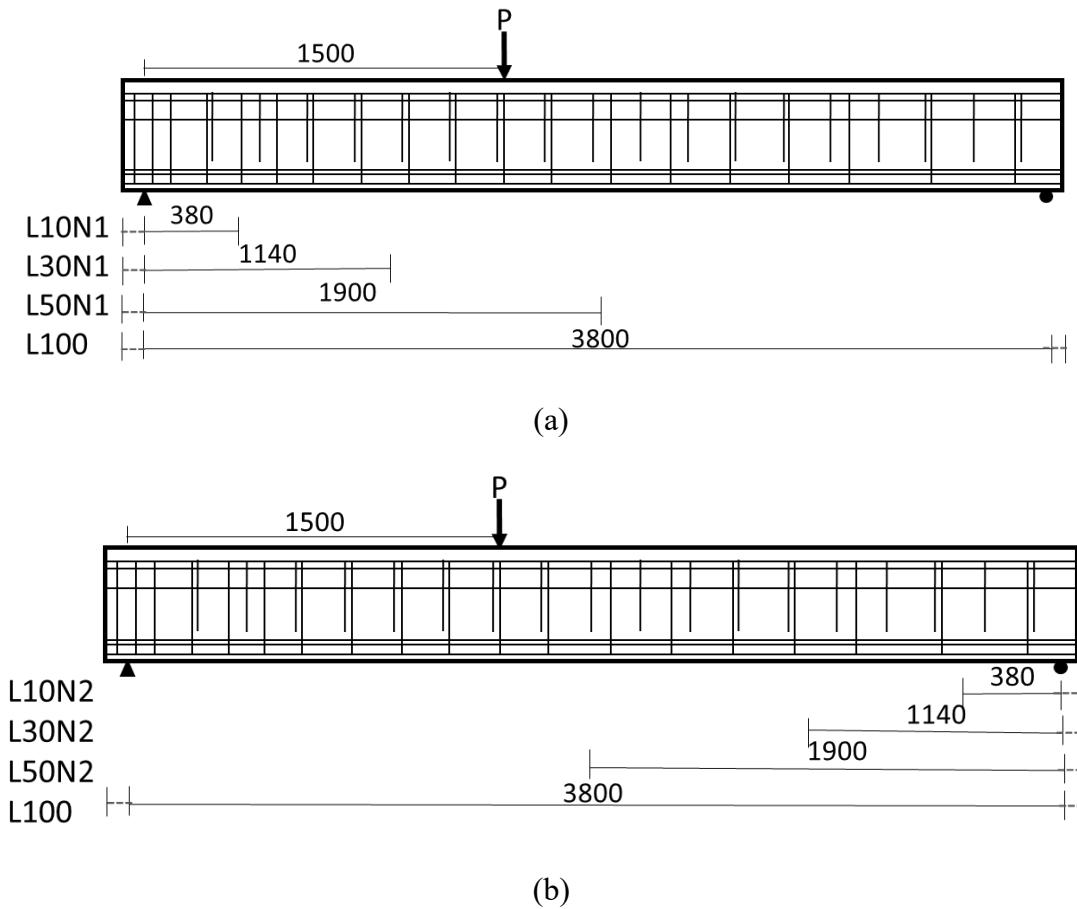
Figure 5-7: Parametric analysis cases for corrosion-affected anchorage bond loss of (a) N1 series and (b) N2 series

5.3.2 Deterioration Implementation in FE Model

The same modelling approach for corroded flexure girder is used for the corroded shear girder. Namely, the corrosion-affected geometric (e.g., steel section loss) and material (e.g., pre-stress loss) can be implemented by modifying the material parameters in the FE model.

However, corrosion-induced topological changes, such as concrete spalling and bond loss, need special treatment. The concrete spalling is modeled by deactivating the concrete elements (as indicated by white) in the spalling area, as shown in Figure 5-8 (a). The imperfect bonding is modeled the same way mentioned in chapter 4, as shown in Figure 5-8 (b).

(a)

(b)
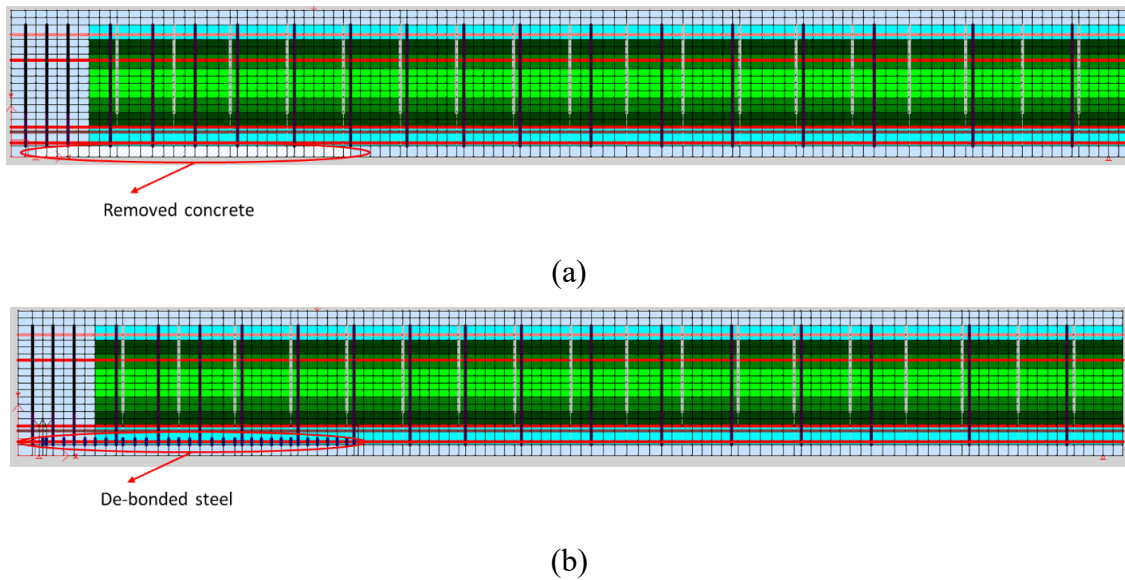
Figure 5-8: Modeling scheme of (a) concrete spalling, and (b) corrosion-affected bonding of steel

5.3.3 Parametric Study Results

5.3.3.1 Steel Cross-section Loss

Figure 5-9 shows the comparisons of load-displacement curves of PC shear girders with corrosion-induced pre-stress loss or reinforcement cross-section area loss under increasing corrosion levels. As shown in Figure 5-9 (a), this study of a wider range of pre-stress loss verifies that the effects of prestress loss observed when predicting the shear behaviour of shear girder #1, i.e., earlier crack initiation and load-carrying capacity reduction. It is also found that when cross-section deduction of pre-stressed strands increases due to corrosion, the post-cracking stiffness and the load-carrying capacity of the girder decrease significantly (see Figure 5-9 b). Moreover, the crack initiation happens earlier due to pre-stress force loss resulting from the cross-section area loss in strands. By contrast, as indicated by Figure 5-9 (c), even when mild steel corrodes with a fairly high level, there is

119

very little effect on the load bearing capacity and only slight decrease in stiffness can be observed. The combined effects of the corrosion-induced cross-section loss in both mild steels and strands are shown in Figure 5-9 d. It is worth mentioning that when the corrosion degree reaches 40%, the shear girder becomes more ductile. The comparison between the effects of corroded mild steels and strands on structural deterioration shows that the corroded strands affect more than corroded mild steels. It is found from Figure 5-9 (e) that the effect of corrosion-induced cross-section area loss in stirrups is limited when the corrosion degree is low (i.e., η <= 20%); however, when the corrosion degree is higher (e.g., 30% or more), the girder becomes more brittle with lower load-carrying capacities. In general, corrosion of strands affects more than the mild steels and it is even worse when both corroded: within the corrosion range considered (i.e., 0% - 50%), the decrease in the load carrying capacities is at most 7% for mild steel, 32% for pre-stressed steel, and can be up to 40% for the combined case, as shown in Figure 5-9 (f).

(a) (b)
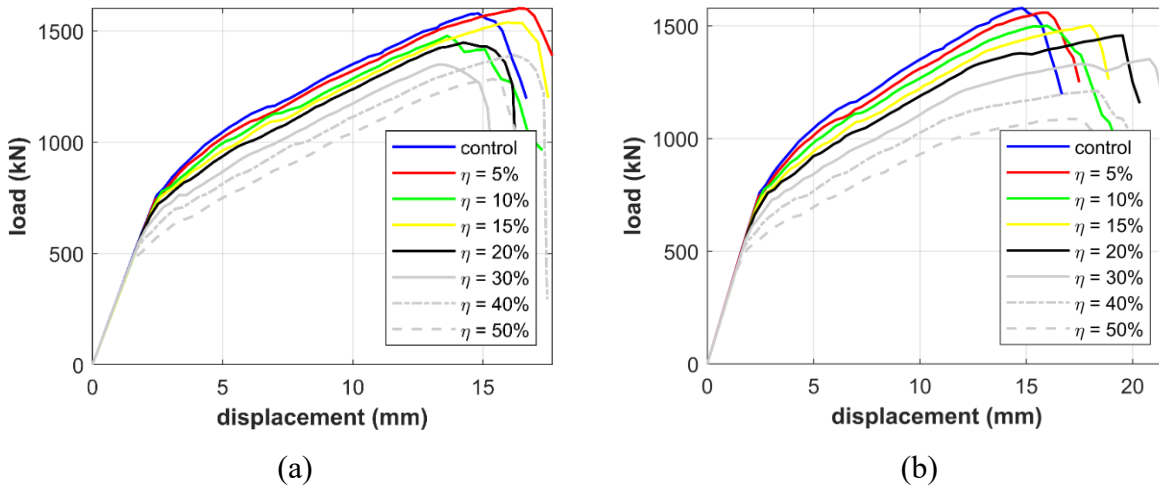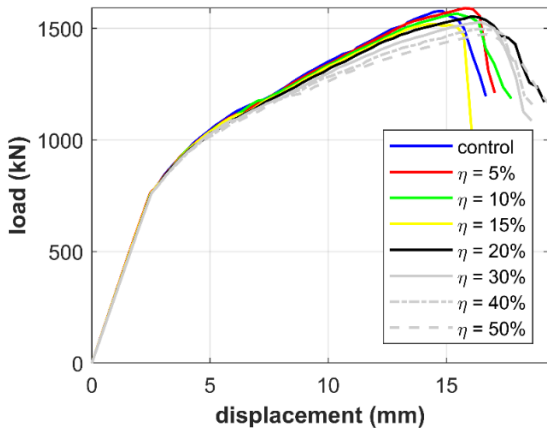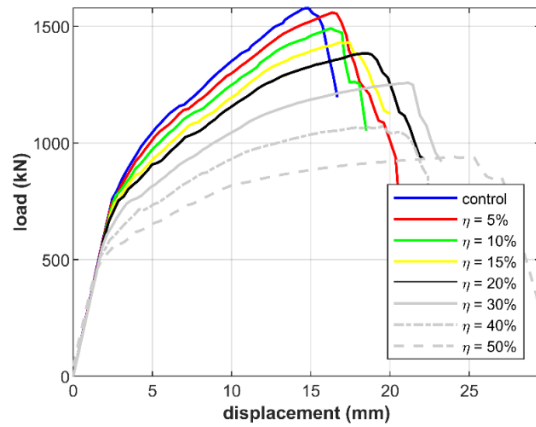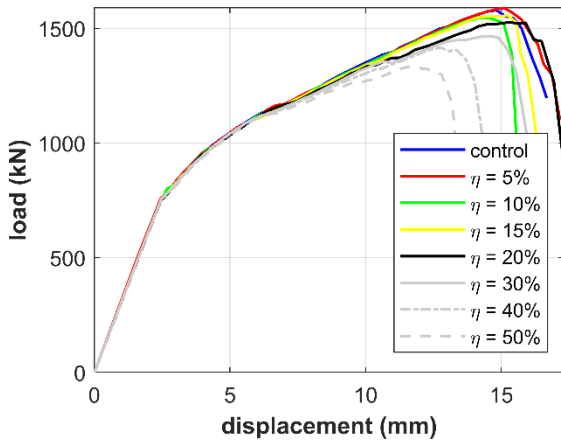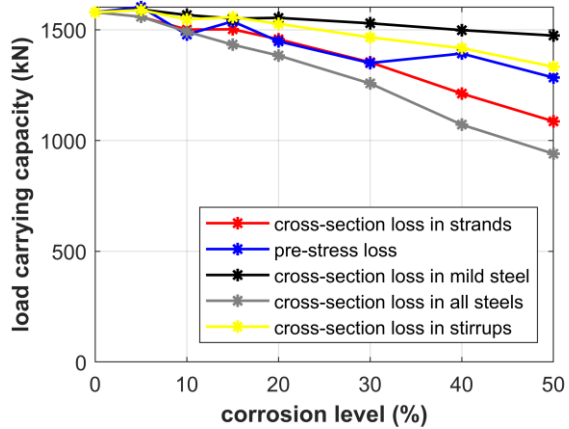
Figure 5-9: Load-displacement comparison of girders with (a) pre-stress loss, (b) 7-wire strands cross-section area loss, (c) mild steel cross-section area loss, (d) all tension steel cross-section loss, (e) stirrups cross-section area loss, and (f) capacities with respect to corrosion degrees in various deterioration features

5.3.3.2 Cover Spalling and Steel De-Bonding in Span

The spalling cases considered are shown in Figure 5-10 to investigate the effects of concrete cover spalling and steel de-bonding in the same ends but of different lengths. The load-displacement curves of the shear girders with bottom concrete cover spalling for N1 and N2 series are presented in Figure 5-11 (a) and (b), respectively. The comparison shows that the only influence of cover spalling is the slight decrease of stiffness and strength due to the geometry change of the girder cross-section when the spalling length is relatively

long (i.e., longer than 50% of span). The load-displacement results of the shear girders with de-bonding of the bottom layer of steel reinforcements for N1 and N2 series are shown in Figure 5-11 (c) and (d), respectively. Similar to spalling, there is no other effects than a slight decrease in the load-carrying capacity and post-cracking stiffness when the de-bonding length is longer than 50% of span. Overall, no noticeable effect of cover spalling or steel de-bonding in span is observed; thus, the influence of these two deterioration types are negligible for shear girders. Note that full anchorage is assumed at the ends of the girder here. The effect of deteriorated anchorage due to corrosion will be studied in the next section.

(a)

(b)
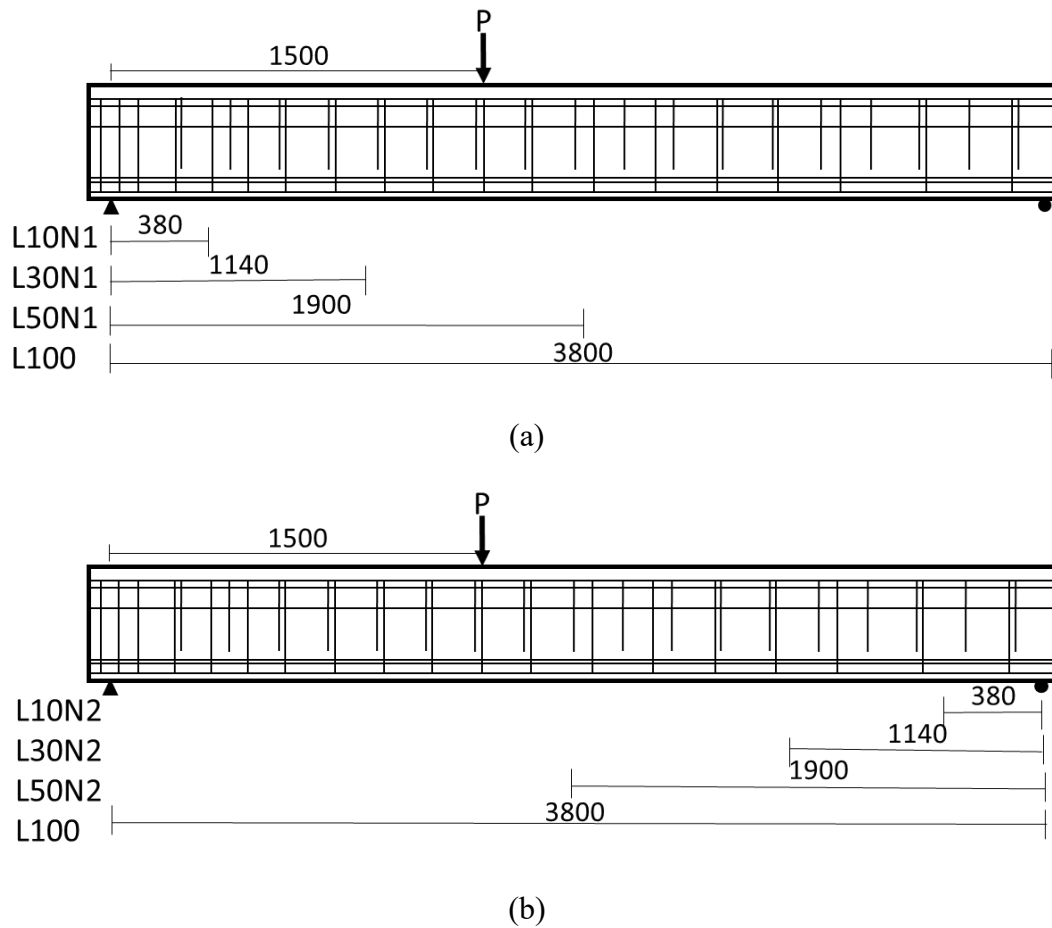
Figure 5-10: Design cases for steel de-bonding for (a) N1 series, and (b) N2 series
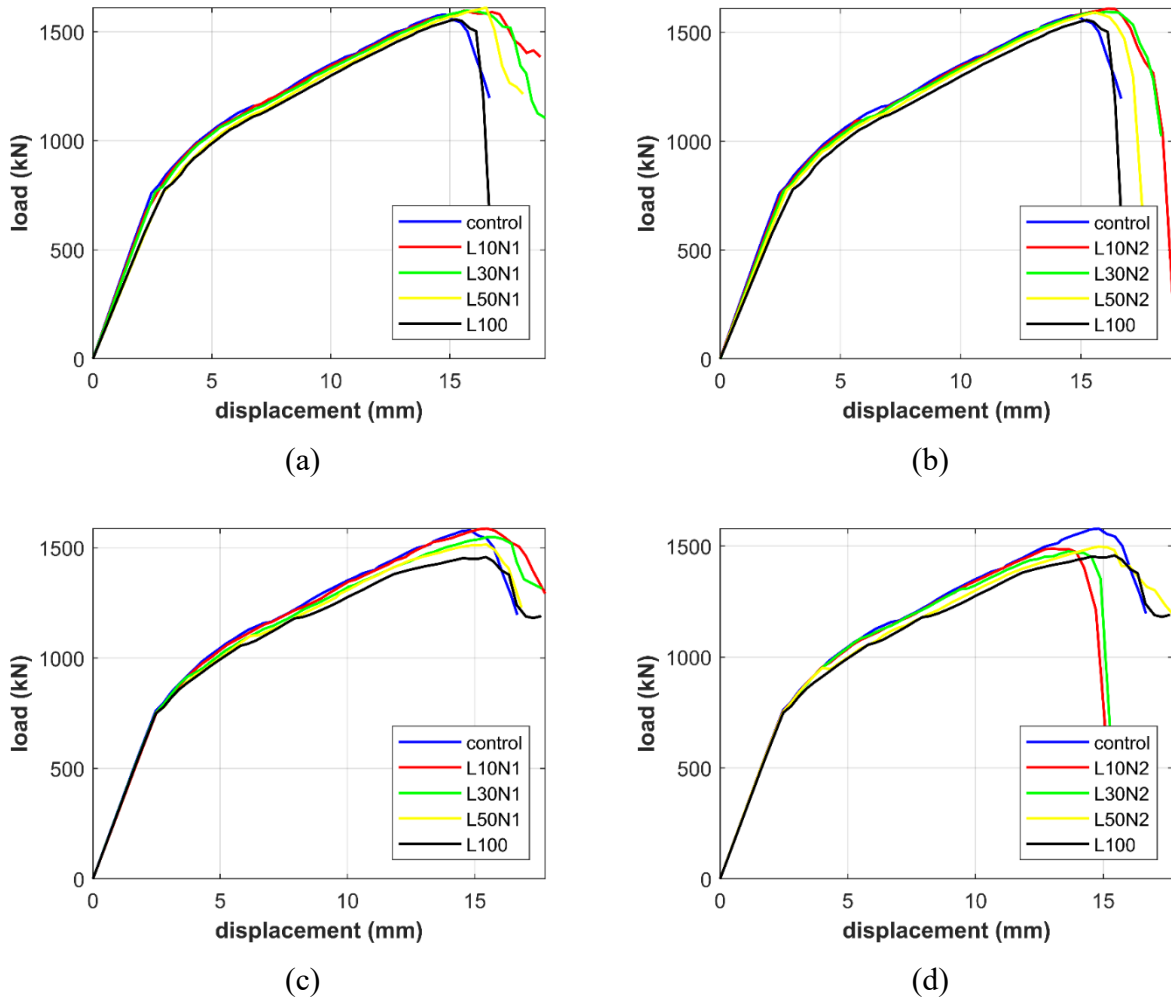
Figure 5-11: Comparison of load-displacement curves of PC shear girders with (a) concrete spalling in N1 series, (b) concrete spalling in N2 series, (c) de-bonding in N1 series with full anchorage at the ends, and (d) de-bonding in N2 series with full anchorage at the ends

5.3.3.3 Bond Loss in the End Anchorage

Figure 5-12 summarizes the comparison of load-displacement curves of PC shear girders with corrosion-affected bond loss in both the span and end anchorage (e.g., N1 series). The effect of bond loss with imperfect end anchorage on the girder behaviour depends on both the corrosion degree and the corrosion-affected length. When the corrosion-affected length measured from the end to the middle of the girder is short (e.g. L10N1), not much corrosion effect is observed for low the corrosion degrees (i.e., $\eta < 20\%$); but when the corrosion degree is larger than 30%, moderate drops in the load-carrying capacity and post-cracking

stiffness are observed in Figure 5-12 (a). When the corrosion-affected length near the shear span is long (e.g., for L30N1, L50N1, and L100), as shown in Figure 5-12 (b) - (d), there is limited effect of corrosion when the corrosion degree is lower than 20%. However, when the corrosion degree reaches 30%, the load-carrying capacity and post-cracking stiffness decrease significantly. In particular, when the corrosion degree is very high (i.e., $\eta > 40\%$), the girder starts to behave extremely ductile. It is interesting to note that further increase of the corrosion degree does not have more effect on the structural behaviour of the girders (e.g., L30N1, L50N1, and L100). This is because the loss of anchorage when $\eta > 40\%$ leads to the loss of the bottom layer of steel reinforcements in these girders. The two typical failure patterns are shown in Figure 5-13 for girders with different corrosion degrees (e.g., $\eta = 30\%$ and 50%) in the case of L100. It is observed that when the corrosion degree is 30%, the inclined shear cracks only form in the short span (see Figure 5-13 a), yet when the corrosion degree is 50%, the inclined cracks are spread in both spans together with some vertical cracks (see Figure 5-13 b).
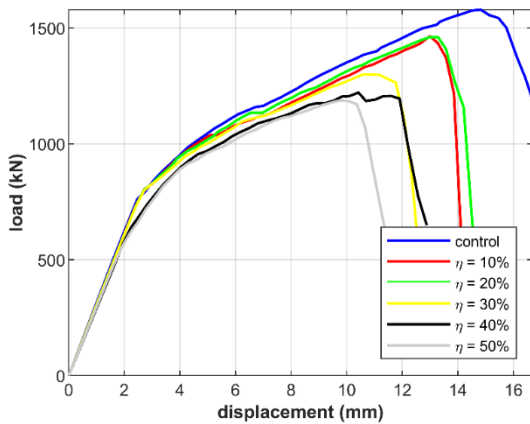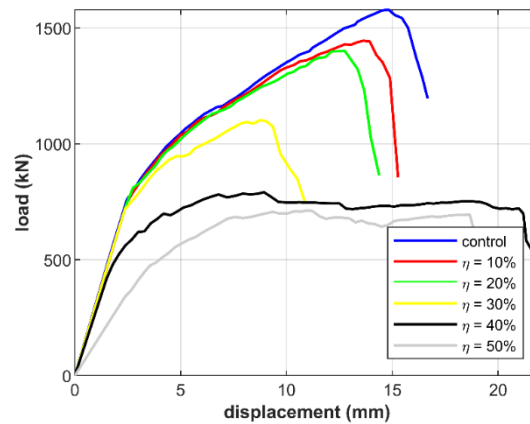
(a)   (b)
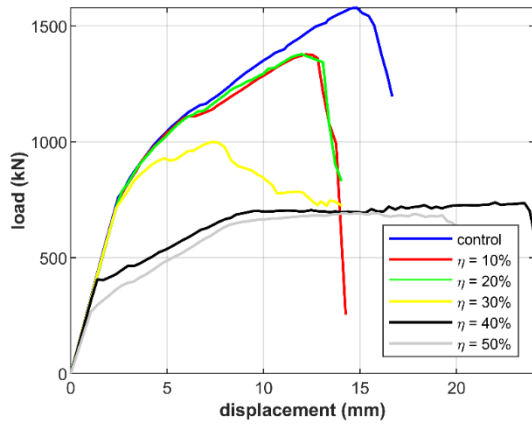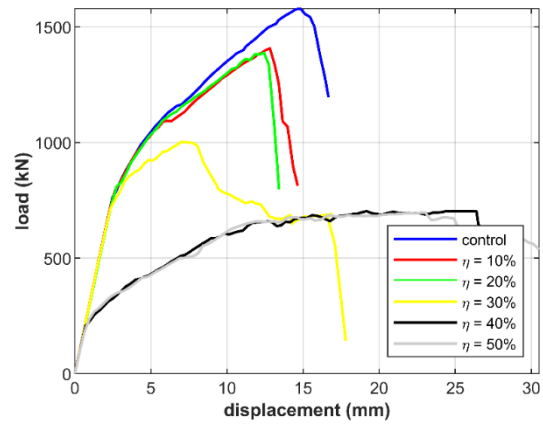
(c)   (d)

Figure 5-12: Comparison of load-displacement curves of PC girders with corrosion-affected end anchorage bond loss for (a) L10N1, (b) L30N1, (c) L50N1, and (d) L100
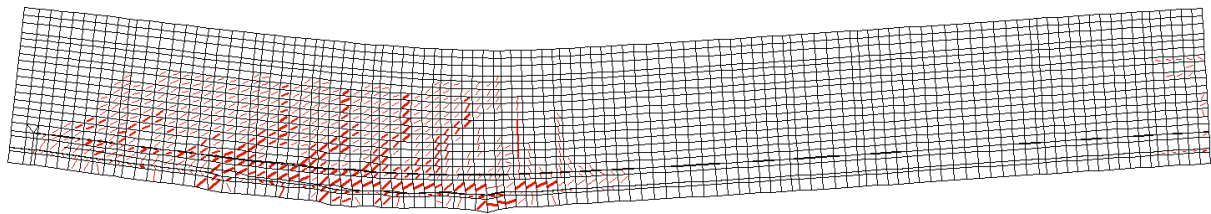
(a)
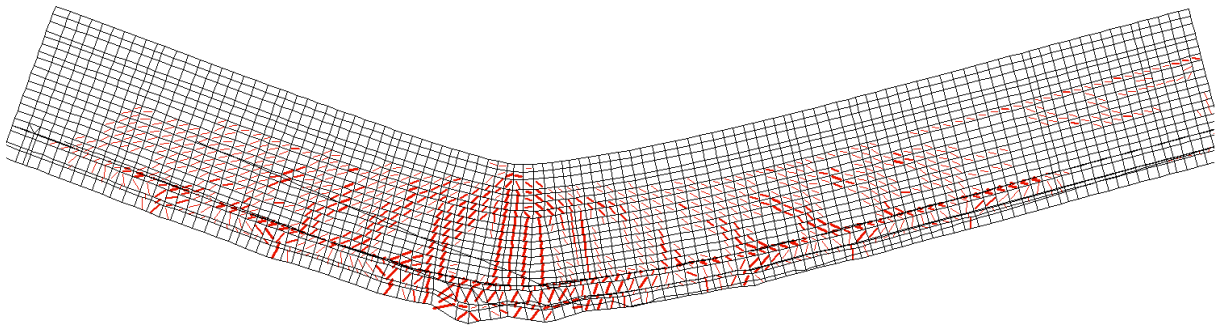
(b)

Figure 5-13: Failure pattern of girders in the case of L100 with a corrosion degree of (a) 30%, and (b) 50%

Figure 5-14 shows the comparison of load-displacement curves of PC shear girders with corrosion-affected bond loss and end anchorage loss (e.g., N2 series). When the corrosion-

125

affected length measured from the end to the middle of the girder is short (e.g., for L10N2), as shown in Figure 5-14 (a), a drop in the load-carrying capacity and post-cracking stiffness can be observed if the corrosion degree is high (i.e., $\eta > 30\%$). When the length of corrosion-affected zone is long (e.g., for L30N2 and L50N2), the load-carrying capacity decreases moderately as the corrosion degree increases. However, when the corrosion degree is high (i.e., $\eta = 40\%$ and 50%), the girder becomes more ductile and can have a lower initial stiffness.
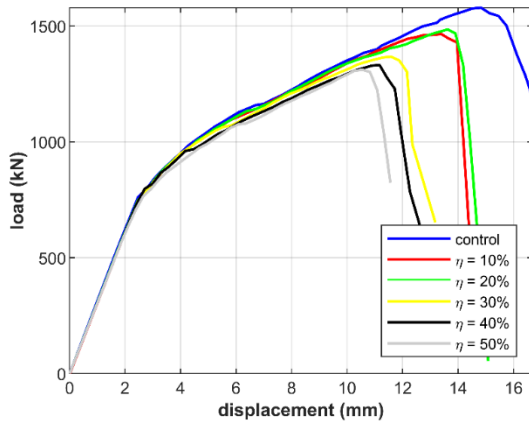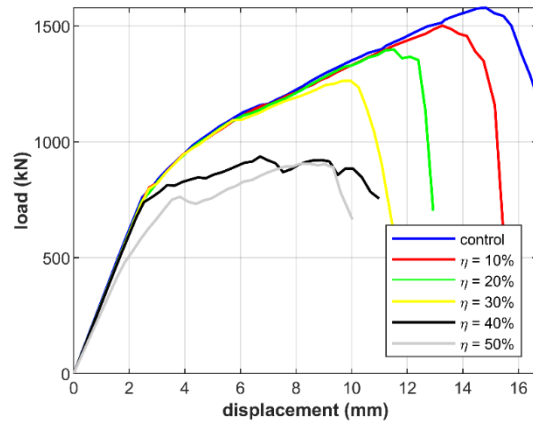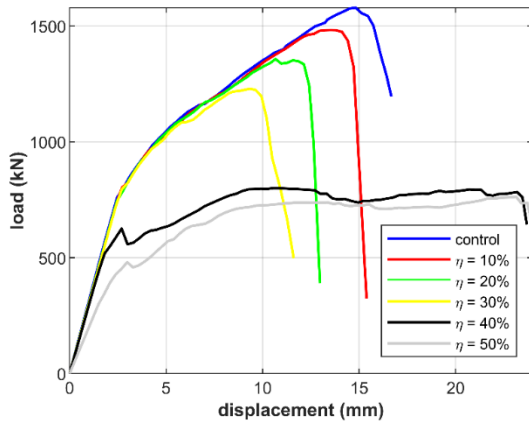
Figure 5-14: Comparison of load-displacement curves of PC girders with corrosion-affected end anchorage bond loss for (a) L10N2, (b) L30N2, and (c) L50N2

5.4   Other Girders Tested

In addition to shear girder #1, which was considered as the one in the best condition, shear girders with more deteriorations were tested to further study the effect of deteriorations. Therefore, a shear girder was cut from girder #2, which had the most severe deterioration, after the flexural test to conduct the shear test. The tested data was used to infer the deterioration states in the PC shear girder according to the parametric study performed earlier. The shear girder #2 had a length of 3,950 mm and the same cross-sectional dimensions as the flexure girder #2. Before the shear test, complete bottom concrete cover spalling along the whole span of the girder was observed, exposing the longitudinal reinforcement, as shown in Figure 5-15. Additionally, corrosion on the mild steels and strands caused the cross-section area deduction of the reinforcement. The shear test followed the same setup as shear girder #1 except that the loading point was 1,500 mm from the support (see Figure 5-16 a) to avoid the strut mechanism. The modelling strategy is same as that for shear girder #1, as shown in Figure 5-16 (b). Similarly, material models and properties used in the FE model are the same as the ones used for girder #1 since they are from the same bridge. Nevertheless, the concrete spalling measured in inspection is incorporated into the FE model for shear girder #2.

Figure 5-15: Picture of shear girder #2

(a)

(b)
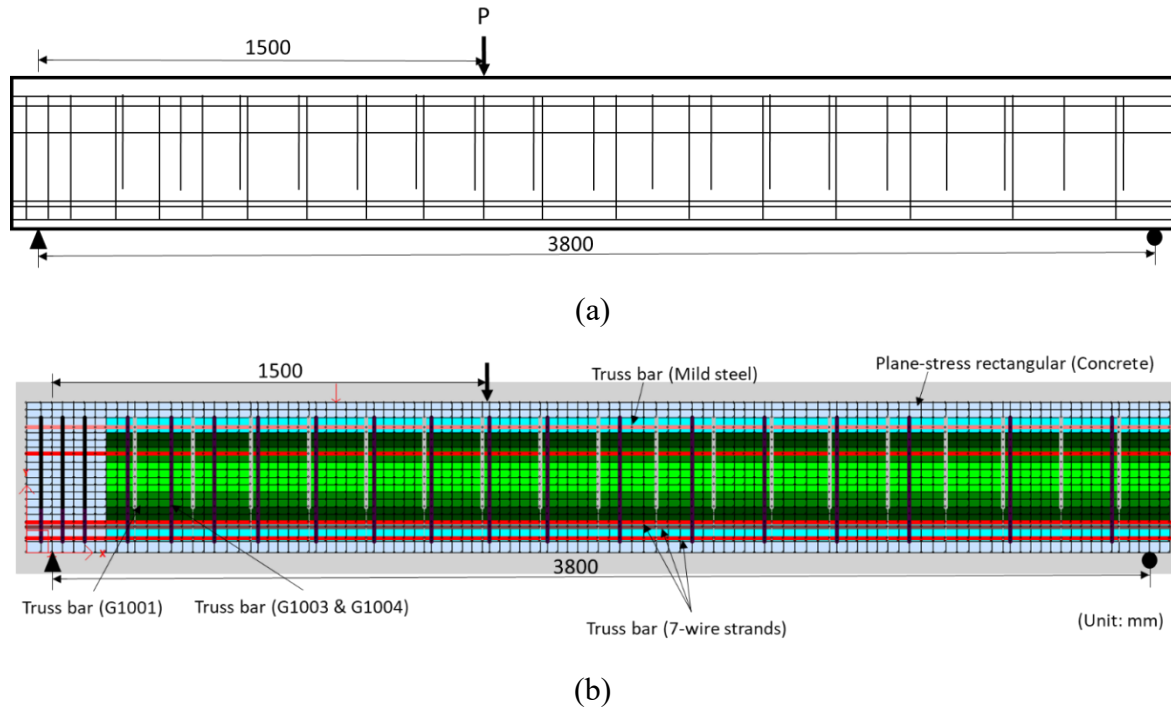
Figure 5-16: (a) sketch of test setup, and (b) modelling scheme of shear girder #2

5.4.1　Possible Deteriorations Analysis

Since shear girder #2 is cut from girder #2, four possible cases proposed for girder #2 in chapter 4 are tried on the shear girder #2 to further infer the possible deteriorations. The load-displacement curves from four cases are compared with experimental result and preliminary prediction in Figure 5-17. The preliminary load-displacement curve predicted from 2D model that considers only concrete spalling overestimates the stiffness and load-carrying capacity dramatically (see Figure 5-17). The predicted load-carrying capacity (1610 kN) is more than double the tested one (769.1 kN). It shows that cases 1, 2 and 4 have very close stiffness and general trend but overestimate the load-carrying capacity and stiffness significantly compared to the test. Case 3 provides the load displacement curve that agrees relatively well to the tested one for its well-matched trend, closest load carrying capacity (877.8 kN) and lower stiffness compared to the other 3 cases.
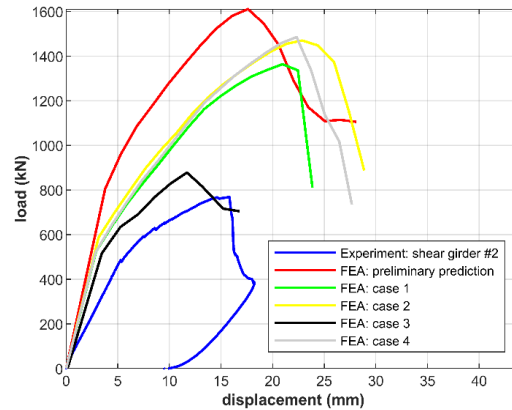
Figure 5-17: Load displacement curves of 4 deterioration cases on shear girder #2

5.4.2 Preliminary Analysis of Shear Girder #3

After the flexural test of girder #3, it was cut at two ends of the girder into two 3,800 mm span shear girders and tested with a 1,500 mm shear span. One of the two shear girders was modified by cutting 7 stirrups in the shear span to simulate fractured stirrups. The test showed that the modified shear girder #3 failed at 701 kN and the un-modified one failed at 692 kN and the post-peak behaviour was not captured in the lab due to sensor failure.

The load-displacement curves of modified and unmodified shear girder #3 from the tests are compared with the simulated curve of the intact shear girder and the case #3 of shear girder #2 in Figure 5-18 (a) to infer deterioration states. Compared to the model assuming the intact girder condition, which overestimates the load-carrying capacity and stiffness significantly, the model assuming girder #2 condition (case #3) provides better prediction in terms of general trend and the stiffness. However, it slightly overestimates the load-carrying capacity and post-cracking stiffness.

For the modified shear girder #3, additional stirrup removal is considered in the FE model, compared with the model for the un-modified shear girder #3. The comparison of experimental and simulated load-displacement curves is shown in Figure 5-18 (b) and it is observed that the predicted initial stiffness and load-carrying capacity agreed reasonably well with the test results though the post-cracking stiffness is overestimated. Comparing the predicted load-displacement curve of modified girder #3 with the unmodified one, it is

observed that the modified girder fails earlier due to the stirrup loss. Due to this early failure, simulation result fails to capture the failure of modified shear girder #3.
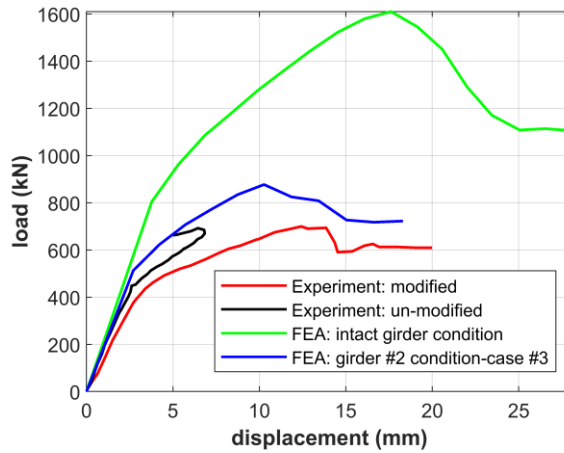
(a)
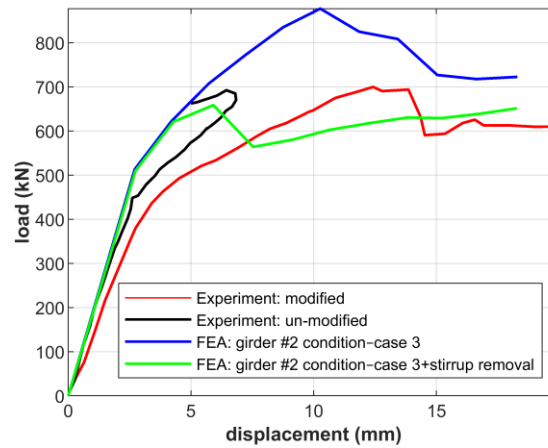
(b)

Figure 5-18: Comparison of load-displacement curves for the un-modified and modified shear girder #3 between the test results and FE predictions: (a) using the model assuming shear girder #2 condition case 3, and (b) using the model assuming shear girder #2 condition case 3 plus additional stirrup removal

5.5   Summary and Discussion

The shear test of a girder cut from tested flexural PC bridge girder is simulated by a 2D finite element model in this chapter. It was shown that the predicted structural behaviour of the shear girder #1 from FE model agreed well with the experimental result when

considering 40% pre-stress loss. A comprehensive parametric study was performed based on the developed numerical model to investigate the structural deterioration due to corrosion-related damage, including steel cross-section area loss (in mild streel, strands, and stirrups), concrete spalling, steel de-bonding, pre-stress loss, and intermediate bond loss including the end anchorage of steel reinforcements. It is shown that the concrete cover spalling and steel de-bonding in span have little influence on the residual shear behaviour of girders. In contrast, the steel cross-section loss, pre-stress loss and bonding loss with end anchorage failure could have a significant influence on the structural behaviour.

With reference to the parametric studies and the condition learnt from flexural girder #2, 2D FE model was used to study possible causes of structural deterioration in shear girder #2, which had the most severe deteriorations. It was found that the deterioration case #3 of flexural girder #2 can provide the load displacement curve that agrees relatively well to the tested one. The same deterioration case was then considered on girder #3. It was observed that the simulated load-displacement curve matched the test results well in terms of the general trend and the initial stiffness, although the load-carrying capacity and post-cracking stiffness are overestimated. Similarly, the simulated load-displacement curve of modified shear girder #3 generally captured the initial stiffness and the carrying capacity. However, the girder was predicted to fail earlier due to the removal of the stirrups.

CHAPTER 6: CORROSION EFFECT ON PROBABILISTIC CAPACITY OF PC GIRDERS

6.1   Introduction

The behaviour and capacity of PC girders with corrosion-induced deterioration was studied in a deterministic manner in previous chapters. However, uncertainties inherent with the PC bridge girders should be taken into account when assessing the effects of corrosion-induced deterioration on the capacity of existing PC girders.

Recognizing such a need, many researchers applied various probabilistic or stochastic methods to existing bridge girders. For example, Darmawan and Stewart (2007) developed probabilistic models for the strength of 7-wire strands, which were then combined with a non-linear model and probabilistic models for corrosion initiation and propagation to study the pitting corrosion effects on a typical PC bridge girder. In addition, Bin et al. (2010) and Guo et al. (2010) investigated the lifetime or time-dependent performance reliability of existing PC bridges under general corrosion attacks by considering the corrosion process. They mainly focused on the evolution of the structural performance as a function of time due to corrosion, instead of focusing on the conditional performance for given corrosion states. Since the corrosion process is highly environment-dependent and thus un-predictable even with current non-destructive testing and health monitoring techniques. To understand of corrosion effects on the probabilistic capacity of PC girders, it is important to investigate the effects of corrosion given a certain corrosion condition, i.e., conditional probabilistic capacity of PC girders.

To this end, this chapter will assess the probabilistic capacities of the PC girder considering two different corrosion levels, and compare those with the capacity of the intact PC girder (no corrosion). The most influencing corrosion features (e.g., cross-section area reductions in both longitudinal steels and stirrups, bond deteriorations) are considered in the PC girders under the flexure and shear loading conditions. The uncertainties in critical material properties (i.e., concrete, mild steel and pre-stressing steel) in PC girder are assumed to be unaffected by corrosion. The 2D FE model developed earlier is integrated with a reliability analysis technique (i.e., subset simulation) for probabilistic capacity analysis.

6.2   Subset Simulation for Probabilistic Capacity Analysis

Due to the limitation of approximate reliability methods (e.g., FORM, SORM), stochastic sampling approach is commonly used nowadays for uncertainty quantification/propagation. It is well known that Monte Carlo simulation is widely used for its robustness in terms of the type and dimension of random variable space in the problems with uncertainty (Rubinstein 1981, Fishman 1996). However, when the probability of interest is small (e.g., $P_F < 10^{-3}$), the sample size required to achieve the given accuracy is fairly high (i.e., proportional to $1/P_F$) and in turn a large number of system analyses (e.g., FE simulations) are needed. Importance sampling technique (e.g., Hammersley and Handscomb 1964, SchueÈller 1987, Shinozuka 1983) has been developed and used widely since it is efficient if an excellent choice of the importance sampling density can be made according to the information of the system in the failure region. Nevertheless, this is usually difficult if the uncertain parameter space is large and the problem is complicated. In reality, the probability of failure for structures is usually small since safety is the top concern in the design, and thus subset simulation is a promising method for structural reliability analysis. This is mainly because subset simulation can adaptively generate samples that explore the failure region efficiently, and at the same time keep the robustness of Monte Carlo simulation related to the dimension of the uncertain parameter space and the complexity of the failure region (Au and Beck 2001).

Subset simulation computes the probability of failure P_F by estimating the sequence of conditional probabilities $\{P(F_{i+1}|F_i) : i = 1, \ldots, m-1\}$ and $P(F_1)$, where F indicates the failure event, the subscript i indicates the corresponding failure region in the uncertain parameter space, and $F_1 \supset F_2 \supset \ldots \supset F_m = F$ is a decreasing sequence of failure events. Even when P_F is small, the conditional probabilities will be sufficiently large so that the effective simulation can be achieved if the intermediate failure events $\{F_i : i = 1, \ldots, m-1\}$ are chosen appropriately. As a result, a sequence of more frequent events in the conditional probability spaces are simulated instead of original probability space in subset simulation using appropriate simulation techniques.

In order to simulate conditional samples efficiently, Markov Chain Monte Carlo (MCMC) method based on the modified Metropolis algorithm is used. MCMC, especially Metropolis method, is a powerful technique for simulating samples based on an arbitrary probability distribution (Metropolis 1953). In this method, samples are simulated as the states of a Markov chain, which, under the assumption of ergodicity, has the target distribution as its limiting stationary distribution. However, it has difficulty for the Metropolis algorithm to simulate random vectors with many independent components, so a modified Metropolis algorithm was developed for the subset simulation (Hastings 1970, Au and Beck 2001).

6.3   Probabilistic Capacity of Corroded PC Girders

6.3.1   Corroded PC Girder Models

6.3.1.1   Flexural Girder

The 2D nonlinear FE model developed in software VecTor2, has been proved to be able to well predict the structural behaviour of PC girder with corrosion-induced deterioration. The same FE modelling strategies are used here for the full girder under four-point bending (referred to as the flexural girder). The flexural PC girder considered in this study is same bridge girder as the one used for parametric analysis in chapter 4. As shown in Figure 6-1, the girder is 11,000 mm long, simply supported with a span of 10,800 mm, and having the cross-section of dimension 1219 mm × 515 mm with three circular voids. The girder is loaded under four-point bending condition to study the flexural capacity, i.e., the loads are applied in the same manner as the flexure tests.
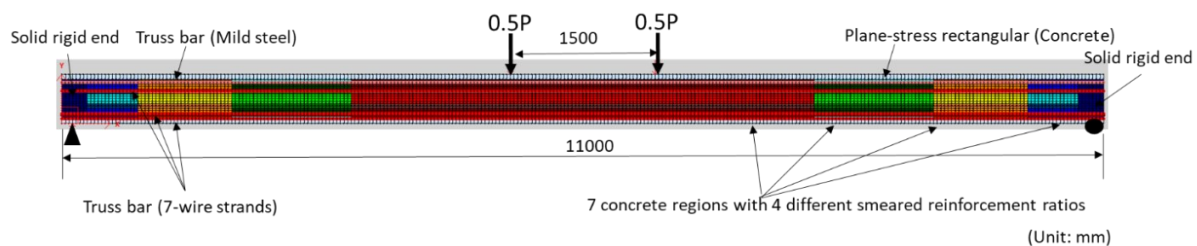
(a)
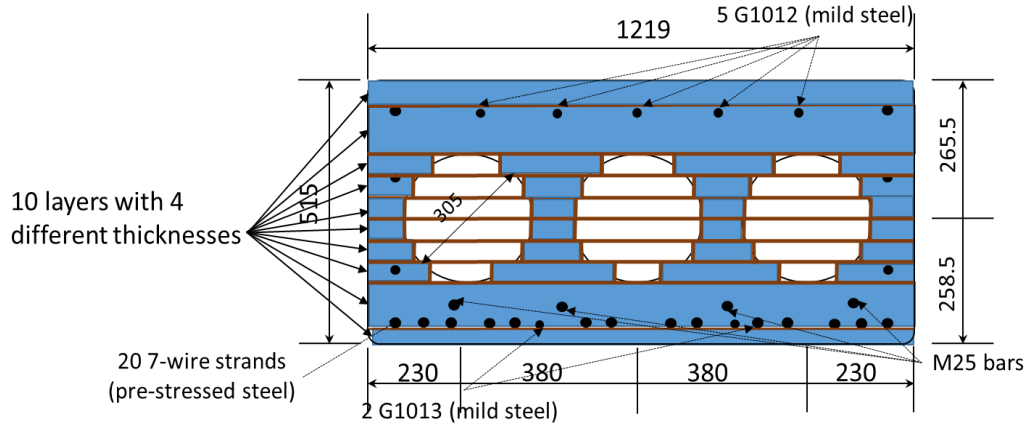
(b)

Figure 6-1: 2-D FE modeling scheme of the studied flexural bridge girder: (a) elevation view of the bridge girder, and (b) cross-section of the middle span

Three corrosion degrees investigated are 0%, 10% and 30%, which are defined as cross-section area loss of longitudinal steels. The corrosion deterioration features considered are based on the parametric study for PC girders with corrosion-induced deteriorations, and the most significant deteriorations are taken into account. Specifically, cross-section loss of all tension steels (i.e., both mild steel and 7-wire strands) are considered in view of their remarkable effect on stiffness and load-carrying capacity. Note that the pre-stress loss is also taken into account indirectly since the pre-stressing force will decrease proportionally to the deduction of cross-section area of 7-wire strands. Stirrups cross-section loss is also considered since it may change the failure mode of the flexural girder. Additionally, the deterioration on bond between steel and the surrounding concrete along whole length of the girder is considered together with imperfect anchorage. The bond-slip model is related to the corrosion degree indicated by Kivel et al (2015) as follows:

$$\frac{\tau_{R,\eta}}{\tau_{R,0}} = 1.2 e^{-7.6\eta} \qquad (6\text{-}1)$$

$$\frac{\tau_{f,\eta}}{\tau_{R,\eta}} = \begin{cases} 0.26 + 13\eta & 0\% \leq \eta < 3\% \\ 0.65 & 3\% \leq \eta < 13\% \\ 0.65 - 0.06(100\eta - 13) & 13\% \leq \eta < 20\% \\ 0.23 & 20\% \leq \eta \end{cases} \tag{6-2}$$

where $\tau_{R,\eta}$ is the rupture stress remained after corrosion, $\tau_{R,0}$ is the original rupture stress before corrosion, and $\tau_{f,\eta}$ represents the remaining ultimate frictional stress. S and H is lug spacing and lug height, respectively. Note that a uniform corrosion degree (η) is assumed for all deterioration features considered.

6.3.1.2 Shear Girder

The FE model for the shear girder is almost the same as the flexural one except that the stirrups are explicitly modelled by 2-node truss bar elements considering the importance of the amount and position of the stirrups in shear girder. The shear PC girder considered in this study is under the same loading condition as the shear girder test introduced in chapter 5, and thus the modelling scheme is shown in Figure 6-2.
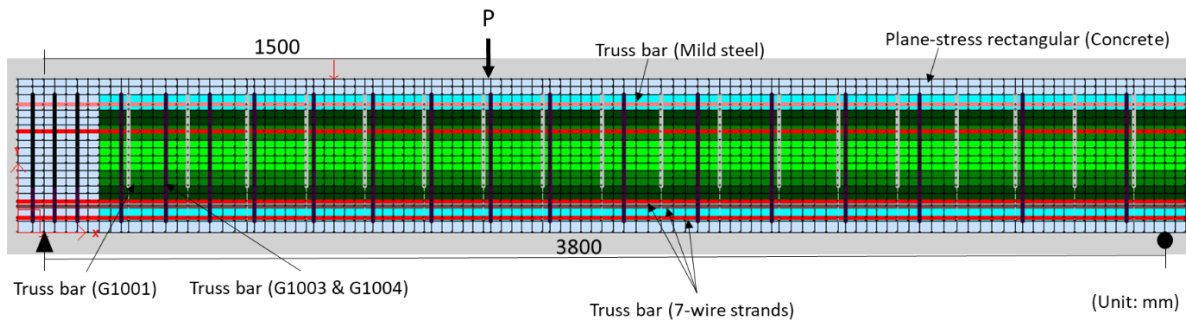
Figure 6-2: Modeling scheme of the shear girder in VecTor2

Similar to the flexure girder, three corrosion degrees 0%, 10% and 30% are investigated. The corrosion deterioration features considered are based on the parametric study for PC girders with corrosion-induced deteriorations, and the most significant deteriorations are taken into account. Specifically, cross-section loss of stirrups and all tension steels (i.e., both mild steel and 7-wire strands) are considered in view of their remarkable effect on stiffness and load-carrying capacity. Note that the pre-stress loss is also taken into account

indirectly since the pre-stressing force will decrease proportionally to the deduction of cross-section area of 7-wire strands. Additionally, the deterioration on bond between steel and the surrounding concrete along whole length of the girder is considered together with imperfect anchorage.

6.3.2   Random Variables and Statistics

The strength of a pre-stressed concrete girder is greatly affected by the variability of the material properties of concrete, mild steel, pre-stressing steel. From the literature available, uncertainties of these variables are summarized (e.g., statistics, the probability distribution types) and used in this study. The mean compressive strength f'_c for the concrete in the girder is taken as 42.7 MPa for concrete with a nominal strength of 35 MPa, as concluded from the concrete cylinder compressive strength tests by Nowak et al. (2012). The coefficient of variation (COV) of f'_c and elasticity modulus E_c of pre-tensioned concrete beam are calculated according to Kikuchi et al. (1978). All considered properties of concrete follow normal distributions as learned from the compressive tests of concrete conducted by Dayaratnam and Ranganathan (1976).

The statistics of the yield strength f_y of mild steels are based on the data summarized by Mirza and MacGregor (1979). The mean and COV of yield strength are 490 MPa and 9.3%, respectively, for grade 400 steel. The mean and COV of modulus of elasticity E_s, which are taken from Kikuchi et al. (1978), are 199,948 MPa and 3.3%, respectively. All considered properties of mild steels are assumed to follow lognormal distributions (Mansour et al. 1984). The mean and COV of pre-stressing strands are primarily calculated from Kikuchi et al. (1978), where the mean f_y was assumed to have the same bias factor with the ultimate tensile strength (1.04). The statistical characteristics of PC girders used in the probabilistic analysis are compared with the nominal values, as well as the tested values of material coupons extracted from the girder (Table 6-1).

Table 6-1 Statistical characteristics of basic random variables

Concrete	Test (MPa)	Nominal (MPa)	Mean (MPa)	COV	Distribution	Reference
f'_c	55.5	35	42.7	15.84%	normal	Nowak et al. 2012
E_c	25500	21401	24390	8%	normal	Mirza et al. 1979
Steel						
M10						
f_y	417	400	490	9.3%	lognormal	Mirza and MacGregor 1979
E_s	198000	200000	199948	3.30%	lognormal	Kikuchi et al. 1978
M25						
f_y	413	400	490	9.3%	lognormal	Mirza and MacGregor 1979
E_s	203000	200000	199948	3.30%	lognormal	Kikuchi et al. 1978
Strands						
f_y	1692	1676.5	1743.6	2.5%	normal	Mirza et al. 1980
E_s	197700	196500	195811	2%	normal	Kikuchi et al. 1978

The probability density function (PDF) of all the random variables considered in this study are shown in Figure 6-4 with the nominal values and tested values indicated. It is shown that the nominal values of the material strengths are lower than the mean values, and the tested values are generally higher than the nominal values as expected. The tested strength for concrete is higher than the mean value, but slightly lower than the mean values for both mild steel and strands. The low tested yield strengths of both mild steel and 7-wire strands compared to the mean values can potentially be attributed to either the natural variability of the yield strength or the reduced yield strength of steel due to corrosion-induced cross-sectional area reduction.
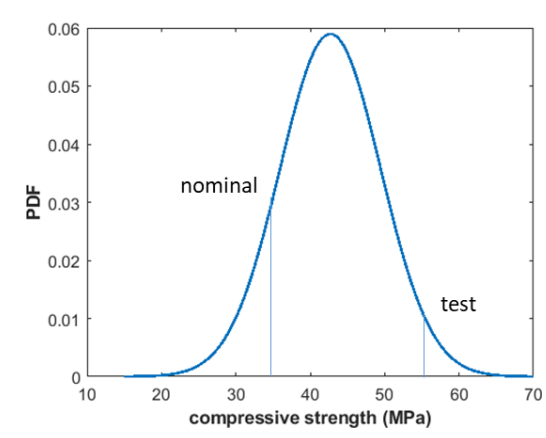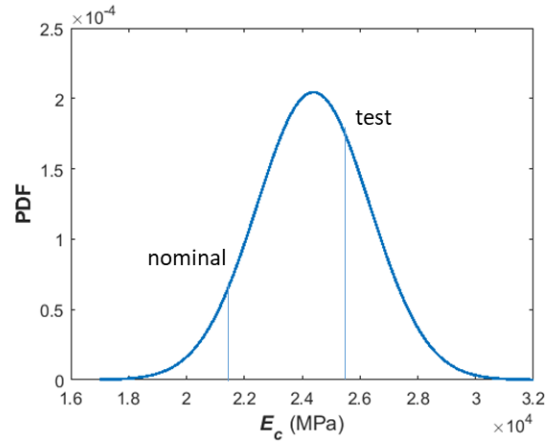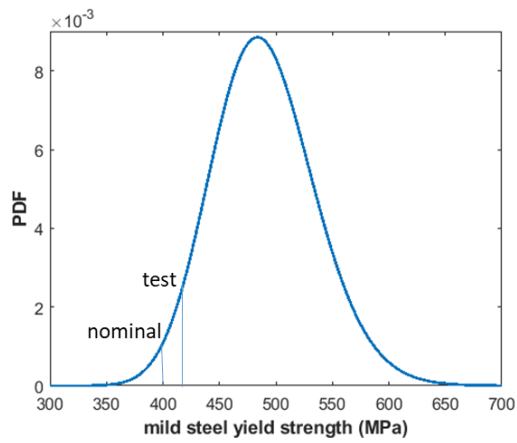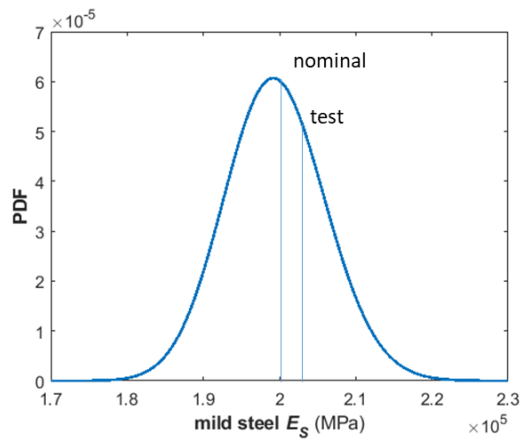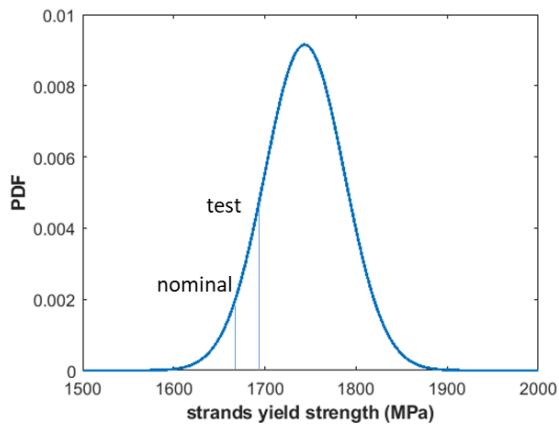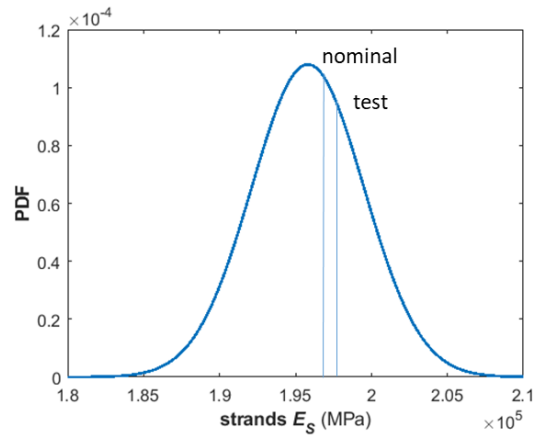
Figure 6-3: PDF curves of (a) f'_c for concrete, (b) E_c for concrete, (c) f_y for mild steel, (d) E_s for mild steel, (e) f_y for strands, and (d) E_s for strands
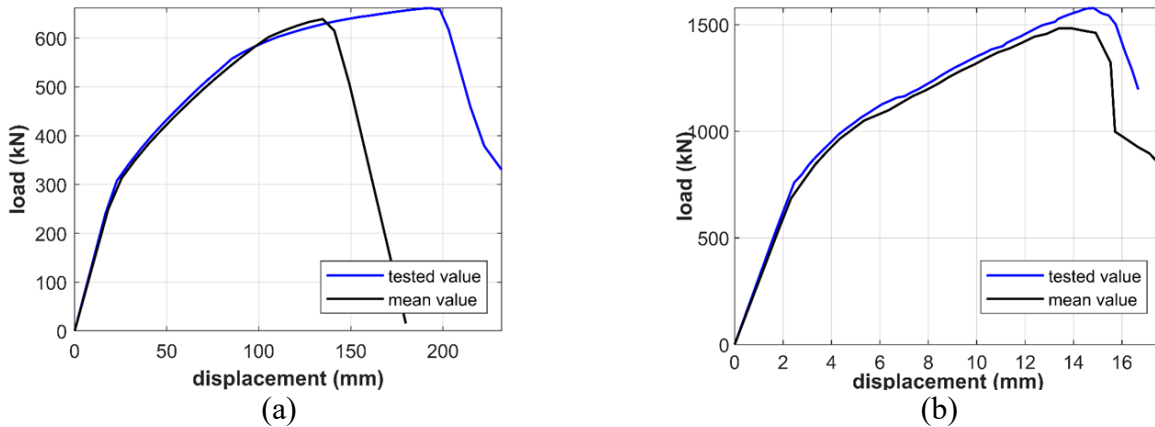
Figure 6-4: Comparison of the load-deflection curves predicted using the mean values and those predicted using tested values: (a) flexural girder, and (b) shear girder

Load-displacement curves of flexural girder and shear girder under corrosion degrees of 0%, 10%, and 30% using all mean values for variables are compared in Figure 6-5 (a) and (b), respectively. It is observed that for flexural PC girder, increasing corrosion reduces the post-cracking stiffness and load-carrying capacity without changing failure mode. However for shear PC girder, 10% degree corrosion decreases the stiffness and capacity slightly and 30% corrosion causes the failure mode change and a drastic reduction in load-carrying capacity.
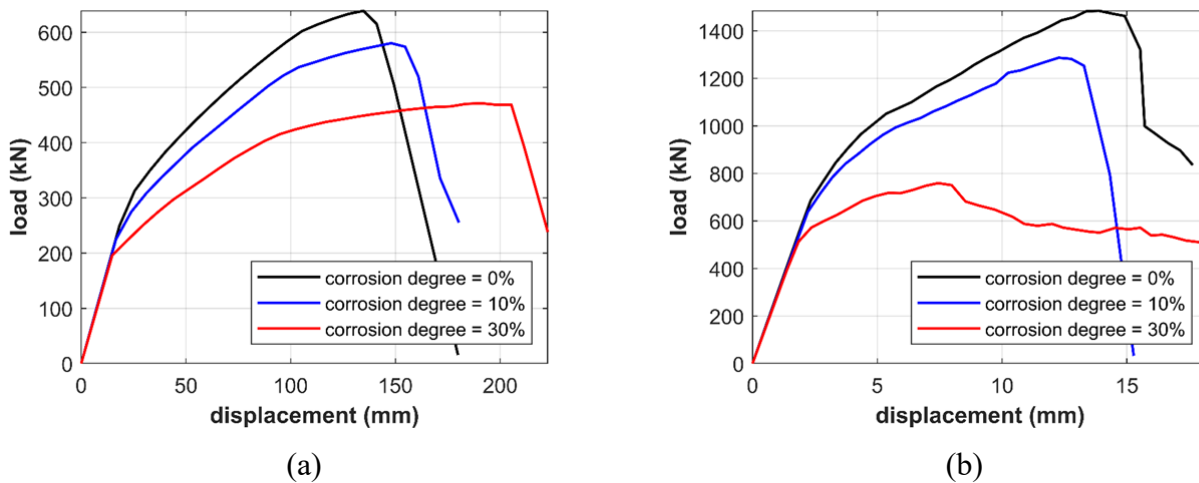
Figure 6-5: Load-displacement curve comparison of girders under various corrosion states: (a) flexural girder, and (b) shear girder

6.3.3 Probabilistic Capacity Results

6.3.3.1 *Flexural Girder*

The cumulative distribution function (CDF) curves of load bearing capacities for the flexural girders with different corrosion degrees are compared in Figure 6-6. Figure 6-6 (a) and (b) show the CDF curves in the normal scale and logarithmic scale (to show the low probability region), respectively. It is observed that as corrosion degree increases, the CDF curve shift to the left, implying higher probability of low load-carrying capacity events. In other words, the probability of failure increases for a given load effect. For example, given the factored load level (415 kN) corresponding to the ultimate limit state (ULS), the probability of failure is 2×10^{-6} when girder has no corrosion, 10^{-5} when girder has 10% corrosion, and 10^{-4} when girder has 30% corrosion, as shown in Figure 6-6 (b). Note that the ULS load is calculated based on legal non-permit truck loads according to the Bridge Load Evaluation Manual (Alberta Government 2016) and the Canadian Highway Bridge Design Code (CSA S6-14).
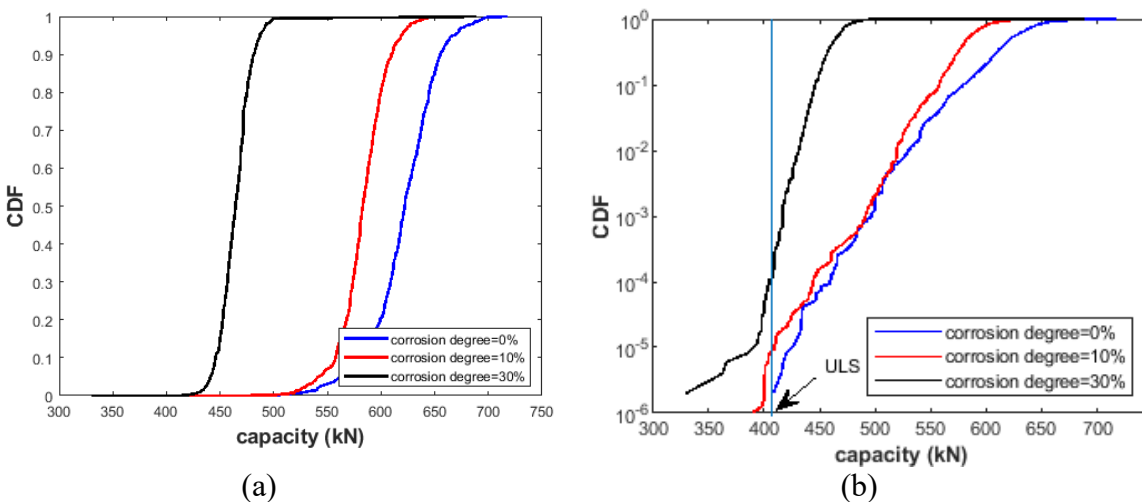
Figure 6-6: CDF comparison of the capacity for flexural PC girders with different corrosion degrees presented in (a) normal scale, and (b) log scale

The empirical PDF of the load bearing capacities of the girder under different degrees of corrosion are approximated with normal distributions as shown in Figure 6-7 (a) – (c). The mean capacity is 522 kN for the un-corroded girder, 485 kN for the girder with 10% corrosion, and 365 kN for the girder with 30% corrosion. Figure 6-7 (d) compares the PDFs

of the load bearing capacity of girders with all corrosion degrees, which shows that PDF of the girder with 10% corrosion is relatively close to that of the un-corroded girder, but PDF for the girder with 30% corrosion is far away from them, which indicates that the capacity drop due to 30% degree corrosion is much larger than 10% corrosion. Furthermore, as corrosion degree increases, the PDF curve becomes narrower, which indicates uncertainty in the capacity is reduced due to corrosion or the role of uncertainty in the material properties is less important.
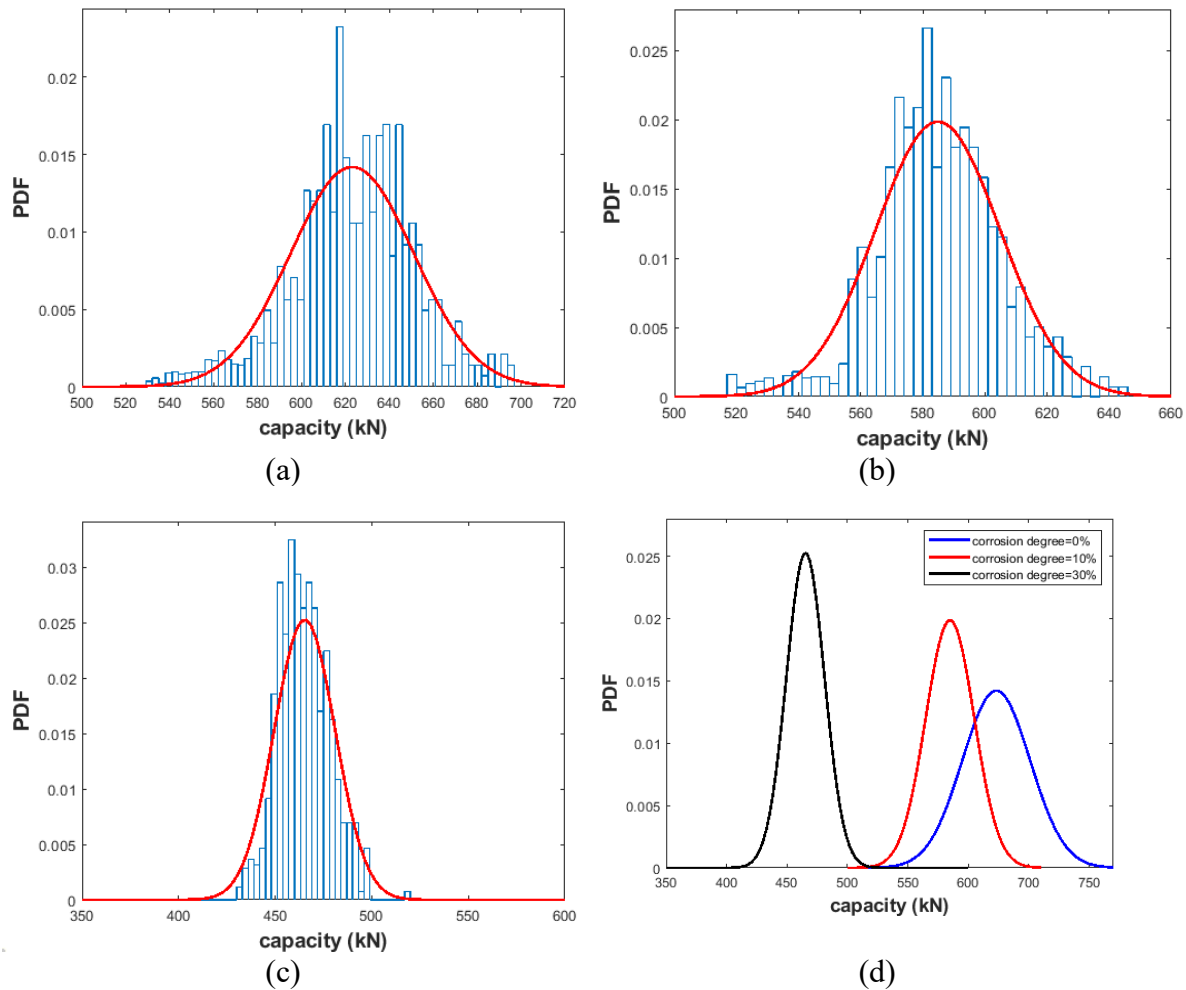
Figure 6-7: PDF curves of the capacity for flexural girders with the corrosion degree of (a) 0%, (b) 10%, (c) 30%, and (d) all three cases

6.3.3.2 Shear Girder

Figure 6-8 (a) and (b) shows the comparison of CDF curves of the load bearing capacities for the shear girders with different corrosion degrees in the normal and logarithmic scale, respectively. It is found that the increasing degree of corrosion on the shear girder can shift the probabilistic capacity curves to the left. This implies that corrosion can cause higher probability of failure. For example, given a 700 kN load applied at the shear girders (see Figure 6-8 b), the probability of failure is 3×10^{-8} when the girder has no corrosion, 3×10^{-7} when the girder has 10% corrosion, and 2×10^{-2} when the girder has 30% corrosion.
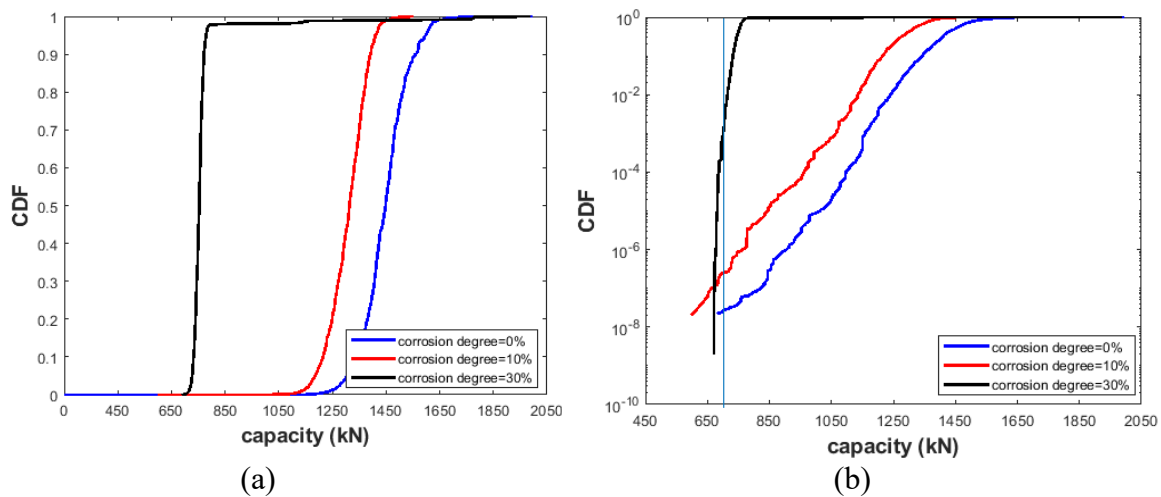
Figure 6-8: CDF comparison of the capacities for shear PC girders with different corrosion degrees presented in (a) normal scale, and (b) log scale

The empirical PDF of the load bearing capacities of the shear girders under different degrees of corrosion are approximated with normal distributions as shown in Figure 6-9 (a) – (c). The mean capacity is 1200 kN for the un-corroded girder, 1065 kN for the girder with 10% corrosion and 503 kN for the girder with 30% corrosion. Figure 6-9 (d) shows the comparison of the PDFs of all shear girders with different corrosion degrees. It is observed that PDF of girder with 10% corrosion has a moderate distance to that of the un-corroded girder in terms of capacity (i.e., x axis), but the PDF for the girder with 30% corrosion is much away from them. This indicates that the capacity drop due to corrosion is significant when the corrosion degree is 30%. Furthermore, the standard deviation of the

143

capacity reduces as the increase of corrosion degree since the PDF curve becomes narrower, especially for the girder with 30% corrosion degree.
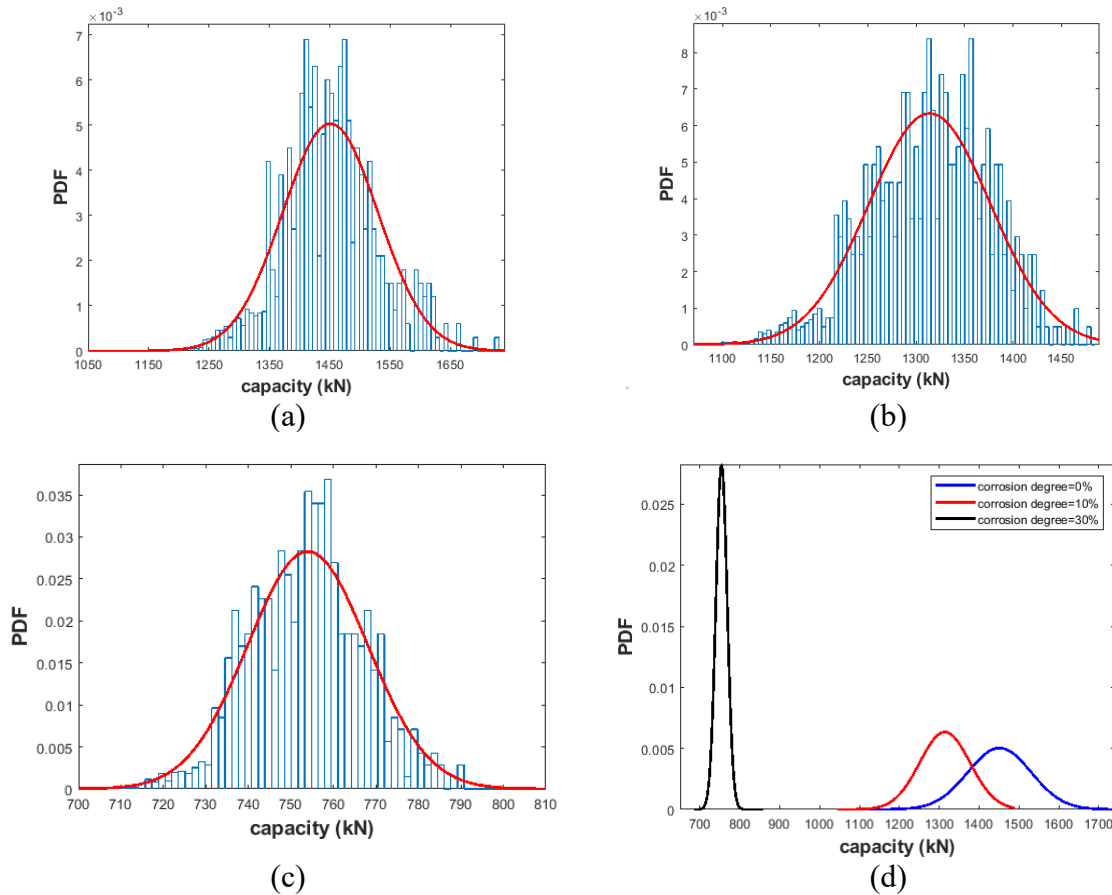
Figure 6-9: PDF curves of the capacity for shear girders with the corrosion degree of (a) 0%, (b) 10%, (c) 30%, and (d) all cases

6.4   Summary and Discussion

In order to understand the corroded PC girders more realistically, a FE-based probabilistic capacity analysis is performed in this chapter by combining the 2D FE model with subset simulation for both flexural and shear girders. Uncertainties in the principal material properties (e.g., those for concrete, mild steel and pre-stressing steel in PC girder) were considered. The probabilistic capacities of the girders under three different corrosion levels (i.e., 0%, 10%, and 30%) were analyzed. It is found that for both flexural and shear girders, the corrosion not only reduces the mean value of the capacity, but also reduces the uncertainty (measured by the standard deviation). The probability of failure for the girder

with higher corrosion degree under a given load is much higher. The effect of corrosion is higher for high corrosion degrees. For example, the mean and standard deviation of load-carrying capacity of the PC girder decreases significantly when corrosion degree reaches 30%, and thus the probability of failure increases considerably for a given load.

CHAPTER 7: CONCLUSIONS AND RECOMMENDATIONS

7.1   Summary

The increasing number of deteriorated bridges reported around the world have aroused the concerns of bridge engineers and the interests of researchers. In order to help authorities to optimise the rehabilitation strategies for aged bridges or focus on the important aspects of deterioration features using non-destructive testing techniques or visual inspection, understanding and quantifying the corrosion effects on the flexural and shear behaviours of PC bridge girders of significant value. To this end, finite element (FE)-based parametric and probabilistic analysis of structural deteriorations in pre-stressed concrete (PC) girders was performed.

Two-dimensional (2D) FE models were developed for corroded concrete beams/girders under both flexural and shear loading conditions. The FE modelling strategies used for concrete beams/girders considering deteriorations were first validated by simulating the experimental test results of reinforced concrete (RC) beams with artificial corrosion deteriorations from literature. Sequentially, they were used to simulate the experimental tests of a visually intact PC girder salvaged from an abandoned bridge (1990 - 2017) near Barrhead in central Alberta. Based on 2D FE model, a comprehensive parametric study with a full range of deterioration types (i.e. steel area loss, concrete spalling, concrete material deterioration, de-bonding, pre-stress loss, and intermediate bond loss) and corrosion degrees was performed. Several other girders from the same bridge with different deterioration levels were also simulated and analyzed using the 2D FE model based on the knowledge learned from the parametric study. Furthermore, to further understand the effect of corrosion on the capacity of PC girders, the FE models for corroded girders were integrated with probabilistic analysis algorithms (e.g., subset simulation) to study the residual capacity of PC girders.

7.2   Conclusions

The main conclusions of this research are outlined as follows:

1. 2D nonlinear FE modelling (i.e., VecTor2 used in this research) was an effective method for modeling the structural deterioration in corroded concrete beams (RC/PC) with reasonable accuracy, given that the information on the corrosion features was well-known. This was verified by the simulated load-displacement responses for RC beams with artificial corrosion-induced deteriorations.

2. The study of the RC beams with deteriorated bonding between steel and concrete (e.g., de-bonding) revealed that given full anchorage at the ends, the load-carrying capacity reduced only moderately in flexural-critical RC beams due to the increasing length of un-bonded region from end supports towards the mid-span. For shear-critical RC beams (e.g., with no stirrups), the increase of the un-bonded length from the loading point towards the supports within the shear span could increase the load carrying capacity and the ductility of the beam.

3. The 2D FE model developed for tested PC girders implied an additional 30% ∼ 40% pre-stress loss based on the comparison of the predicted load-deflection curves with the experimental results of a 27-year-old bridge PC girder. This inference was built on the confidence in the well-calibrated material behaviours and was further confirmed by 1D FE model using fibre-based beam elements for the flexure test, 2D FE model developed for the shear test. The FE models captured the structural behaviour of the tested girders fairly well.

4. The parametric study performed using the developed 2D FE models of PC girders indicated that corrosion-induced cross-section deduction of reinforcing steels and pre-stress loss of pre-stressed strands could significantly decrease the stiffness and load-carrying capacity of the girder; spalling and de-bonding in span have little effect on structural behaviour; and intermediate bond loss considering imperfect anchorage could reduce the strength of the girder significantly and even change the failure mode. Based on parametric study, the 2D FE model was used to uncover the possible deterioration states in other girders from the same bridge.

5. Parametric study conducted for shear PC girder based on the 2D FE model developed showed that the concrete cover spalling and steel de-bonding in span only had slight influence on the residual shear behaviour of girders, while the steel cross section loss and bonding loss with end anchorage failure could have a significant influence. Based on parametric study, the 2D FE model was used to study the possible deterioration states in other shear girders from the same bridge.

6. For both flexural and shear girders, the corrosion degree affected both the mean and variance of the residual capacities. The higher corrosion degree in PC girders can cause higher probability of failure given a certain load level. The effect of corrosion is very significant particularly when the corrosion degree is high (e.g., 30%).

7. Based on the numerical study along with experimental tests of PC girders salvaged from the bridge, it is found that the experimental load-carrying capacity (637 kN) of girder #1, which is in a visually intact condition, is 53% higher than the equivalent design load (415 kN) calculated corresponding to the ultimate limit state. However, due to the deterioration in girder #2 and #3, the capacity dropped to 490 kN and 546 kN, respectively. In particular, the failure mode changed to brittle failure due to strand rupture, which was undesired. Though the tested capacities for each girder are higher than the design load levels, the safety margin is reduced significantly for girders with deteriorations. This implied a need for repair or replacement of girders that are deteriorated significantly such as girder #2 for safety concerns. It is worth mentioning that the residual capacity would be much lower if there were no extra M25 bars. To assist rational decision-making, a rigorous system reliability assessment considering multiple girders needs to be conducted with well-quantified corrosion state of the girders in the bridge.

8. The parametric analysis results presented in this work can help bridge inspectors to focus more on the important deterioration features, such as steel area reduction and bond loss, particularly the anchorage bond loss. This is because the study in this thesis shows that they have significant influence on the residual strength of corroded PC girders. Furthermore, change in the load-carrying capacities under flexure and shear loading as a

function of corrosion degrees can help (1) bridge evaluators assess the bridge girder condition with more confidence on the severity of girder conditions, and (2) forensic engineers to infer the possible causes of bridge performance degradation.

7.3   Recommendations for Future Work

The presented work is limited in various aspects, and thus recommendations for future work are suggested as follows:

1. The preliminary forensic analysis using computer modeling for the visually intact PC girder (i.e., girder #1) signified an additional prestress loss in the PC girders. Further verification using experimental evidence is needed.

2. The FE-based parametric analysis was conducted in one-at-a-time manner, to understand how individual corrosion-related deterioration feature affects the girder behaviour. Thus, the effect of the interaction of different corrosion features needs further study.

3. The FE modeling of corroded PC girders is based on the good knowledge of corrosion features or degrees. Actually, obtaining such information is challenging in practice. To advance the use of FE modeling for condition assessment of corroded structures, appropriate non-destructive testing techniques need to be sought for those influencing factors identified in this research.

4. Only material model parameter uncertainties were considered in the FE-based probabilistic capacity analysis of corroded PC girders, where the corrosion state was assumed to be known deterministically. In reality, the uncertainty in corrosion states should be taken into account to perform unconditional probabilistic performance analysis of PC girders, since uncertainty in corrosion states depends on the techniques used for corrosion defect detection.

REFERENCE

Alberta Government, 2016. Alberta Transportation Bridge Load Evaluation Manual v. 1.1

American Association of State Highway Officials, 1989. *Standard Specifications for Highway Bridges*, 14th Edition, Washington, D.C.

AASHTO, 1992. *Standard Specifications for Highway Bridges*, 15th edition, American Association of State Highway and Transportation Officials, Washington, D.C.

AASHTO, 2009. *AASHTO LRFD bridge design specifications*, 4th Ed., Interim, Washington, D.C.

AASHTO, 2012. *LRFD bridge design specifications*, 6th Ed., Washington, D.C.

American Association of State Highway and Transportation Officials (AASHTO), 2015. *AASHTO LRFD Bridge Design Specifications*. 7th ed. Washington, DC: AASHTO

ACI Committee 318, 1989. *Building Code Requirements for Reinforced Concrete* (ACI 318-89), American Concrete Institute, Detroit, MI.

ACI Committee 318, 2014. *Building Code Requirements for Structural Concrete* (ACI 318-14) and Commentary (ACI 318R-14). Farming- ton Hills, MI.

Akgül, F. and Frangopol, D.M., 2004. Lifetime performance analysis of existing prestressed concrete bridge superstructures. *Journal of Structural Engineering, 130*(12), pp.1889-1903.

Andrade, C., Alonso, C. and Molina, F.J., 1993. Cover cracking as a function of rebar corrosion: Part II–Numerical model. *Materials and structures*, *26*, pp.532-548.

Aquino, W. and Erdem, I., 2007. Implementation of the modified compression field theory in a tangent stiffness-based finite element formulation. *Steel and Composite Structures, 7*(4), pp.263-278.

Au, S.K. and Beck, J.L., 2001. Estimation of small failure probabilities in high dimensions

by subset simulation. *Probabilistic engineering mechanics, 16*(4), pp.263-277.

Azad, A.K., Ahmad, S. and Azher, S.A., 2007. Residual strength of corrosion-damaged reinforced concrete beams. *ACI Materials Journal, 104*(1), p.40.

Bartlett, F.M. and MacGregor, J.G., 1996. Statistical analysis of the compressive strength of concrete in structures. *Materials Journal, 93*(2), pp.158-168.

Bartlett, F.M. and MacGregor, J.G., 1999. Variation of in-place concrete strength instructures. *Materials Journal, 96*(2), pp.261-270.

Bartlett, F.M., 2007. Canadian Standards Association standard A23. 3-04 resistance factor for concrete in compression. *Canadian Journal of Civil Engineering, 34*(9), pp.1029-1037.

Bertolini, L., Bolzoni, F., Pastore, T. and Pedeferri, P., 2004. Effectiveness of a conductive cementitious mortar anode for cathodic protection of steel in concrete. *Cement and Concrete Research, 34*(4), pp.681-694.

Bin, D., Zhao, R.D. and Xiang, T.Y., 2010. Lifetime reliability analysis of flexural cracking for existing prestressed concrete bridge under corrosion attack. In *ICCTP 2010: Integrated Transportation Systems: Green, Intelligent, Reliable* (pp. 3810-3818).

Böhni, H., 2000. Influence of temperature on the localized corrosion of stainless steels. *Russian journal of electrochemistry*, *36*(10), pp.1122-1128.

BRIME, 2001. Research project no.: RO-97-SC.2220, *The European Union: transport research and technological development, final report*. Bridge management in Europe

Broomfield, J.P., 1997. Corrosion of steel in concrete: Understanding. *Investigation and Repair, E&FN, London*, pp.1-15.

Bruce, S.M. and McCarten, P.S., 2006. Deterioration of prestressed concrete bridge beams in New Zealand. In *AUSTROADS BRIDGE CONFERENCE, 6TH, 2006, PERTH,*

WESTERN AUSTRALIA.

BSI, 1990. Steel, concrete and composite bridges. *Code of practice for design of concrete bridges*. BS 5400. London: British Standards Institution.

Bureau of Transportation Statistics, 2008. *National transportation statistics*. US Department of Transportation.

CSA Canadian Standards Association, 2014. Canadian Highway Bridge Design Code S6-14.

Cairns, J., Plizzari, G.A., Du, Y., Law, D.W. and Franzoni, C., 2005. Mechanical properties of corrosion-damaged reinforcement. *ACI Materials Journal*, *102*(4), p.256.

Cairns, J. and Zhao, Z., 1993. Behaviour of concrete beams with exposed reinforcement. *Proceedings of the Institution of Civil Engineers-Structures and Buildings*, *99*(2), pp.141-154.

Cairns, J., 1995. Strength of concrete beams during concrete breakout. *In IABSE Symposium on extending the lifespan of Structures*. San Francisco (pp. 500-504).

Cairns, J., 1995. Strength in shear of concrete beams with exposed reinforcement. *In Proceedings of the Institution of Civil Engineers. Structures and Buildings* (Vol. 110, No. 2).

Capé, M., 1999. Residual service-life assessment of existing R/C structures. In *Chalmers University of Technology, Goteborg (Sweden) and Milan University of Technology, Italy Erasmus Program*.

Cartz, L., 1995. Nondestructive testing.

Castel, A., Coronelli, D., Vu, N.A. and François, R., 2010. Structural response of corroded, unbonded posttensioned beams. *Journal of Structural Engineering, 137*(7), pp.761-771.

Castel, A., François, R. and Arliguie, G., 2000a. Mechanical behaviour of corroded reinforced concrete beams—Part 1: experimental study of corroded beams. *Materials and Structures, 33*(9), pp.539-544.

Castel, A., François, R. and Arliguie, G., 2000b. Mechanical behaviour of corroded reinforced concrete beams—Part 2: Bond and notch effects. *Materials and Structures, 33*(9), p.545.

Cavell, D.G. and Waldron, P., 2001. A residual strength model for deteriorating post-tensioned concrete bridges. *Computers & Structures, 79*(4), pp.361-373.

CDN Infrastructure, 2016. Canadian infrastructure report card (roads and bridges). http://canadianinfrastructure.ca/en/municipal-roads.html

Cheng, J., 2013. Serviceability reliability analysis of prestressed concrete bridges. *KSCE Journal of Civil Engineering, 17*(2), pp.415-425.

Chotickai, P., 2001. *Acoustic emission monitoring of prestressed bridge girders with premature concrete deterioration* (Doctoral dissertation, University of Texas at Austin).

Coggins, F.B. and French, C.W., 1990. Chloride ion distribution in twenty-year-old prestressed bridge girders. *Materials Journal*, *87*(5), pp.479-488.

Coombs, W., 1957. The Sorell causeway bridge: Longest pre-stressed concrete bridge in Australia. *Tasmanian Architect*, pp.24-5.

Coronelli, D. and Gambarova, P., 2004. Structural assessment of corroded reinforced concrete beams: modeling guidelines. *Journal of structural engineering, 130*(8), pp.1214-1224.

Coronelli, D., Castel, A., Vu, N.A. and François, R., 2009a. Corroded post-tensioned beams with bonded tendons and wire failure. *Engineering Structures, 31*(8), pp.1687-1697.

Coronelli, D., Castel, A., François, R. and Cleland, D., 2009b. Modelling the response of prestressed beams with corroded reinforcement. *European Journal of Environmental and Civil Engineering, 13*(6), pp.653-669.

CSA Group, 2014. Canadian Highway Bridge Design Code S6-14. *Canadian Standards Association*.

Cullington, D.W. and Raggett, S.J., 1991. Shear strength of some 30-year-old prestressed beams without links.

Council of the Federation, 2005. *Looking to the Future: A Plan for Investing in Canada's Transportation System.*

Czaderski, C. and Motavalli, M., 2006. Determining the remaining tendon force of a large-scale, 38-year-old prestressed concrete bridge girder. *PCI journal*, 51(4).

Dang, V.H. and François, R., 2013. Influence of long-term corrosion in chloride environment on mechanical behaviour of RC beam. *Engineering Structures, 48*, pp.558-568.

Darmawan, M.S. and Stewart, M.G., 2007. Spatial time-dependent reliability analysis of corroding pretensioned prestressed concrete bridge girders. *Structural Safety, 29*(1), pp.16-31.

Darmawan, M.S., 2009. Pitting corrosion model for partial prestressed concrete (PC) structures in a chloride environment. *IPTEK The Journal for Technology and Science, 20*(3).

Darmawan, M.S., 2010. Probabilistic Assessment of Pitting Corrosion Effect on Flexural Strength of Partial Prestressed Concrete Structures in a Chloride Environment. *Journal of Civil Engineering and Architecture, 4*(2), pp.25-32.

Dayaratnam, P. and Ranganathan, R., 1976. Statistical analysis of strength of concrete. *Building and Environment, 11*(2), pp.145-152.

Dasar, A., Irmawaty, R., Hamada, H., Sagawa, Y. and Yamamoto, D., 2016. Prestress loss and bending capacity of pre-cracked 40 year-old PC beams exposed to marine environment. In *MATEC Web of Conferences* (Vol. 47, p. 02008). EDP Sciences.

Dekoster, M., Buyle-Bodin, F., Maurel, O. and Delmas, Y., 2003. Modelling of the flexural behaviour of RC beams subjected to localised and uniform corrosion. *Engineering Structures*, *25*(10), pp.1333-1341.

Du YG, Clark LA, Chan AHC. Impact of reinforcement corrosion on ductile behaviour of reinforced concrete beams. *ACI Struct J 2007;104*(3):285–93

Enright, M.P. and Frangopol, D.M., 1998. Service-life prediction of deteriorating concrete bridges. *Journal of Structural engineering, 124*(3), pp.309-317.

Eligehausen, R., Popov, E., and Bertero, V. 1983. "Local Bond Stress-Slip relationship of Deformed Bars under Generalized Excitations", *Report No. UCB/EERC-83/23, Earthquake Engineering Center, University of California, Berkeley.*

El Maaddawy, T., Soudki, K. and Topper, T., 2005. Analytical model to predict nonlinear flexural behaviour of corroded reinforced concrete beams. *ACI structural journal, 102*(4), p.550.

Federal Highway Administration (FHWA), 2011. *Bridge preservation guide. Rep. no.FHWA-HIF-11042*. US Department of Transportation.

Floyd, R., Pei, J.S., Tang, P.F. and Murray, C.D., 2016. *Understanding the behaviour of prestressed girders after years of service* (No. FHWA-OK-16-03). Oklahoma. Dept. of Transportation.

Fishman, G.S., 1996. Monte Carlo Concepts, Algorithms and Applications. Springer-Verlag.

François, R., Castel, A. and Vidal, T., 2006. A finite macro-element for corroded reinforced concrete. *Materials and structures, 39*(5), pp.571-584.

Guo, T., Frangopol, D.M., Han, D. and Chen, Y., 2010. Probabilistic assessment of deteriorating prestressed concrete box-girder bridges under increased vehicle loads and aggressive environment. *Journal of Performance of Constructed Facilities, 25*(6), pp.564-576.

Halsey, J.T. and Miller, R., 1996. Destructive testing of two forty-year-old prestressed concrete bridge beams. *PCI journal*, *41*(5).

Hammersley, J.M. and Handscomb, D.C., 1964. Monte Carlo methods, methuen & co. *Ltd., London, 40.*

Harries, K.A., 2009. Structural testing of prestressed concrete girders from the Lake View Drive Bridge. *Journal of Bridge Engineering, 14*(2), pp.78-92.

Hastings, W.K., 1970. Monte Carlo sampling methods using Markov chains and their applications.

Hellier, C., 2001. Handbook of nondestructive evaluation.

Huston, D., 2010. *Structural sensing, health monitoring, and performance evaluation*. CRC Press.

Jeppsson, J. and Thelandersson, S., 2003. Behaviour of reinforced concrete beams with loss of bond at longitudinal reinforcement. *Journal of Structural Engineering, 129*(10), pp.1376-1383.

Jnaid, F. and Aboutaha, R.S., 2016. Residual flexural strength of corroded reinforced concrete beams. *Engineering Structures, 119*, pp.198-216.

Juarez, C.A., Guevara, B., Fajardo, G. and Castro-Borges, P., 2011. Ultimate and nominal shear strength in reinforced concrete beams deteriorated by corrosion. *Engineering Structures*, *33*(12), pp.3189-3196.

Kallias, A.N. and Rafiq, M.I., 2010. Finite element investigation of the structural response

of corroded RC beams. *Engineering Structures, 32*(9), pp.2984-2994.

Kikuchi, D.K., Mirza, S.A. and MacGregor, J.G., 1978. Strength variability of bonded prestressed concrete beams.

Kim, W. and White, R.N., 1999. Shear-critical cracking in slender reinforced concrete beams. *Structural Journal, 96*(5), pp.757-765.

Kivell, A., Palermo, A. and Scott, A., 2015. Complete model of corrosion-degraded cyclic bond performance in reinforced concrete. *Journal of Structural Engineering*, *141*(9), p.04014222.

Kotsovos, G.M., Cotsovos, D.M., Kotsovos, M.D. and Kounadis, A.N., 2011. Seismic behaviour of RC walls: an attempt to reduce reinforcement congestion. *Magazine of Concrete Research, 63*(4), pp.235-246.

Kotsovos, G.M., Vougioukas, E. and Kotsovos, M.D., 2015. Behaviour of reinforced concrete beams with non-bonded flexural reinforcement. *Magazine of Concrete Research, 67*(10), pp.503-512.

Kotyaev, O., Shimada, Y. and Hashimoto, K., 2006. Laser-based non-destructive detection of inner flaws in concrete with the use of lamb waves. In *European Conf. for Non Destructive Testing* (pp. 25-29).

Kramer, W., Martin, W. and Viljoen, H., 2018. Demolition of Old Oak Bridge B4113: Condition of a 54-year old prestressed concrete bridge. In *MATEC Web of Conferences* (Vol. 199, p. 06002). EDP Sciences.

Labia, Y., Saiidi, M.S. and Douglas, B., 1997. Full-scale testing and analysis of 20-year-old pretensioned concrete box girders. *Structural Journal*, *94*(5), pp.471-482.

Lau, M., Pochanart, A. and Eden, R., 2010. Load Testing and Ratings of Salvaged Precast Prestressed Concrete Channel Bridge Girders. In *2010 Annual Conference of the Transportation Association of* Structures Standing Committee, Halifax, Nova Scotia,

Canada.

Li, C.Q., Yang, Y. and Melchers, R.E., 2008. Prediction of reinforcement corrosion in concrete and its effects on concrete cracking and strength reduction. *ACI materials journal*, *105*(1), p.3.

Li, F. and Yuan, Y., 2010. Experimental study on bending property of prestressed concrete beams with corroded steel strands. *Journal of Building Structures*, pp.78-84.

Li, F. and Yuan, Y., 2013. Effects of corrosion on bond behaviour between steel strand and concrete. *Construction and Building Materials*, *38*, pp.413-422.

Li, H., Lan, C.M., Ju, Y. and Li, D.S., 2012. Experimental and numerical study of the fatigue properties of corroded parallel wire cables. *Journal of Bridge Engineering, 17*(2), pp.211-220.

Luckai, J., Polak, M.A. and Walbridge, S., 2014. A methodology for evaluating the effects of spalling on the structural capacity of reinforced concrete bridge girders. *Canadian Journal of Civil Engineering, 41*(3), pp.197-205.

Maes, M.A., Wei, X. and Dilger, W.H., 2001. Fatigue reliability of deteriorating prestressed concrete bridges due to stress corrosion cracking. *Canadian Journal of Civil Engineering*, *28*(4), pp.673-683.

Mallett, G.P., 1994. *Repair of concrete bridges*. Thomas Telford.

Malumbela, G., Alexander, M. and Moyo, P., 2010. Variation of steel loss and its effect on the ultimate flexural capacity of RC beams corroded and repaired under load. *Construction and Building Materials, 24*(6), pp.1051-1059

Mander, J.B., Priestley, M.J.N., and Park. R., 1988. Theoretical Stress-Strain Model for Confined Concrete. *ASCE Journal of Structural Engineering*, 114(8), pp. 1804-1826.

Mangat, P.S. and Elgarf, M.S., 1999. Flexural strength of concrete beams with corroding

reinforcement. *Structural Journal, 96*(1), pp.149-158.

Mansour, A.E., Jan, H.Y., Zigelman, C.I., Chen, Y.N. and Harding, S.J., 1984. Implementation of reliability methods to marine structures. *Transactions-Society of Naval Architects and Marine Engineers, 92*, pp.353-382.

Mathy, B., Demars, P., Roisin, F. and Wouters, M., 1996. Investigation and strengthening study of twenty damaged bridges: A Belgium case history. In *Bridge management 3. Inspection, maintenance and repair. Papers presented at the third international conference on bridge management, University of Surrey, Guildford, UK, 14-17 April 1996.*

Metropolis, N., Rosenbluth, A.W., Rosenbluth, M.N., Teller, A.H. and Teller, E., 1953. Equation of state calculations by fast computing machines. *The journal of chemical physics, 21*(6), pp.1087-1092.

Minh, H., Mutsuyoshi, H. and Niitani, K., 2007. Influence of grouting condition on crack and loadcarrying capacity of post-tensioned concrete beam due to chloride-induced corrosion. *Construction and Building Materials, 21*(7), pp.1568-1575.

Minkarah, I. and Ringo, B.C., 1981. Behaviour and repair of deteriorated reinforced concrete beams. *Transportation research record*, (821).

Mirza, S.A. and MacGregor, J.G., 1979. Variations in dimensions of reinforced concrete members. *Journal of the Structural Division, 105*(4), pp.751-766.

Mirza, S.A. and MacGregor, J.G., 1979. Variability of mechanical properties of reinforcing bars. *Journal of the Structural Division, 105(*ASCE 14590 Proceeding).

Mohamed, O.A. and Rens, K.L., 2001. Ultrasonic testing of properties of 50 year old concrete. *Materials evaluation*, *59*(12), pp.1426-1430.

Mousa, M.I., 2016. Effect of bond loss of tension reinforcement on the flexural behaviour of reinforced concrete beams. *HBRC Journal, 12*(3), pp.235-241.

Nowak, A.S., Rakoczy, A.M. and Szeliga, E.K., 2012. Revised statistical resistance models for R/C structural components. *Special Publication, 284*, pp.1-16.

Murray, C.D., Cranor, B.N., Floyd, R.W. and Pei, J.S., 2017. Shear Behaviour of 45-Year-Old AASHTO Type II Bridge Girders. *Paper*, *57*

Naqvi, A., Nagadi, M. and Al-Amoudi, O., 2007. Non-destructive evaluation of concrete samples using PGNAA technique. *Journal of radioanalytical and nuclear chemistry*, *271*(1), pp.151-154.

Ngo, D. and Scordelis, A.C., 1967. Finite Element Analysis of Reinforced Concrete Beams. *ACI Journal, 64*(3), pp. 152-163.

Nokhasteh, M.A., Eyre, J.R. and Mcleish, A., 1992. The effect of reinforcement corrosion on the strength of reinforced concrete members. *Proceedings of Structural Integrity Assessment.*

OpenSees command language manual

Osborn, G.P., Barr, P.J., Petty, D.A., Halling, M.W. and Brackus, T.R., 2012. Residual prestress forces and shear capacity of salvaged prestressed concrete bridge girders. *Journal of Bridge Engineering*, *17*(2), pp.302-309.

Pape, T.M. and Melchers, R.E., 2013. Performance of 45-year-old corroded prestressed concrete beams. *Proceedings of the Institution of Civil Engineers-Structures and Buildings*, *166*(10), pp.547-559.

Parmar, D.S. and Sharp, S.R., 2009. Acoustic emission for non-destructive testing of bridges and other transportation infrastructure. In *Beyond the Crossroads: A National Conference on Transportation Infrastructure & Regulatory Policy; University of Denver: Denver, CO, USA.*

Pandey, M.D. and Nessim, M.A., 1996. Reliability-based inspection of post-tensioned concrete slabs. *Canadian Journal of Civil Engineering*, *23*(1), pp.242-249.

PCI Committee on Prestress Losses, 1975, Recommendations for Estimating Prestress Losses, *PCI JOURNAL, 20*(4), pp. 45-70.Peng, L. and Stewart, M.G., 2014. Spatial time-dependent reliability analysis of corrosion damage to RC structures with climate change. *Magazine of Concrete Research*, *66*(22), pp.1154-1169.

Pettigrew, C.S., Barr, P.J., Maguire, M. and Halling, M.W., 2016. Behaviour of 48-year-old double-tee bridge girders made with lightweight concrete. *Journal of Bridge Engineering, 21*(9), p.04016054.

Rao, C. and Frantz, G.C., 1996. Fatigue tests of 27-year-old prestressed concrete bridge box beams. *PCI journal*, *41*, pp.74-83.

Raoof, M. and Lin, Z., 1993. Implications of structural damage to concrete elements. *In Bridge Management 2: Inspection, Maintenance Assessment and Repair*. Papers Presented at the Second International Conference on Bridge Management Held 18-21 April 1993, University of Surrey, Guildford.

Raoof, M. and Lin, Z., 1995. Implications of exposure of main steel during patch repairs. *In International Association for Bridge and Structural Engineering* (Vol. 73, No. 1, pp. 499-504).

Raoof, M. and Lin, Z., 1997, February. Structural characteristics of RC beams with exposed main steel. *In Proceedings of the Institution of Civil Engineers: Structures and Building* (Vol. 122, No. 1).

Rinaldi, Z., Imperatore, S. and Valente, C., 2010. Experimental evaluation of the flexural behaviour of corroded P/C beams. *Construction and Building Materials, 24*(11), pp.2267-2278.

Rodriguez, J., Ortega, L.M. and Casal, J., 1997. Load carrying capacity of concrete structures with corroded reinforcement. *Construction and building materials, 11*(4), pp.239-248.

Rubinstein, R.Y. and Kroese, D.P., 1981. Simulation and the monte carlo method. john wiley&sons. *Inc. Publication*.

Ryan, T.W., Hartle, R.A., Mann, J.E. and Danovich, L.J., 2006. Bridge inspector's reference manual. *Report No. FHWA NHI*, pp.03-001.

Schuëller, G.I. and Stix, R., 1987. A critical appraisal of methods to determine failure probabilities. *Structural Safety, 4*(4), pp.293-309.

Setty, C.J., 2012. Truck testing and load rating of a full-scale 43-year-old prestressed concrete adjacent box beam bridge (Doctoral dissertation, Ohio University).

Sharaf H, Soudki K. Strength assessment of reinforced concrete beams with debonded reinforcement and confinement with CFRP wraps. In: *4th Structural specialty conference of the Canadian Society for Civil Engineering, Montreal, Quebec, Canada.* pp. 1–10. (2002)

Shenoy, C.V. and Frantz, G.C., 1991. Structural tests of 27-year-old prestressed concrete bridge beams. *Pci Journal, 36*(5), pp.80-90.

Shinozuka, M., 1983. Basic analysis of structural safety. *Journal of Structural Engineering, 109*(3), pp.721-740.

Tabsh, S.W. and Nowak, A.S., 1991. Reliability of highway girder bridges. *Journal of structural engineering*, *117*(8), pp.2372-2388.

Tassios, T. and Aligizaki, K., 1990. Evaluation of an Old Prestressed Concrete Bridge. In *Bridge Evaluation, Repair and Rehabilitation* (pp. 435-443). Springer, Dordrecht.

Toutanji, H., 2000. Ultrasonic wave velocity signal interpretation of simulated concrete bridge decks. *Materials and Structures*, *33*(3), pp.207.

Vecchio, F.J. and Collins, M.P., 1986. The modified compression-field theory for reinforced concrete elements subjected to shear. *ACI Structural Journal., 83*(2),

pp.219-231.

Vecchio, F.J. and Collins, M.P., 1988. Predicting the response of reinforced concrete beams subjected to shear using modified compression field theory. *ACI Structural Journal, 85*(3), pp.258-268.

Vecchio, F.J., 2000. Disturbed stress field model for reinforced concrete: formulation. *Journal of Structural Engineering, 126*(9), pp.1070-1077.

Wang, L., Hu, Z., Yi, J., Dai, L., Ma, Y. and Zhang, X., 2020. Shear Behavior of Corroded Post-Tensioned Prestressed Concrete Beams with Full/Insufficient Grouting. *KSCE Journal of Civil Engineering*, pp.1-12.

Wang, X.H., 2008. Modeling the flexural carrying capacity of corroded RC beam. *Journal of Shanghai Jiaotong University (Science), 13*(2), pp.129-135.

Wang, X. and Chung, D.D.L., 1998. Short carbon fibre reinforced epoxy coating as a piezoresistive strain sensor for cement mortar. *Sensors and Actuators A: Physical*, *71*(3), pp.208-212.

Wang, L., Zhang, X., Zhang, J., Dai, L. and Liu, Y., 2017. Failure analysis of corroded PC beams under flexural load considering bond degradation. *Engineering Failure Analysis, 73*, pp.11-24.

Wong, P.S., Vecchio, F.J. and Trommels, H., 2013. Vector2 & Formworks user's manual second edition. *University of Toronto, Canada*.

Woodward, R.J. and Williams, F.W., 1989. Collapse of Ynys-Y-Gwas Bridge, West-Glamorgan-Discussion. *Proceedings of the Institution of Civil Engineers Part 1-D1Design and Construction, 86*, pp.1177-1191.

Xia, J., Jin, W.L. and Li, L.Y., 2011. Shear performance of reinforced concrete beams with corroded stirrups in chloride environment. *Corrosion Science, 53*(5), pp.1794-1805.

Xiong, G., Liu, J. and Xie, H., 2000. Flexural behaviour of reinforced concrete beams with unbonded repair patch. *Structural Journal, 97*(5), pp.783-786.

Xu, S.H. and Niu, D.T., 2004. The shear behaviour of corroded simply reinforced concrete beam. *Journal of Building Structures, 25*(5), pp.98-104.

Zandi Hanjari, K., Kettil, P. and Lundgren, K., 2011. Analysis of mechanical behaviour of corroded reinforced concrete structures. *ACI Structural Journal, 108*(5), pp.532-541.

Zhang, W., Shang, D. and Gu, X., 2006. Stress-strain relationship of corroded steel bars. *JOURNAL-TONGJI UNIVERSITY*, *34*(5), p.586.

Zhang, X., Wang, L., Zhang, J., Ma, Y. and Liu, Y., 2017a. Flexural behaviour of bonded posttensioned concrete beams under strand corrosion. *Nuclear Engineering and Design, 313*, pp.414-424.

Zhang, X., Wang, L., Zhang, J. and Liu, Y., 2017b. Corrosion-induced flexural behaviour degradation of locally ungrouted post-tensioned concrete beams. *Construction and Building Materials, 134*, pp.7-17. 49

Zhu, W. and François, R., 2014. Corrosion of the reinforcement and its influence on the residual structural performance of a 26-year-old corroded RC beam. *Construction and Building Materials, 51,* pp.461-472.

APPENDIX A: TRUCK LOAD CALCULATION TO DETERMINE LOADING PROTOCOL FOR THE GIRDER TESTING

1. General

In order to assist determining the loading protocol for the girder testing, legal non-permit truck loads were used to estimate the service load and ultimate load of the girder according to the Bridge Load Evaluation Manual (Alberta Government 2016) and the Canadian Highway Bridge Design Code (CSA S6-14). The CL-W truck, which is the five-axle truck specified in CSA code as shown in Figure A-1, was used here. Three evaluation levels (i.e., a vehicle train, a two-unit vehicle, and a single-unit vehicle) were considered. For each evaluation level, the lane load was also considered. The lane load consists of a CL-W Truck with each axle reduced to 80% of the truck load superimposed with a uniformly distributed load of 9 kN/m and 3.0 m wide as shown in Figure A-2. Additionally, a multiple-lane load factor and a dynamic load factor were used to consider the load distribution among girders and the dynamic amplification effect, respectively. Assuming the flexural failure as the dominant limit-state, the mid-span moments in the critical cases of all evaluation levels were compared to determine the governing load: i.e., the largest moment was selected to calculate the equivalent load in the four-point bending test with the pure bending span of 1.5 m.
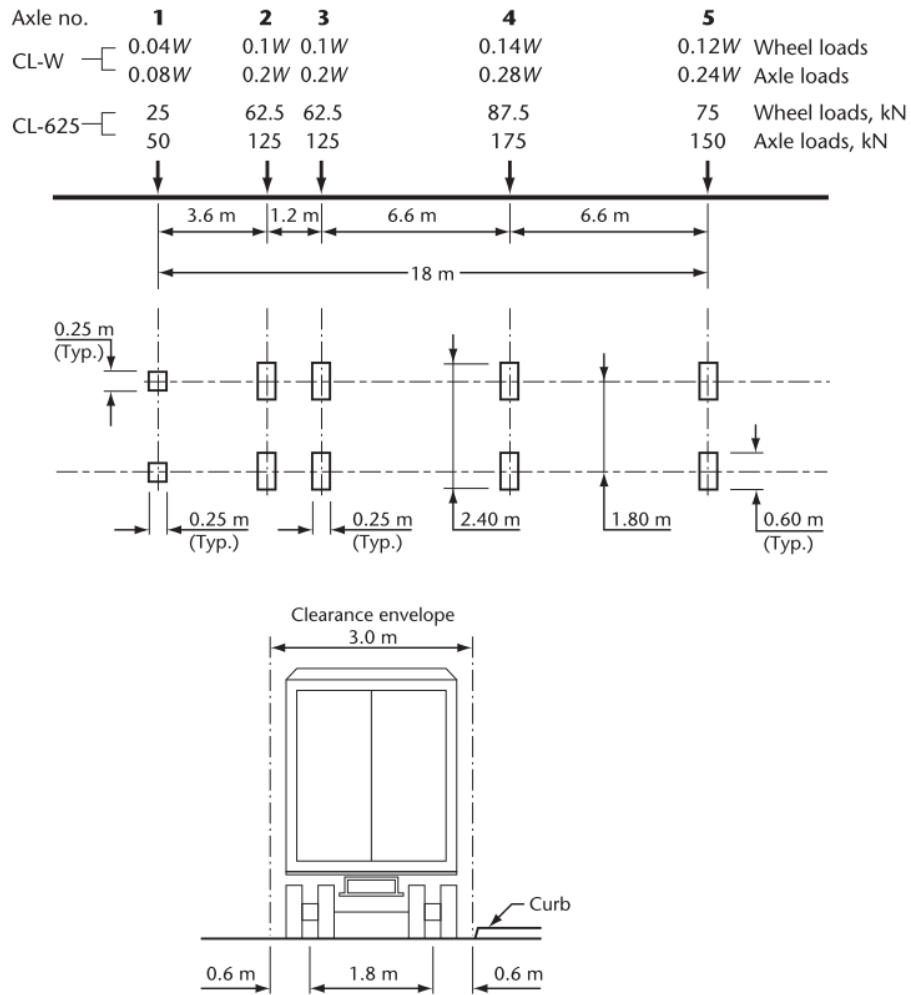
Figure A-1: CL-W truck (CSA S6-14)
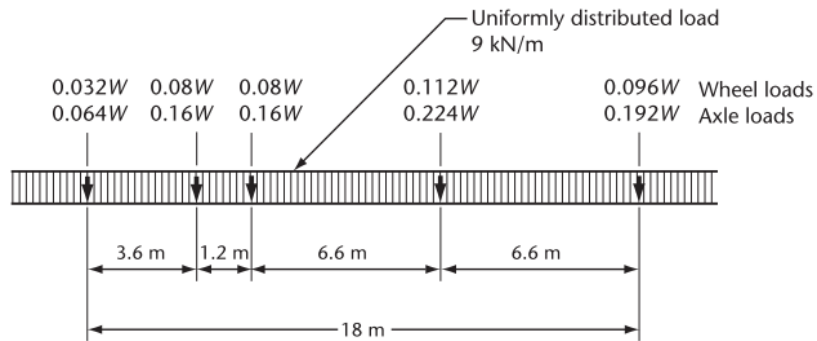
Figure A-2: CL-W lane load (CSA S6-14)

2. Maximum mid-span moment calculation

CL-W truck is a vehicle train with five axles and the axle load distribution is shown in Figure A-1. The value of W is taken as 625 kN here. The truck length (18 m), is longer than the length of girder (11 m); thus only part of the truck can be placed on the girder. As a result, two loading cases from the truck load were considered to estimate the maximum moment at the middle span (point C) of the beam. These two loading cases differed in the position of the truck on the girder as shown in Figure A-3 (a) and (b), respectively, denoted as case 1 and 2. Figure A-3 (c) shows a lane load case (denoted as case 3). Case 1 considers that most axles of the CL-W truck are positioned on the girder with the middle of the three axles located at point C; case 2 considers that the heaviest axle is located at point C; and case 3 is lane load considered. The maximum moments calculated for each of the three cases are listed below.

$$M_{c1} = 495 \text{ kN-m}$$

$$M_{c2} = 360.934 \text{ kN-m}$$

$$M_{c3} = 532.25 \text{ kN-m}$$

It is found that case 1 is more critical case for the truck load and case 3 is the most critical one among all three cases. Note that CL2-W and CL3-W truck for the evaluation level 2 and 3 have fewer axles but the same axle load and layout with CL1-W truck. As such, the critical cases of evaluation level 2 and 3 are believed to be included in the evaluation level 1, and thus not repeated here.

(a)
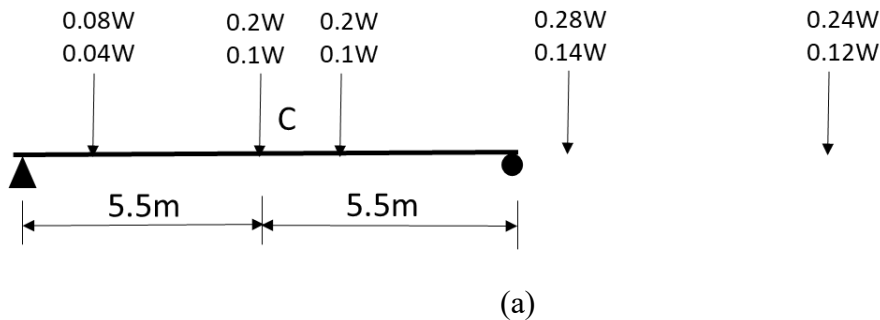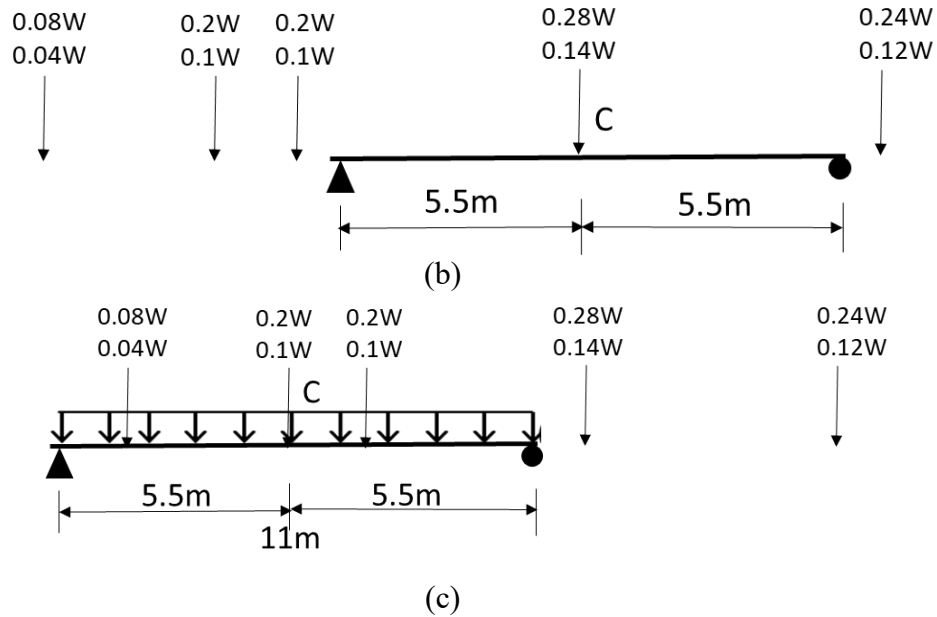
Figure A-3: Critical loading scenarios for CL1-W (a) Case 1: 3 axles on the girder, (b) Case 2: heaviest axle at the middle span of the girder, and (c) Case 3: lane load considered

3. Factors considered

A dynamic load allowance should be applied to the CL-W Truck load to amplify the truck loads but should not be applied to the CL-W lane load. According to the clause 3.8.4.5.3 in CSA S6-14, a dynamic load allowance of 0.3 is considered for axle no. 1 to 3 of the CL-W Truck positioned on the bridge. With dynamic amplification considered for the truck load, M_{c1} for the case 1 in Figure A-2 becomes the most critical case instead of M_{c3} since

$$M_{c1} = 495 \times 1.3 = 643.5 \text{ kN-m} > M_{c3}$$

Multiple lane load is considered and relevant modification factors are specified in Table 3.6 in CSA S6-14. For the two-lane bridge (i.e., with 9 girders with the interior girder 1.206 m in width) considered here, a factor 0.9 is considered assuming the highway class of A. As a result, the critical moment is

$$M_c = M_{c1} \times 0.9 = 643.5 \times 0.9 = 579.15 \text{ kN-m}$$

4. Equivalent load for four-point bending test

In order to determine the equivalent load for the four-point bending test with the pure bending span of 1.5 m, the moment diagram (see Figure A-4) for the critical case

determined earlier. The maximum moment (579.15 kN-m) at the mid-span in the girder as shown in Figure A-4 is used to determine the equivalent load P = 243.85 kN in the four-point bending test. The serviceability (SLS) and ultimate (ULS) limit-states are considered according to the load combination factors in Table 3.1 in CSA S6-14. Here, the SLS combination 2 and the ULS combination 1 are used to determine service truck load for ultimate truck load as below.

$$P_s = 0.9 \times P = 219.465 \text{ kN}$$

$$P_u = 1.7 \times P = 414.545 \text{ kN}$$

(a)   (b)
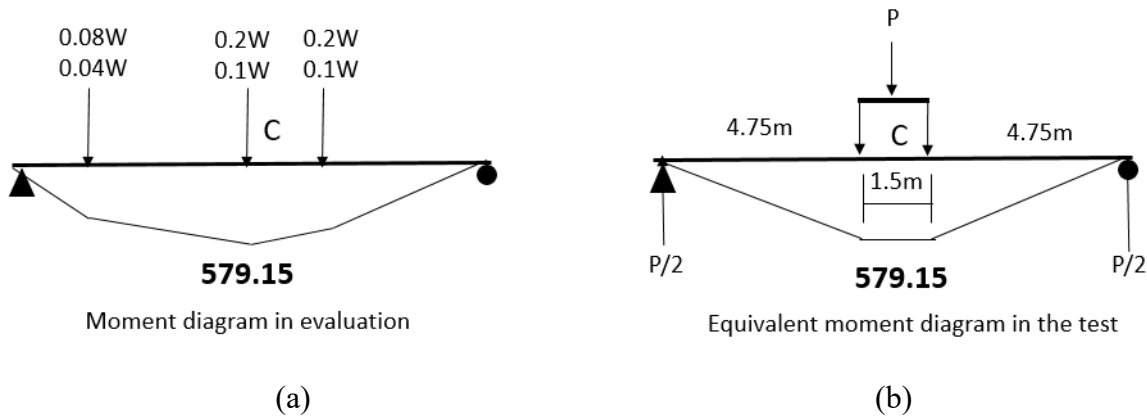
Figure A-4: Moment diagram (a) from the truck loads, and (b) for the four-point bending test with equivalent critical moment in (a)

5. Reference

Alberta Government, 2016. Alberta Transportation Bridge Load Evaluation Manual v. 1.1

CSA Canadian Standards Association, 2014. Canadian Highway Bridge Design Code S6-14.